

**Aus der Medizinischen Klinik und Poliklinik IV
der Ludwig-Maximilians-Universität München
Direktor: Prof. Dr. med. Martin Reincke**

Inflammasome-Independent NLRP3 Signaling in Chronic Kidney Disease

Dissertation
zum Erwerb des Doktorgrades der Medizin
an der Medizinischen Fakultät der
Ludwig-Maximilians-Universität zu München

vorgelegt von
Melissa Sofia Grigorescu Vlass
aus
Caracas, Venezuela

2018

Mit Genehmigung der Medizinischen Fakultät
der Universität München

Berichterstatter: Prof. Dr. med. Hans-Joachim Anders

Mitberichterstatter: PD Dr. Christoph Küper
PD Dr. Stephan Lederer

Mitbetreuung durch den promovierten Mitarbeiter: PD.Dr. hum.biol. Shrikant Ramesh Mulay

Dekan: Prof. Dr. med. dent. Reinhard Hickel

Tag der mündlichen Prüfung: 26.07.2018

Diese Arbeit wurde von August 2013 bis May 2015 im Nephrologischen Zentrum der Medizinischen Klinik und Poliklinik IV in der Arbeitsgruppe Prof. Anders der LMU München angefertigt. Die Betreuung erfolgte durch Herrn Prof. Dr. med. Hans-Joachim Anders und PD. Dr. hum. biol. Shrikant Ramesh Mulay.

Förderung: Die Arbeit wurde im Rahmen des DFG Graduiertenkolleg 2012 der LMU München vom Januar 2014 bis September 2014 unter Leitung von Prof. Dr. med. Stefan Enders gefördert.

Aus dieser Arbeit hervorgegangene Veröffentlichungen:

Poster-Präsentation:

Melissa Grigorescu, Shrikant R. Mulay, Hans-Joachim Anders. The inflammasome component NLRP3 drives renal fibrogenesis by augmenting TGF- β -signaling and not via caspase-mediated interleukin release, 6^a Jahrestagung der Deutschen Gesellschaft für Nephrologie, Berlin September 2014

Originalarbeit:

Hans-Joachim Anders*, Beatriz Suárez-Álvarez*, **Melissa Grigorescu***, Orestes Foresto-Neto*, Shrikant R. Mulay, et.al. The inflammasome component NLRP3 contributes to nephrocalcinosis-related chronic kidney disease independent from IL-1-mediated tissue injury. Role of macrophage phenotypes and NLRP3-mediated fibrogenesis. *Kidney International* (im Druck).

* equal contribution



Table of Contents

| | |
|---|----|
| Zusammenfassung..... | 7 |
| Summary | 8 |
| 1. Introduction | 9 |
| 1.1 Chronic Kidney Disease..... | 9 |
| 1.1.1 Definition and epidemiology | 9 |
| 1.1.2 Etiology and Classification..... | 10 |
| 1.1.3 Clinical features and complications..... | 11 |
| 1.2 Pathophysiology | 13 |
| 1.3 The innate immune system..... | 16 |
| 1.3.1 The role of pattern recognition receptors in PAMP and DAMP recognition..... | 18 |
| 1.3.3 The NLRP3 inflammasome: structure, activation and function | 24 |
| 1.3.4 Role of the NLRP3 inflammasome in disease..... | 27 |
| 1.4 Mesenchymal healing and fibrosis | 29 |
| 1.4.1 Biomolecular basis of mesenchymal healing and fibrosis: TGF- β signaling..... | 32 |
| 1.5 The NLRP3 inflammasome in kidney diseases..... | 35 |
| 1.5.1 Inflammasome in AKI and CKD pathology..... | 35 |
| 1.5.2 Inflammasome-independent NLRP3 signaling in kidney disease..... | 36 |
| 1.6 Mouse models of CKD..... | 37 |
| 1.7 Hypothesis..... | 40 |
| 2. Materials and Methods | 41 |
| 2.1 Materials..... | 41 |
| 2.2 Methods..... | 50 |
| 3. Results | 66 |
| 3.1 <i>In vivo</i> studies..... | 66 |
| 3.1.1 Unilateral ureteral obstruction model..... | 66 |

| | |
|---|-----|
| 3.1.2 Chronic oxalate nephropathy model..... | 79 |
| 3.2 <i>In vitro</i> studies..... | 91 |
| 3.2.1 NIH-3t3 fibroblast express NLRP3 and its expression augments upon stimulation with LPS and TGF- β 1 | 91 |
| 3.2.2 LPS and TGF- β increased the expression of profibrotic and inflammasome genes in NIH-3t3 fibroblasts in a time-dependent manner. | 93 |
| 3.2.3 NIH-3t3 cells proliferate independently of Casp-1 | 94 |
| 3.2.4 LPS and TGF- β 1 stimulation increase <i>Nlrp-3</i> expression in primary mouse embryonic fibroblasts | 95 |
| 3.2.5 LPS and TGF- β 1 stimulation increased profibrotic gene expression in WT pMEFs and not in <i>Nlrp-3</i> -deficient pMEFs | 96 |
| 3.2.6 TGF- β induced proliferation of pMEFs involves NLRP3 and ASC | 100 |
| 3.2.7 NIH-3t3 fibroblasts and pMEFs do not release IL-1 β | 101 |
| 4. Discussion..... | 102 |
| 4.1 NLRP3 and ASC in the UUO model | 103 |
| 4.2 The NLRP3 inflammasome and the Chronic Oxalate Model | 106 |
| 4.3 Fibroblasts and the NLRP3 inflammasome | 108 |
| 4.4 Study limitations | 110 |
| 4.5 Conclusion and further perspectives | 111 |
| 5. Abbreviations..... | 112 |
| 6. References | 114 |
| 7. Eidesstattliche Versicherung | 125 |
| 8. Acknowledgments | 126 |

Zusammenfassung

Chronische Nierenerkrankungen sind mit steigender Morbidität und Mortalität weltweit verbunden. Unabhängig von der Ätiologie sind alle Nierenschädigungen, die zu irreversiblen Nephronverlusten führen, mit Nierenfibrose assoziiert. Das NLRP3 Inflammasom ist ein Multiprotein-Komplex, der die Erkennung von Selbst- und Nicht-Selbst-Gefahrensignalen vermittelt und diese in die Freisetzung von Interleukinen übersetzt, was wesentlich zu entzündungsreaktionen beiträgt. Allerdings haben neuere Studien gezeigt, dass die NLRP3 Komponente auch andere Inflammasom-unabhängige (d.h. nicht IL-1 β - oder IL-18-abhängige) Funktionen ausüben kann, insbesondere bei der Regulierung des TGF- β Signalwegs. Wir postulierten, dass NLRP3 eine wichtige Rolle bei der Entwicklung der renalen interstitiellen Fibrose spielt, indem es den TGF- β Signalweg reguliert.

Unsere *in vivo* Experimente im Modell der einseitigen Ureterobstruktion (UUO) zeigten, dass die Caspase-1 (Casp-1) Inhibition die Mäuse vor der renalen interstitiellen Fibrose im Vergleich zu *Nlrp-3*-defizienten Mäusen nicht schützt. Eine zweite *in vivo* Studie mit Hyperoxalurie-induzierter chronischer Niereninsuffizienz verdeutlichte, dass die Hemmung des IL-1 Rezeptors mit Anakinra keine große Bedeutung bei der Oxalat-induzierten Nephropathie spielt. Die genaue Rolle des NLRP3 oder ASC in diesem Modell konnte nur eingeschränkt beurteilt werden, da *Nlrp-3*- sowie *Asc*-defiziente Mäuse keine intrarenalen Kalziumoxalat Kristalle entwickelten. Zusätzlich zeigte das UUO *in vivo* Modell eine reduzierte Phosphorylierung von Smad 2/3 bei *Nlrp3* Defizienz, was darauf hindeutet, dass NLRP3 die Signalübertragung des TGF Rezeptors durch Regulierung der Smad 2/3 Phosphorylierung erhöht. Ferner konnten *in vitro* Experimente mit embryonalen Maus Fibroblasten verdeutlichen, dass NLRP3 die Proliferation und Aktivität dieser Zellen stark reguliert, dies allerdings unabhängig von der Sekretion von Interleukinen erfolgt.

Diese Arbeit zeigt, dass NLRP3 die renale interstitielle Fibrose beim renalen Gewebsumbau und chronischer Niereninsuffizienz durch die Verstärkung des TGF Rezeptor Signalwegs unabhängig von Casp-1-vermittelter IL-1 β Freisetzung fördert.

Summary

Chronic kidney disease (CKD) is associated with increasing morbidity and mortality worldwide. Regardless of the etiology, all kidney injuries that lead to irreversible nephron loss are associated with renal fibrosis. The NLRP3 inflammasome is a multiprotein-complex, which translates self and non-self danger signals for the activation and release of IL-1 β and IL-18, contributing significantly to inflammatory responses. However, recent studies have shown that the NLRP3 component also exerts other inflammasome-independent (i.e. IL-1 β - or IL-18-independent) functions, especially in regulating TGF- β signaling. We postulated that NLRP3 plays an important role in the development of renal interstitial fibrosis by regulating TGF- β signaling in an inflammasome-independent manner.

Our *in vivo* experiments using the unilateral ureteral obstruction (UUO) mouse model showed that Caspase-1 (Casp-1) inhibition does not protect mice from renal interstitial fibrosis compared to *Nlrp-3*-deficient mice. A second *in vivo* study using a chronic hyperoxaluria-induced CKD model showed that inhibition of the IL-1 receptor with anakinra does not protect mice from nephrocalcinosis-induced CKD, whereas *Nlrp-3*- and *Asc*-null mice were unable to develop intrarenal calcium oxalate crystals, compromising any conclusions regarding the role of NLRP3 in nephrocalcinosis-induced CKD. The UUO *in vivo* model showed a reduced phosphorylation of SMAD 2/3 upon *Nlrp-3* deficiency, suggesting that NLRP3 augments TGF- β receptor signaling by regulating SMAD 2/3 phosphorylation. Furthermore, *in vitro* studies using mouse embryonic fibroblasts revealed that the inflammasome component NLRP3 regulates fibroblast activation, function and proliferation, and that this is independent of the release and activation of IL-1 β .

Taken together, this thesis demonstrates that the inflammasome component NLRP3 drives renal fibrogenesis and tissue remodeling in CKD by augmenting TGF receptor signaling independent of a Casp-1-mediated interleukin release.

1. Introduction

1.1 Chronic Kidney Disease

1.1.1 Definition and epidemiology

Definition: Kidney Disease: Improving Global Outcomes (KDIGO) defines chronic kidney disease as *abnormalities of kidney structure or function present for over three months with implications for health* [4]. These abnormalities encompass increased albuminuria, urine sediment or histological irregularities, electrolyte and acid-base disorders, imaging abnormalities (as marker of kidney damage) or decreased **G**lomerular **F**iltration **R**ate (GFR) ($< 60 \text{ ml/min/1.73m}^2$). The latter is the best-known parameter for estimating kidney function. It declines from $125 \text{ ml/min/1.73m}^2$ starting from the third decade of age at an approximate of 1 ml/min/1.73m^2 per year in healthy adults, thus leading to CKD stage G1 or G2 in the older population. KDIGO refers to a GFR under $60 \text{ ml/min/1.73m}^2$ as decreased, whereas a GFR under $15 \text{ ml/min/1.73m}^2$ is considered as kidney failure, reflecting a state of **E**nd **S**tage **R**enal **D**isease (ESRD) [4].

Epidemiology: CKD and its complications have increasingly contributed to the morbidity and mortality in industrialized and developing countries. In the U.S. 4 to 5% of the adult population has CKD stages G4 to G5 [3]. Between 2007 and 2012 a study called NHANES was performed in the U.S., which revealed a total of 13.6% prevalence of CKD in patients with 20 years of age and older. Also, the number of patients with CKD stage G3 increased from 4.5% to 6.0% in 10 years [5]. In Germany, 175 out of one million people have ESRD and the incidence increases 3 to 5% every year [6]. It is also one of the most expensive diseases for the health-care system with costs of up to 500 million Euros (2002) for patients between 65 and 85 years of age. This number significantly expanded in 2008 to an approximate of 724 million Euros [7], defining CKD as one of the most expensive non-communicable chronic diseases that involve a significant reduction of lifespan. The increased incidence of CKD in industrialized countries is mainly a result of improved cardiovascular-disease management and survival rates of the population [3]. On the other hand, ESRD has not changed its incidence in these countries, probably because of the improved management possibilities. However, developing countries show a rising trend in the development of both CKD and ESRD. This is expected to increase dramatically in the next two decades [8]. Overall, epidemiological studies signalize the growing importance of CKD worldwide and the need for improved and more economical strategies in the management of the disease.

1.1.2 Etiology and Classification

Etiology: Diabetic nephropathy, glomerulonephritis, hypertensive nephropathy (as primary glomerulonephritis with hypertension or vascular and ischemic renal disease), diverse congenital anomalies of the kidney and urinary tract (CAKUT) and tubulointerstitial nephropathies are the most frequent causes of CKD in Germany (Figure 1). This distribution varies worldwide depending on the geographic region. Still, diabetic nephropathy remains the leading cause in both industrialized and developing countries, mainly secondary to type 2 diabetes mellitus [3]. However, the number of people with CKD not secondary to diabetes or hypertension is significantly higher in developing countries, especially in younger patients. One study from 2007 revealed 43% of CKD patients in China, Mongolia, and Nepal did not have diabetes or hypertension [9]. Other factors affecting developing countries such as poor nutrition during pregnancy, result in low nephron number in the fetus, increasing the risk for CKD development later in life [10].

Among the highest risk factors for the development, progression and worsening of CKD today are hypertension, diabetes mellitus, older age, smoking, metabolic syndrome, prolonged treatment with nephrotoxic drugs, family history for CKD and acute kidney injury (AKI) in the past medical history [11]. Genetic factors like the presence of the APOL1 gene in CKD patients with African ancestries have shown higher rates for progression of kidney disease and development of ESRD [12].

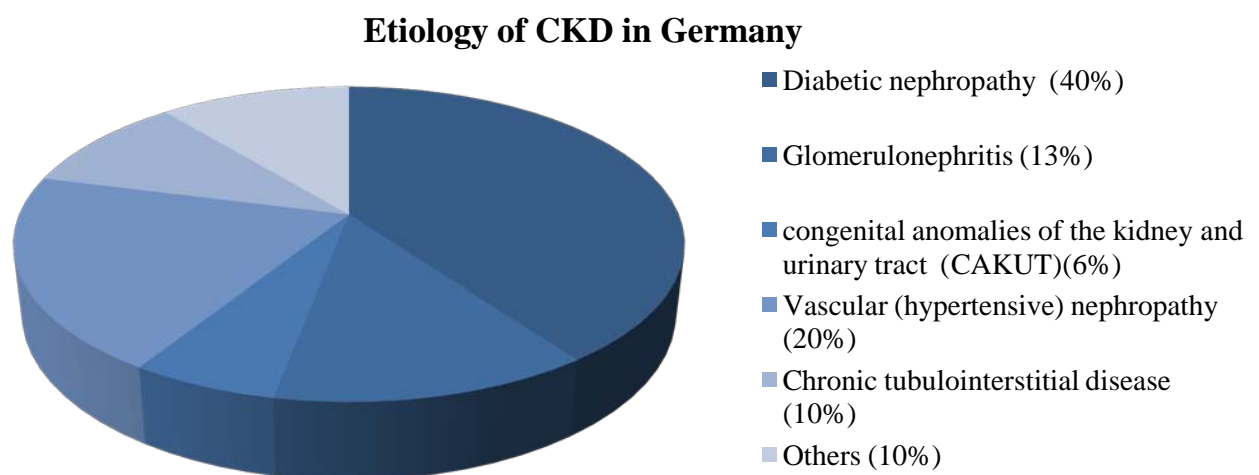


Figure 1: Adapted from *Daten und Fakten zur Nephrologie* (DGFN) [6]

Classification: The CKD classification is based on cause, GFR category (G1 to G5) and albuminuria category (A1 to A3). Due to recent evidence, both categories were combined and used for the prediction of disease progression and prognosis [4].

1.1.3 Clinical features and complications

Kidneys are multifunctional organs, responsible for the elimination of metabolites and toxins, water and electrolyte balance, acid-base homeostasis, regulation of the hematopoietic (erythropoietin secretion) and cardiovascular system (angiotensin II and prostaglandin regulation), bone-mineralization homeostasis (calcitriol formation) and arterial blood pressure control, taking a pivotal role in the function of almost every organ system in the body [3, 13].

Interestingly, patients with an early stage of the disease (CKD G1 to 3) are generally asymptomatic. They may present with unspecific symptoms such as fatigue, sleep disturbances, hypertension or decreased urine output. In most cases, the underlying pathology is the key symptomatic feature (e.g. systemic manifestations of type 2 diabetes mellitus, arterial hypertension or lupus erythematosus). Patients with advanced stages of CKD (G4 to 5) may present with diverse signs and symptoms including metabolic or endocrine derangements (e.g. anemia), signs of acid-base dysbalance (e.g. malnutrition and muscle weakness), water and electrolyte disturbances (e.g. edema and hypertension due to fluid overload), and many others. Patients with kidney failure or ESRD present with a wide group of symptoms that reflect the presence of uremia. It results mostly from the accumulation of internal and external toxins, the inability to regulate the endocrine system, acid-base and fluid homeostasis disturbances, and the progressive and systemic inflammation with subsequent vascular and nutritional consequences. Table 1 shows clinical manifestations of this syndrome in different organ systems [3]. The clinical manifestations of uremia have almost disappeared among European countries mainly due to the growing implementation of renal replacement therapies such as chronic dialysis and renal transplantation. Nevertheless, not all symptoms are ameliorated by dialysis. Many of them persist and worsen during this procedure, while others appear as a consequence of the treatment itself.

Conceptual model of CKD: For a better understanding of CKD with its risk factors, progression and complications, a conceptual model was developed by the KDOQI in 2002, later modified by KDIGO 2012. This displays in a simplified diagram the continuous development, progression and complications of CKD, which serves as a guideline in disease prevention programs of the public health care system (Figure 2).

Complications of CKD: Kidney malfunction implies systemic complications. Commonly, patients with advanced stages of CKD present with metabolic acidosis, hyperkalemia, calcium and phosphate disturbances and respective bone and cardiovascular complications, including low turnover and high turnover hyperparathyroidism (starting from a GFR < 60 ml/min/1.73m²). The cardiovascular complications as well the significantly higher risk for infections are the leading causes of morbidity and mortality in patients with CKD [14].

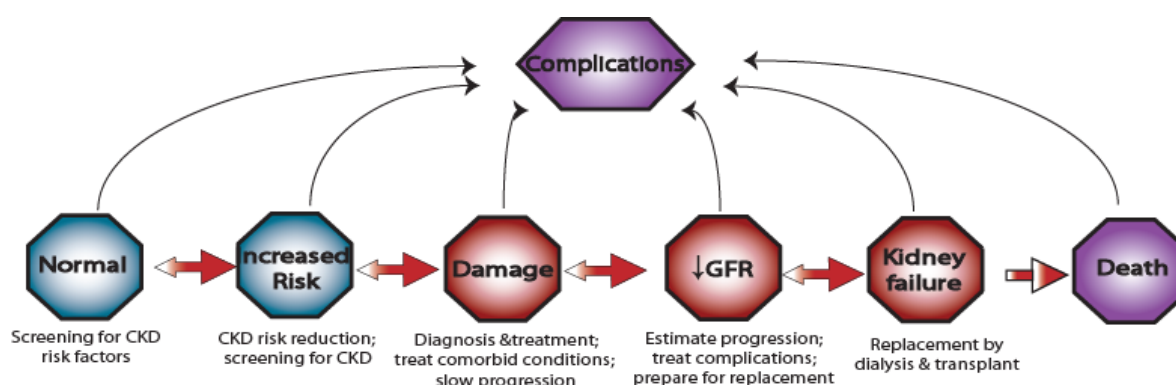


Figure 2: Conceptual model of CKD. Adapted from KDIGO 2012 [4]. Blue: potential antecedents of CKD; red: stages of CKD; purple: consequences of CKD; thick arrows: left to right: development and progression of CKD, white right to left arrows: remission (less frequent than progression). Abb.: GFR: Glomerular filtration rate.

Table 1: Clinical manifestations of uremia

| Organ system | Symptoms |
|-----------------------------------|---|
| Fluid, electrolyte, and acid-base | Volume expansion, hyperkalemia, hyperphosphatemia. |
| Endocrine – metabolic | Secondary hyperparathyroidism, a-dynamic bone, Vitamin-D deficient osteomalacia, carbohydrate resistance, hyperuricemia, hypertriglyceridemia, decreased HDL, protein-energy malnutrition, infertility and sexual dysfunction, amenorrhea, amyloidosis. |
| Cardiovascular | Arterial hypertension, pericarditis, uremic lung, accelerated atherosclerosis, hypotension and vascular calcifications. |
| Hematologic and immunologic | Anemia, lymphocytopenia, bleeding diathesis, increased susceptibility to infection, thrombocytopenia. |
| Gastrointestinal and nutritional | Nausea, vomiting, peptic ulcer and gastrointestinal bleeding, ascites, peritonitis. |
| Neuromuscular | Fatigue, sleep disorders, lethargy, muscular irritability, myopathy. |
| Dermatological | Pallor, hyperpigmentation, pruritus, uremic frost. |

Adapted from Harrisons: Principles of Internal Medicine [3]

1.2 Pathophysiology

Nephrons are the functional units of the kidney and work in a defined and organized manner. Neal Bricker's 1969 *intact nephron hypothesis* describes from a functional perspective, how surviving nephrons either function normally or do not function at all [15]. When an injurious trigger causes relevant damage to the kidney parenchyma with significant nephron loss, adaptive mechanisms of the remaining nephrons activate and lead to their "hyperfunction" and progressive hypertrophy with the aim of compensating the lost functionality. Such mechanism can be observed in patients who undergo unilateral nephrectomy, where the remaining kidney is able to regain the function by rising the GFR up to 80% of the normal population with two kidneys and show a hypertrophic parenchyma [15]. This initial adaptive response involving nephron hyperfunction and hypertrophy can become from a certain point maladaptive, leading to disease progression and CKD, especially with ongoing kidney injury like in chronic glomerulonephritis or with persistent proteinuria.

From a molecular perspective, CKD pathology is mostly a product of the deregulation of the four "danger response programs"; these include *hemostasis*, *inflammation*, *epithelial-* and *mesenchymal healing* [16]. They are responsible for regaining tissue structure and function after any kind of injury. In most cases, nature has achieved an adequate balance between these mechanisms. Occasionally these act in a dysregulated manner, being either insufficient or overshooting [16, 17].

Certainly, whether glomerular, vascular or tubulointerstitial, continuous injury to the kidney will almost always lead to interstitial nephritis, a product of overshooting inflammation. In diabetic and hypertensive nephropathy, for example, the intraglomerular capillary pressure rises, increasing the single nephron GFR. The activated renin-angiotensin-aldosterone system also known as RAAS, and concomitant elevation of angiotensin II further worsen the scenario by constricting the efferent arteriole, reducing glomerular filtration selectivity, inducing protein ultrafiltration and increasing shear stress for podocytes. The elevated concentration of proteins in the ultrafiltrate induces its uptake in the proximal convoluted tubule cells via megalin/cubulin into the lysosomes [18], disturbing cell homeostasis and activating them to secrete proinflammatory cytokines such as interleukin 6 (IL-6), IL-8, among others [18, 19]. The released cytokines stimulate resident immune cells such as macrophages and dendritic cells (DCs), which in turn augment the reaction by recruiting additional mononuclear cells, sustaining the inflammatory process [20]. The exaggerated and continuous inflammation persists as long as the injurious trigger is not removed. Interstitial

nephritis, oxidative stress, and cytokines damage tubular cells, resulting in an epithelial imperfection that hardly recovers, especially under these conditions.

Mesenchymal cells, namely activated fibroblasts from the interstitial compartment, will then try to cover up the defect by producing extracellular matrix (ECM) components such as collagen I and III, leaving eventually an acellular scar, which when overshooting results in interstitial fibrosis [21]. This pathological feature is the hallmark of advanced CKD, which further aggravates the organ architecture destruction and function impairment, and is thus thought to worsen the prognostic outcome of the disease [22]. Figure 3 displays a schematic presentation of the pathomechanisms leading to CKD. The following chapters will carefully describe the molecular mechanisms regarding interstitial nephritis and mesenchymal healing leading to CKD.

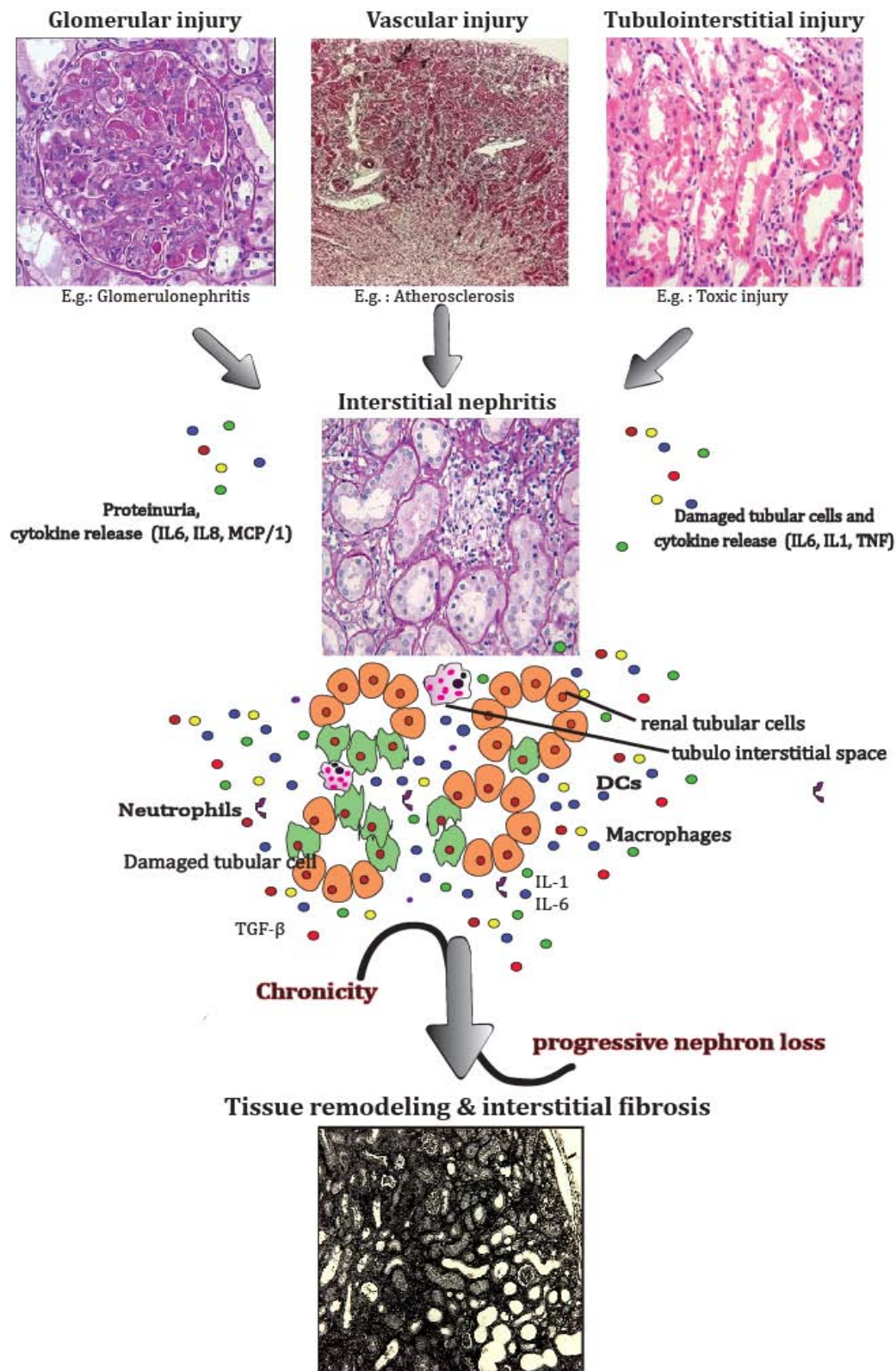


Figure 3: Pathomechanisms leading to CKD. Glomerular, vascular and tubulointerstitial injuries lead to interstitial nephritis. Damaged tubular cells (green) release cytokines, activating resident immune cells (DCs, neutrophils and macrophages) who recruit additional immune cells and release proinflammatory (IL-6, IL-1) and profibrotic cytokines (TGF- β). Disease chronification enhances progressive nephron loss and leads to overshooting activation of fibroblasts and therefore the mesenchymal healing process, leading to renal interstitial fibrosis. Abb.: DCs: dendritic cells; IL-1, IL-6: interleukin 1 and 6; TGF- β : transforming growth factor β , TNF: tumor necrosis factor, MCP1: monocyte chemoattractant protein 1.

1.3 The innate immune system

Humans possess two types of immune system: the innate or unspecific and the adaptive or specific immunity. Both systems consist of soluble molecules and cells that act against invading microorganisms. The innate immunity is found in both vertebrates and invertebrates, and it is characterized as a rather unspecific and ancient defense system. The adaptive system, on the other hand, is only found in more evolved organisms such as jawed fish and mammals and is characterized for being a rather specific and more evolutionary recent mechanism [23]. *In vivo*, both systems act together in the immune response. The following mechanisms are required for a proper and accurate response: (1) recognition of the danger signal/microorganism, (2) elimination of the injurious agent, (3) regulation of the immune response and (4) gain of memory. The regulatory and memory functions are mainly achieved by the adaptive immunity [24]. Innate immunity recognizes a large number of pathogens but not in a specific manner like the adaptive immune response does. Nevertheless, specific recognition requires more time and implies a delayed response. This is counteracted by the innate immune system, which is capable of acting instantly against entering invaders. Table 2 shows some of the principal differences between innate and adaptive immunity.

Table 2: Main differences between innate and adaptive immunity

| | Innate | Adaptive |
|------------------------|--|--|
| Specificity | Limited Same response for a variety of agents | Wide Response only to stimulating agent |
| Protagonists | Mononuclear phagocytic system Granulocytes (neutrophils, basophils) | T- and B-lymphocytes |
| Reaction | Immediate | Delayed |
| Immune response | Phagocytosis Co-stimulating molecules: cytokines IL-6, IL-1 | Clonal expansion (IL-2) Effector cytokines (IFN- γ , IL-4) |
| Receptors | PRRs, invariant, germline encoded | T-cell receptor, B-cell receptor, somatic gene encoded; rearrangement, diversity extended to a wide range of receptors |
| Recognition | Conserved molecular patterns (LPS) | Structural unities (peptides, carbohydrates) |
| Memory | Absent, same response for subsequent exposure. Non-anticipatory | Present, amplified responses for subsequent exposure. Anticipatory |

Adapted from Janeway, C.A, et al. Abb.: PRRs: pattern recognition receptors, LPS: lipopolysaccharide, IL: interleukin, IFN: interferon [25]

After pathogens cross the physical barriers (skin, epithelial respiratory, gastrointestinal and urogenital tract), chemical barriers (gastric acid with low pH and vaginal secretions) and biological defense barriers (bactericide lysozyme in mucosal secretion), innate immunity awaits as first line host defense to prevent their further propagation [26, 27]. Cells of the innate immunity include monocytes, tissue macrophages and their precursors (Langerhans cells, mesangium cells of the kidney and microglia) [28], recognize pathogens *via* specific molecular patterns named *Pathogen-associated molecular patterns* or PAMPs using specific receptors called *Pattern recognition receptors* or PRRs. Upon recognition, cells eliminate the invading agent through instant mechanisms such as phagocytosis, where pathogens are “eaten” by neutrophils or monocytes/macrophages and killed in endosomes with the help of nitric oxide (NO), oxygen radicals (O_2^-), hydrogen peroxide (H_2O_2) and other toxic agents. Following activation, these cells induce the recruitment of further inflammatory cells by secreting proinflammatory cytokines (IL-1 β , IL-6, monocyte chemotactic protein 1 (MCP-1)), chemokines, complement factors and antimicrobial peptides, thus amplifying the immune response [29, 30]. Furthermore, antigen presenting cells (APC) such as DCs introduce the pathogen to T-lymphocytes and thereby, activating the adaptive immune system [27]. Table 3 describes the main components of the innate immune system and their functions.

This response is what we call *inflammation*. It may manifest in any organ, either locally (e.g. an abscess of the skin), or systemically (e.g. as in sepsis). All organs possess resident immune cells, and the kidney is not an exception. Under homeostatic conditions, resident DCs localized mainly in the renal interstitium are strongly implicated in the development of interstitial nephritis by secreting cytokines and chemokines that recruit neutrophils; macrophages on the other hand, are found mainly in the medulla and cortex crucial for keeping tissue homeostasis and repair; and finally a few lymphocytes, whose function under normal conditions is still not fully understood [31-34].

Table 3: Main components of the innate immune system and their main function

| System | Characteristics | Function |
|-------------------------------|--|---|
| Cells | Monocytes and macrophages, | Phagocytosis, antimicrobial peptides; secretion of inflammatory cytokines (IL-1 β , IL-6) |
| | NK-cells, dendritic cells (DCs) | NK-cells: cellular toxicity DCs: part of the adaptive immune system, but play a key role in innate immunity as APC. Strong producers of IFN- γ , IL-12 |
| | Granulocytes (neutrophils, eosinophiles, basophiles) | Phagocytose and kill bacteria, produce antimicrobial peptides |
| | Mast cells | Release TNF- α , IL-6, IFN- γ in response to PAMPs |
| | Epithelial cells | Production of mediators local innate immunity |
| Humoral (proteins) | Complement system (C3b, C5a, C7, C9), IFN (alpha, beta, gamma), cytokines (IL, TGF, TNF), pentraxins (CRP), collectins | Complement: opsonization, kill pathogens, lymphocyte activation. IFNs and cytokines: activation of immune cells, response magnification. Pentaxins: acute phase reaction. |
| Antimicrobial peptides | α - and β - defensins, granulysin, secretory leukoprotease inhibitor | Disruption of membrane integrity of pathogens and other mechanisms |

Adapted from Janeway C.A. et al. and Turvey S.E. et al. Abb.: IFN: Interferon, IL: Interleukin, NK-cells: natural killer cells, APC: antigen presenting cells, DCs: dendritic cells, TNF: tumor necrosis factor, PAMPs: pathogen-associated molecular patterns, IFNs: interferons [24, 35].

1.3.1 The role of pattern recognition receptors in PAMP and DAMP recognition

Recognition of the pathogen/danger signal is essential for an optimal immune response. Charles Janeway first proposed in the late 90's that innate immunity uses specific tools for danger recognition. He suggested that the unspecific innate immune system actually uses specific germ-line encoded PRRs, which can detect bacteria, viruses and other invaders in form of PAMPs [36]. The following section describes each part of the recognition system of the innate immunity.

PAMPs: *Pathogen-associated molecular patterns* are conserved molecular patterns throughout evolution, essential for the survival of microorganisms. Host cells do not express these molecular patterns, allowing automatically a self/non-self discrimination by the innate immune system [37]. PAMPs are the pathogens' signature, allowing the innate immune system to differentiate which kind of pathogen (bacterial, fungal or parasite) is present at the site of infection. Through this, the innate immunity may recognize a wide range of microorganisms and danger signals, in a reasonably

specific manner using only a limited number of germ-line encoded receptors, as opposed to the adaptive immunity, which constantly renews the genome that encodes the receptor [38, 39].

Damage-associated molecular patterns or DAMPs: Immunology was dominated by the self/non-self theory since the 1950's. In 1994, Polly Matzinger proposed a novel theory, "the danger theory", which explained how the immune system is more concerned about "danger" or "no danger", rather than self/non-self [40]. This theory introduced the term DAMP "*Danger-associated molecular patterns*", which covers what we understand as a danger or alarm signal produced by the organism itself. They can be constitutively expressed or induced; located in the intracellular space (ICS) or secreted to the extracellular space (ECS), or part of the ECM. When cells undergo programmed cell death, for example, such as apoptosis, cell detritus is scavenged by the remaining living cells annexed to it. This is a process that constantly takes place in the gut mucosa and does not lead to the activation of the immune response. Necrosis, on the other hand, is also a form of programmed cell death, but instead, leads to the release of intracellular material to the ECM. The surrounding cells recognize the residuals of the diseased cell and translate them into danger signals, thus inducing an immune response. Nucleotides (ATP, UTP) and other hydrophobic molecules such as oxidized LDL, β -defensin, protein A, and fibronectin, which are found normally in the ICS, alarm and activate the immune system when released to the ECS [40, 41]. Situations like cell stress, necrosis, and allograft implantation, promote DAMP release and induce sterile inflammation. Among the most studied DAMPs are proteins such as high mobility group box 1 (HMGB-1) or S100 localized to the cytoplasm, heat shock proteins (HSP) in endosomes, hyaluronic acid products from the ECM, mitochondrial products as mtDNA, mitochondrial reactive oxygen species (ROS), and many others [42-44]. Figure 4 shows a schematic representation of different PAMPs and DAMPs together with their receptors and expression within the cell.

PRRs: Almost every cell of the innate immune system uses PRRs for the recognition of pathogens. Several types of these receptors have been described over the past few years. They are localized in different cell compartments, some being membrane bound, others in the cytosol, and others in the ECS. Toll like receptors (TLRs) are a good example of PRRs. Their discovery in the late 1990's reassured Janeway's theory and changed science's perception of an "unspecific" innate immune system. Till then, innate immunity was known for its antigen-presenting function and phagocytosis system managed by the adaptive immunity. To date, many TLRs have been discovered and classified depending on the activating ligand; these may be self or non-self, soluble or membrane bound. In humans, 13 different types of TLRs (2-10) have been described. These transmembrane proteins can

recognize DAMPs and PAMPs, which may consist of proteins, carbohydrates, nucleotide acids, or other structures. TLR-4, for example, binds PAMPs such as bacterial LPS or DAMPs such as HMGB1 or HSPs. Ligand-receptor complex triggers a downstream signaling cascade, including the activation of MyD88, which then activates and recruits a series of proteins that further can activate the transcription factor NF- κ B [45, 46]. NF- κ B, a well-known transcription factor in the innate immune system, promotes the transcription of multiple cytokines such as interleukins, interferons (IFNs), tumor necrosis factor (TNF), MCP-1 and many others, depending on the triggering stimulus and the type of cell [47]. On the other hand, extracellular, soluble PRRs like pentraxins (a family of multimeric PRRs) have a completely different mechanism. C-reactive protein (CRP) and serum amyloid protein are both short pentraxins released from the liver as acute phase proteins and are widely used as clinical parameters for infection diagnostics. They act as receptors, effectors, and modulators almost simultaneously. PTX3, part of the long pentraxin family, is released from endothelial and inflammatory cells upon inflammation [48]. Table 4 describes different PRRs, together with their ligands, expression and function [49, 50]. This thesis focuses on the cytosolic NOD-like receptors (NLRs). Their discovery and especially the formation of the NLRP3 inflammasome have been of great interest to the scientific community and will be discussed in the next chapter.

Table 4: Pattern recognition receptors

| PRR Family | Sites of expression | Examples | Ligands (PAMP/DAMP) | Functions of PRR |
|------------------------------------|------------------------------------|--------------------------------------|--|--|
| Toll-like receptors (TLR) | Multiple cells | TLR 2-10 | LPS, LTA, HMGB1 | Activate innate immune cells and initiate adaptive immune response |
| C-type lectin (CLR) | Plasma, macrophages, DCs, NK cells | Dectin-1 Macrophage mannose receptor | Bacterial mannose, fungal β glucan | Opsonization of bacteria and virus, activation of complement. Inhibits killing host cells expressing HLA and self-peptides |
| Scavenger receptors | Macrophages | Scavenger receptors | Bacterial cell walls | Phagocytosis of bacteria |
| Pentraxins | Plasma | CRP Serum amyloid P | Phosphatidyl-choline, bacterial cell walls | Opsonization of bacteria, activation of complement |
| Integrins | Macrophages, DCs, NK-cells | CD11b,c; CD18 | LPS | Signals cells, activates phagocytosis |
| NOD-like receptors (NLRs) | Innate cells | AIM2, NLRP3 | Crystals, A-toxin | Cytosolic proteins involved in innate sensing (self/non-self) |
| RIG-I-like receptors (RLRs) | Myeloid cells, epithelial cells, | RIG-I, MDA 5 | Viral RNA | IFN-1 production, activation of innate immunity and infection control |

Adapted from [1-3]. Abb.: LPS: lipopolysaccharide, LTA: lipoteichoic acid, HMGB 1: high-mobility group box 1, HLA: human leukocyte antigen, DCs: dendritic cells, NK-cells: natural killer cells, CRP:c-reactive protein, CD: cluster of differentiation, AIM2: absent in melanoma 2, MDA 5: melanoma differentiation-association, RNA: ribonucleic acid, IFN-1: interferon-1.

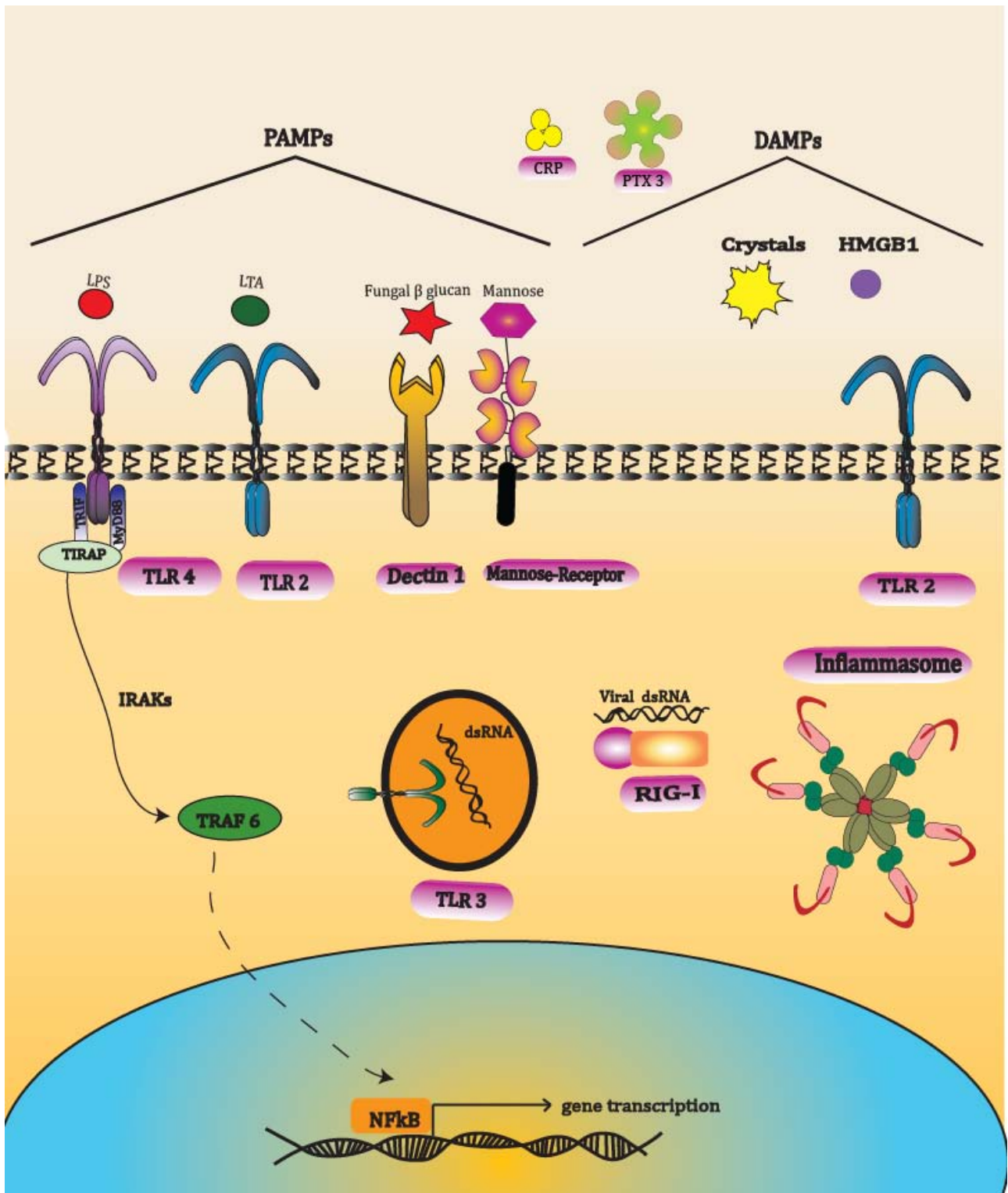


Figure 4: PAMPs and DAMPs with receptors. Pattern recognition receptors and ligands (PAMPs or DAMPs). Depicted are: Extracellular PRRs CRP and PTX3; *Toll-like receptors*: TLR-2,-3 and -4 with respective ligands LTA and the DAMP HMGB1, dsRNA and LPS; *C-type lectins*: dectin-1 and mannose receptor with respective ligands: fungal β glucan and mannose; *Nod-like receptors*: NLRP3 with crystals as respective ligands; *RIG-I like receptors*: RIG I with respective ligand viral dsRNA. Schematic representation of TLR-4 signaling pathway (left) with activation of TIRAP and TRAF and further gene transcription. Abb.: PAMPs: Pathogen-associated molecular patterns, DAMPs: Danger-associated molecular patterns, CRP: C-reactive protein, PTX3: pentraxin 3; TLR: Toll like receptor; LTA: lipoteichoic acid, LPS:lipopolysaccharide, HMGB1: High-mobility group box 1; dsRNA: double strand ribonucleic acid; NLRP3: NOD-like receptor protein 3.

1.3.2 NOD-like receptors and the inflammasome

Nucleotide-binding oligomerization domain (NOD)-like receptors are evolutionarily conserved receptors, present in plants and animals (zebra fish) as R genes [51]. The NLR family consists of 22 proteins in humans and 33 in mice. Their main functions are regulation of cell death, inflammation and innate immune responses, and are mainly expressed in innate immune cells, e.g. DCs, macrophages and neutrophils, as well as in tissue epithelia of the gut, heart, liver, and kidney.

These protein receptors are built of a tripartite structure composed of a central invariable nucleotide binding domain with ATPase activity called NOD domain, NBD, or NACHT domain; a C-terminal domain with leucine rich repeats (LRRs), probably responsible for the ligand recognition and regulation; and a variable N-terminal domain, the effector domain, which is defined by respective binding structures such as CARD (caspase activation and recruitment domain), PYD (pyrin domain), AD (acidic transactivator domain), and BIR (Baculovirus inhibitory N-terminal domains). The CARD and PYD domain belong to the death fold superfamily. These are structure motifs commonly found in apoptosis- or inflammation-related processes.

NLRs are classified in four subfamilies according to the structure binding the N-terminal domain: NLRA (NLR binding AD domain), NLRB (NLR binding BIR), NLRC (NLR bind CARD), NLRP (NLR binding PYD domain) and NLRX (this has an unknown binding domain and only one class has been found in mitochondria) [52]. Figure 5 shows different NLR families with its respective structures.

Upon activation with PAMPs or DAMPs, NLRs will trigger a signaling cascade, which will induce the production of antimicrobial and proinflammatory mediators such as TNF- α , IL-6 and IL-1 β . But not all NLRs use the same signaling pathway. Three end-targets of NLR signaling have been studied to the date, these include the activation of (1) NF- κ B, of (2) MAPKs and (3) Casp-1.

NOD-1 and NOD-2 (two well-studied NLRs belonging to the NLRC subfamily) are known for activating MAPKs as well as NF- κ B. NLRP-3 and two other NLRs including NLRP1 and NLRC4 (also known as IPAF) activate Casp-1 and sometimes caspase-5 in humans (caspase-11 in mice). Caspases are known for their important role in cell death induction and proinflammatory function. These three NLRs including the non-NLR family protein AIM2 (absent in melanoma 2) build multi-protein complexes called inflammasomes which serve as Casp-1 activating platforms and are essential for the secretion of IL-1 β and IL-18, and the induction of pyroptosis, an alternative way of cell death [53-55].

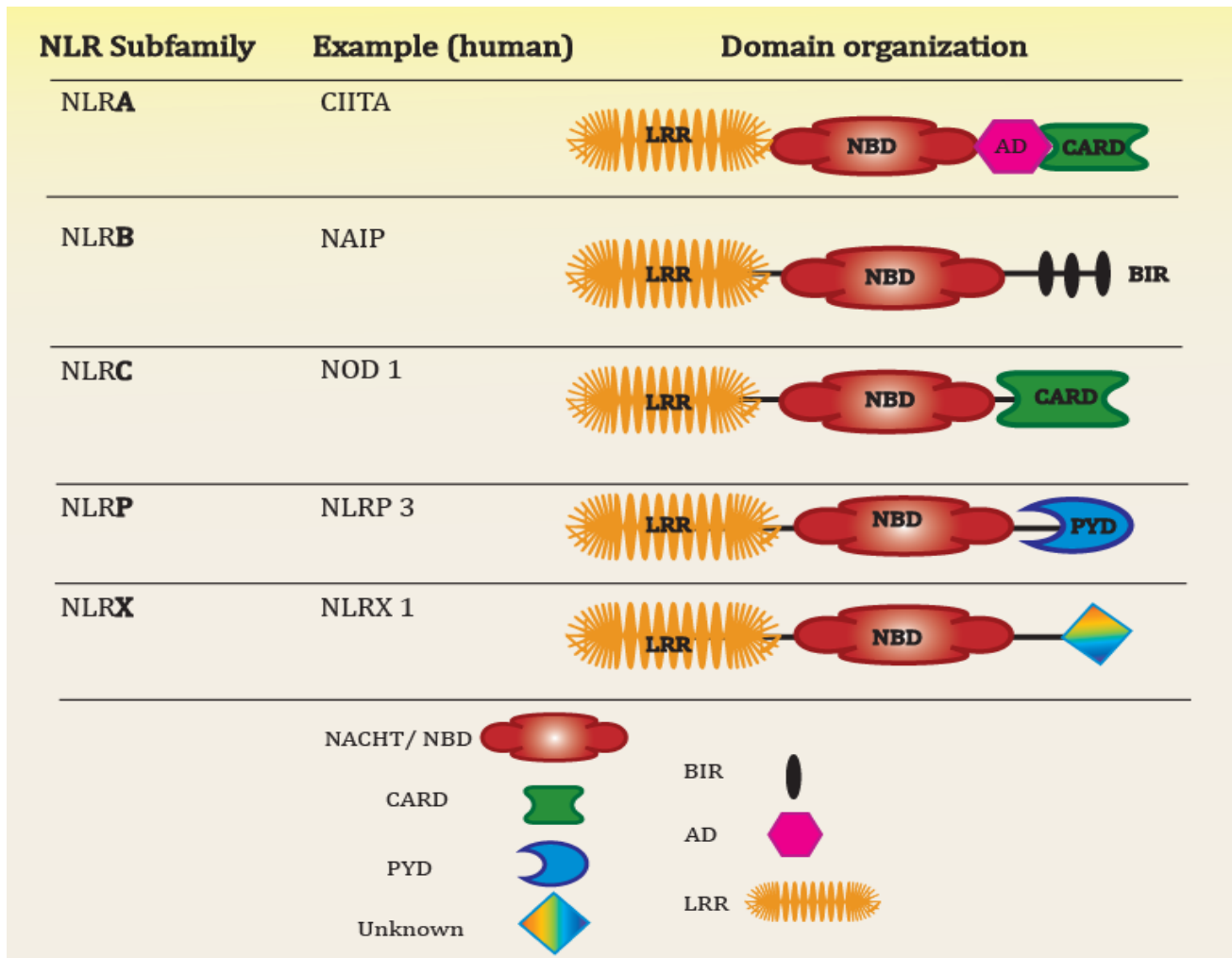


Figure 5: The NLR family and subfamily. Schematic representation of the NLR family members and subfamilies with examples of human NLRs. Abb.: NLR: Nod-like receptor; NBD: Nucleotide-binding domain; LRR: Leucine-rich repeats; CARD: Caspase-activation and recruitment domain; PYD: pyrin domain; AD: acidic transactivator domain; BIR: Baculovirus inhibitory N-terminal domains. Adapted from [53, 56]

1.3.3 The NLRP3 inflammasome: structure, activation and function

The NLRP3 inflammasome or cryopyrin, described for the first time in 2002 by Jürgen Tschopp, is the most studied inflammasome to date [56, 57]. This multi-protein complex serves as a platform for Casp-1 activation and maturation of IL-1 β and IL-18. Both cytokines are part of the IL-1 family, which includes a variety of other cytokines (IL-1 α , IL-1 β , IL-33, IL-18, among others) that play a central role in the inflammatory response. IL-1 β is a potent pyrogenic and inflammatory cytokine mainly produced by blood monocytes, tissue macrophages and DCs. Low concentrations of IL-1 β can cause fever and hypotension, whereby additional proinflammatory cytokines, such as IL-6, are released. Due to its powerful response upon stimuli, nature has developed several mechanisms to regulate its excessive production [58].

Expression: The NLRP3 inflammasome is mainly expressed in spleen myeloid immune cells (neutrophils, macrophages, monocytes, DCs), although it is also present in epithelial cells of the esophagus, oropharynx and urothelial layer of the bladder [59]. Other compartments as bone marrow, blood and liver have shown a predominant expression of NLRP3 in myeloid cells compared to lymphoid cells. Lymph nodes and thymus only poorly express NLRP3 [60]. In most cells, NLRP3 is inducible, showing low expression under homeostatic conditions. Monocytes, for example, express high concentrations of the NLRP3 inflammasome, which is not highly inducible upon stimulation. On the other hand, expression of NLRP3 has been shown to be highly inducible in macrophages, DCs and BMDCs particularly under an inflammatory setting [60, 61].

Structure: The NLRP3 inflammasome has three main components: (1) a sensor protein NLRP3, which recruits upon activation (2) the adaptor protein ASC (adaptor protein apoptosis speck protein with caspase recruitment), also known as PYCARD or CARD5, containing two death-fold domains named PYD and CARD that further bind the “effector” domain of the complex, and (3) the protease Casp-1. Casp-1 auto-activates after binding ASC through the CARD-CARD domains, which leads to pro-IL-1 β and pro-IL-18 cleavage [62].

Function: Inflammasomes are key protagonists of the inflammatory response, not only due to the secretion of the cytokines IL-1 β and IL-18, but also for the instruction of a novel form of cell death: *Pyroptosis*. This name stands for "the falling of fire", which was given due to the high burst of pro-inflammatory signals that result from cells undergoing this type of cell death. Pyroptosis involves membrane disintegration and release of intracellular components into the ECS in a Casp-1-mediated manner, thus representing another type of programmed cell death [63].

Activation: The activation of the NLRP3 inflammasome is mediated by several kinds of molecules, which include PAMPs, e.g. LPS, fungal zymosan, nigericin, and DAMPs such as monosodium urate crystals (MSU), calcium oxalate crystals [64, 65], uromodulin [66], and ATP as shown in Table 5 below. Many of the mechanisms leading to inflammasome activation are still not fully understood. *In vitro* experiments have shown that the activation of NLRP3 inflammasome requires two steps: first, a priming step, in which NLRP3 and pro-IL-1 β are transcribed by induction of the nuclear factor NF- κ B. As pointed above, not all cells express high levels of NLRP3 under resting conditions, which makes this step important for acquiring the needed concentrations of NLRP3. ASC and Casp-1 are constitutively expressed in most cells, and no priming is needed. Ligands like LPS, lead to the activation of the transcription factor NF- κ B through TLR-4-signaling, CpGs and even IL-1 β -mediated IL-1 receptor activation and MyD88 mediated NF- κ B activation are some of the classical priming steps known for NLRP3. The second step will lead to the actual activation of the complex

with oligomerization and ensemble of the three inflammasome components. Several mechanisms have been proposed to date: (1) formation of pore channels in the cell membrane, either by bacterial toxins from the ECS or by increasing extracellular ATP concentration activating P2X₇ channels, which allow potassium (K⁺) efflux, thus lowering the intracellular K⁺ concentration and activating the complex [67]; (2) elevation of intracellular ROS concentrations, related either to the K⁺ efflux or mitochondrial suffering from oxidative stress [68] and (3) phagocytosis of particulate components such as MSU or calcium oxalate crystals, which induce rupture of the lysosomes and thus release cathepsins, consequently activating the inflammasome complex [65]. All these activators suggest an additional function of the NLRP3 inflammasome in sensing cellular homeostasis [69]. Now, how these mechanisms interact with the NLRP3 inflammasome or whether these activation steps (priming and activation) are also required *in vivo*, is still unknown. The mechanisms regulating the assembly and activation of the NLRP3 inflammasome involve conformational changes of the NLR receptor domain, which is “locked” by the LRR-domain, HSP-90 and SGT-1 under resting conditions [56]. Other regulatory proteins including A20, are also involved in the negative regulation of NLRP3 [70]. Figure 6 presents a schematic version of the NLRP3 inflammasome and the postulated priming and activating mechanisms.

Table 5: Ligands involved in inflammasome induction and activation

| Groups | Examples |
|-----------------|--|
| PAMPs | LPS, peptidoglycan Muramyl dipeptide (MDP) [71] Bacterial RNA [72] |
| Bacteria | <i>Neisseria gonorrhoea</i> , <i>Escherichia coli</i> , <i>Listeria monocytogenes</i> [73], <i>Staphylococcus aureus</i> [74] |
| Viruses | Adenovirus, Influenza virus [75], Encephalomyocarditis virus |
| Toxins | A-Toxin (<i>S. aureus</i>), Gramicidin (<i>Bacillus brevis</i>), listeriolysin O Nigericin (<i>Streptomyces hygoscopus</i>) |
| DAMPs | ATP, malarian hemozoin [76], Calciumpyrophosphate dihydrate, calcium phosphate [77], calcium oxalate, monosodium uratecrystals (MSU) [78], cholesterol crystals [79], cystein crystals [80], silica, asbestos, aluminum [81, 82], Uromodulin [66], glycoprotein ASC speck complexes, myoglobin, reactive oxygen species (ROS) |

Adapted from [57, 62]

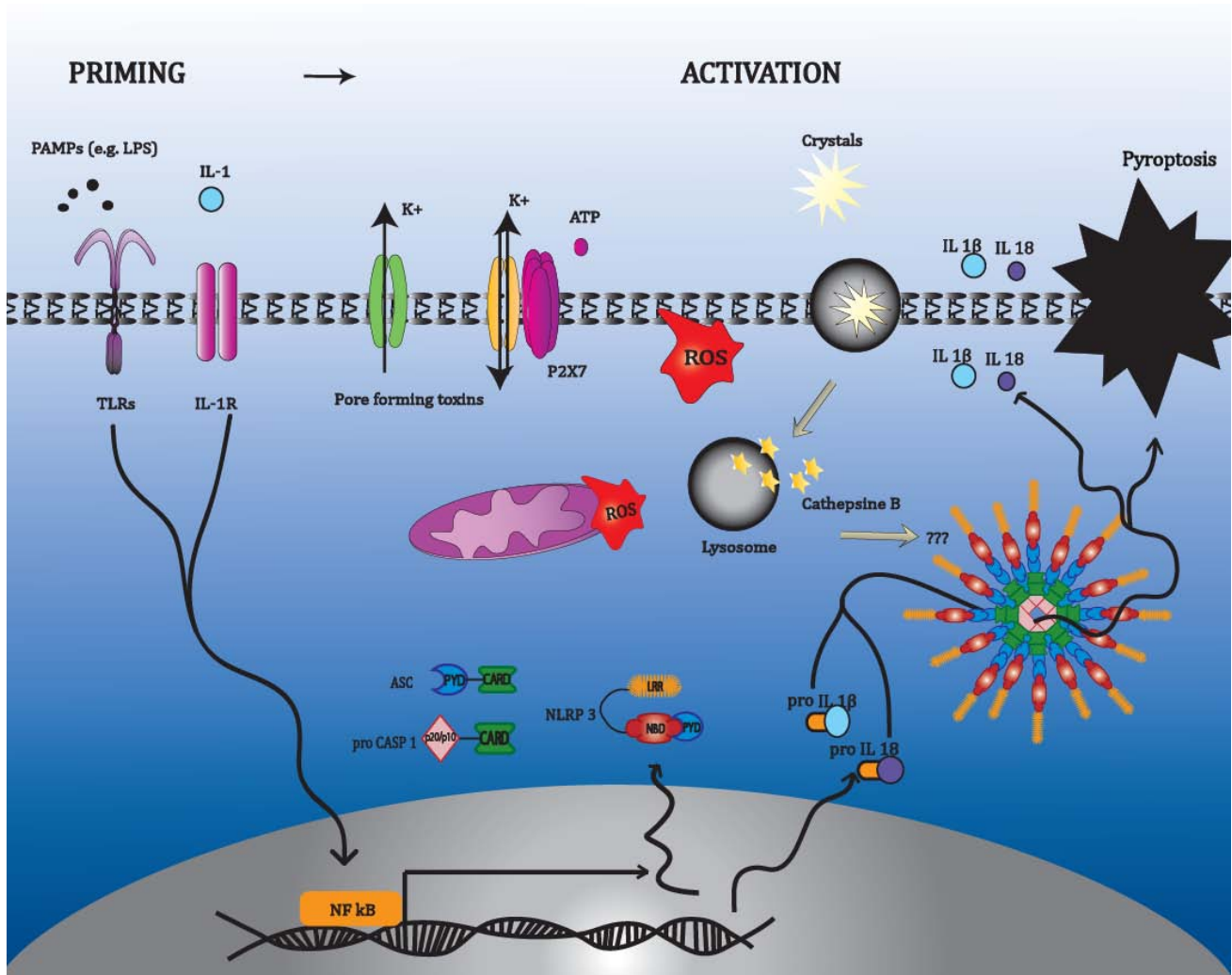


Figure 6: Mechanisms of activation and induction of the NLRP-3 inflammasome. Schematic representation of NLRP3 inflammasome priming and activation. Priming: PAMP or DAMP recognition through TLRs or IL-1R activate NF- κ B induced transcription of NLRP3, pro-IL-1 β and pro-IL-18. Constitutional expression of ASC and pro-Casp-1. Activation: K⁺ efflux through pore-forming toxins, membrane integrity loss or associated to P2X7 receptor activation; cytosolic or mitochondrial ROS production as a result from oxidative stress; crystal induced inflammasome activation through endocytosis and lysosomal rupture with cathepsin B release. The exact ligand-receptor interaction is still unknown. Activated NLRP3 inflammasome cleaves IL-1 β and IL-18 and secretes it out of the cell or activates pyroptosis.

1.3.4 Role of the NLRP3 inflammasome in disease

The NLRP3 inflammasome is pivotal for the inflammatory response. Several human pathologies can be directly associated to the activation of the NLRP3 inflammasome. Mutations in the *Nlrp-3* gene that provoke its persistent activation lead to the auto-inflammatory disease Muckle-Wells syndrome and other CAP associated syndromes (Cryopyrin-associated auto-inflammatory syndromes) [83, 84]. Microbial agents such as bacteria, fungi, viruses and parasites are also known to trigger NLRP3 inflammasome activation *in vivo*. The well-known Influenza A virus has been shown to mediate

innate immunity *in vivo* through NLRP3 activation. This NLRP3-mediated response could result from exposure to specific viral RNA species which was mediated through lysosomal maturation and ROS [75]. Furthermore, viral M2 ion channels lead to potassium efflux and ROS production thus activating the assembling of the protein complex [85]. Also, *Salmonella typhi*, a bacterium known for causing typhoid or enteric fever, which manifests with a sudden onset of fever and diarrhea, activates the NLRP3 inflammasome. Its activation in innate immune cells leads to pyroptosis-mediated cell death, eliminating the bacteria. The importance of this mechanism was observed in *Casp-1*-deficient mice, who severely suffered following infection with this bacterium [86].

Among other potent ligands that activate inflammasomes are particulate compounds, such as exogenous crystals like asbestos and silica, which are endocytosed by pulmonary macrophages, activating the NLRP3 inflammasome and leading to pulmonary disease [87, 88]. Endogenous crystals such as MSU crystal deposits in gout, also activate the NLRP3 inflammasome by endocytosis, inducing an acute inflammatory response in the joints [89, 90]. Several studies have confirmed an association between high levels of IL-1 β in joints of gout patients and crystal-related inflammation [65, 91, 92].

The biomolecular mechanisms of the metabolic syndrome, a disease marked by abdominal obesity, high triglyceride levels, high blood pressure, and type II diabetes mellitus, is also related to activation of the NLRP3 inflammasome [93]. Obesity, for example, has been demonstrated to have an important inflammatory component because large amounts of adipose tissue stimulate NLRP3 in adipocyte-infiltrating macrophages, leading to chronic inflammation [94, 95]. In addition, insulin resistance and later apoptosis of pancreatic β -cells observed in patients with type II diabetes is linked to the activation of NLRP3. Studies have shown that IL-1 β can inhibit insulin signaling and aggravate pancreatic β -cell dysfunction, thus contributing to the mechanisms leading to type II diabetes mellitus [96, 97]. Cholesterol crystals, responsible for atherosclerosis, also activate NLRP3 inflammasomes in macrophages leading to the inflammatory response that is the base of plaque formation in arterial walls and progression of disease [98].

1.4 Mesenchymal healing and fibrosis

The wound healing process concludes with mesenchymal healing. Mesenchymal tissue or connective tissue can be considered as an organ system itself. It is found in all tissues of living organisms (lung, bones and skin), showing different properties in their composition and topology, but keeping the same basic functions and components. Various cells (fibroblasts, adipocytes, and endothelial cells), fibrous proteins (collagens, elastin, fibronectin) and proteoglycans (small leucine-rich proteoglycans –SLRPs-) are the principal components of this organ system. The functions of the ECM involve mainly the physical scaffolding of organs, giving tissues strength, elasticity and protection. Additionally, ECM provides biochemical and biomechanical cues for the morphogenesis of tissues together with its differentiation and extracellular homeostasis [99, 100]. All of this is mediated by several growth factors secreted from surrounding resident cells, which contribute to the dynamic modulation, migration and differentiation of cells [101]. Chronic diseases are characterized by persistent injury of tissues, whereby, mesenchymal healing becomes overshooting, a pathologic process, resulting in the exaggerated ECM deposition and tissue fibrosis. The following section thoroughly describes the main components of mesenchymal tissue and the pathophysiology of fibrosis.

Fibroblasts: Since Virchow's work on the ECM in the 19th century, it is known that fibroblasts are the main producers of ECM in all tissues [102]. They are the lead protagonists of mesenchymal healing, tissue remodeling and fibrosis, and are present in almost every organ of the body. But not all fibroblasts share the same functions. Phenotypical differences within organs or even within one organ itself have been regularly found. In the kidney, one of the fibroblast subpopulations has been shown to produce erythropoietin (EPO), a cytokine hormone that regulates red blood cell homeostasis [103, 104]. Fibroblasts produce fibrous proteins (mostly collagens) in a dynamic manner, maintaining constant tissue and ECM homeostasis and adapting it to the organs' needs. Some organs are under continuous tensional state (prostate, saliva gland), and maintaining tissue homeostasis, especially in these tissues, is key for preventing aberrant fibrosis and tumorigenesis [105]. Additionally, fibroblasts secrete several modulatory cytokines such as transforming growth factor β 1 or (TGF- β 1), connective tissue growth factor (CTGF), both powerful profibrotic cytokines, vascular endothelial growth factor (VEGF a key factor in neo-vascularization and lymphangiogenic processes), matrix metallo proteinases (MMPs) that help rearranging the tissues through degrading ECM components, and tissue inhibiting MMPs or TIMPs, which inhibit MMPs [106-108].

Characterizing fibroblasts has been and still is a very difficult task. No specific markers have been found that would exclusively target fibroblasts. In the kidney, for example, markers such as vimentin, desmin, fibroblast specific protein 1 (FSP-1) and alpha smooth muscle actin (α -SMA, which labels activated fibroblasts or myofibroblasts), are used as markers for mesenchymal cells as are fibroblasts [109]. The origin of these cells has been an intensive subject of discussion. Under normal conditions, parenchymal tissues (liver and kidney) show only a few resident fibroblasts in the interstitial space, which are localized between the tissue epithelia. Upon stimulation, e.g. in tissue injury with concomitant elevated levels of TGF- β , larger quantities of fibroblasts are needed in order to cover the defect. This leads to the differentiation of several endothelial and epithelial cells converting them into fibroblasts. This process is called endothelial to mesenchymal transition (EndMT) and epithelial to mesenchymal transition (EMT) respectively. Recent studies have shown that cells undergoing EMT get arrested in the G2/M phase promoting a phenotype change of the cell [110-112]. This process is characterized by the loss of epithelial markers such as E-cadherin or ZO-1 and the increase of mesenchymal markers such as α -SMA. Other fibroblasts progenitor cells include pericytes, fibrocytes (considered here as circulating precursors of fibroblasts) and bone marrow-derived mesenchymal stem cells. Figure 7 shows a schematic representation of the possible origins of myofibroblasts in the kidney.

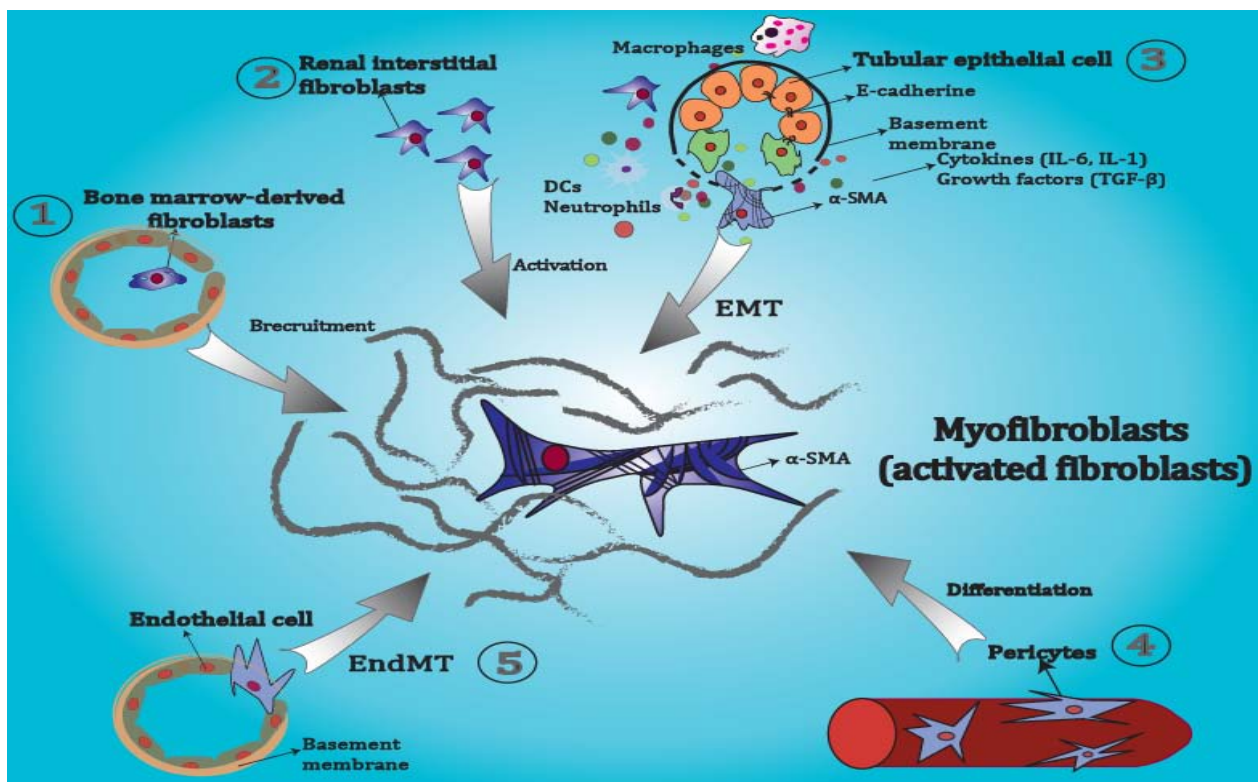


Figure 7: Origin of myofibroblasts (activated fibroblasts) in renal interstitium. Schematic representation of the different myofibroblast origins in the renal interstitium. **1:** Recruitment and activation of bone marrow fibroblasts. **2:** Activation of renal interstitial fibroblasts. **3:** Tubular cells undergo phenotype change, a process called *epithelial to mesenchymal transition* or EMT. **4:** Pericyte differentiation and activation. **5:** Endothelial cell undergo *endothelial to mesenchymal transition* or EndMT.

Fibrosis: Fibrosis is defined as aberrant scarring of tissues during the wound healing process. Under normal conditions, fibroblast proliferation and activation for wound healing purposes are strictly regulated. Many different stimulating agents such as TGF- β and other growth factors including inflammatory cytokines IL-6, *fibroblast growth factors* (FGFs), and IL-13, are key in aberrant scarring processes [113, 114]. ECM's degradation products can also activate macrophages, which in turn secrete more growth factors (GFs), TGF- β , MMPs and other cytokines that will further recruit resident fibroblasts, and promote their migration and proliferation. Collagen I, collagen III, fibronectin, and hyaluronic acid are the main ECM components produced by fibroblasts and represent the hallmark feature of mesenchymal healing [115]. Continuous mechanical stress, tissue injury and interstitial inflammation further enhance migration of bone marrow fibrocytes, together with the promotion of EMT and EndMT, thus recruiting and activating more fibroblasts. Activated fibroblasts or myofibroblasts are defined as highly contractile cells with a high capacity of ECM production and expression of α -SMA [116]. In several pathologic fibrotic processes like in pulmonary fibrosis, liver cirrhosis and renal fibrosis, the presence of high numbers of myofibroblasts has been demonstrated [109, 117]. The rigid collagen deposition and the increasing stiffness of tissue lead to basement membrane disruption, loss of epithelial polarity, as well as cell-cell adhesion, and finally leading to cell death (apoptosis). Compared to an acute injury, where tissue homeostasis restores with no or few fibrotic lesions, chronic injuries such as in diabetic nephropathy, liver cirrhosis or idiopathic pulmonary fibrosis show persistent tissue remodeling, increasing infiltration of myofibroblasts and ECM production, and vascular remodeling that finally result in the aberrant stage of fibrosis. The altered mechanical stability, reduced elasticity and loss of epithelial functional cells (replaced by an acellular scar), deteriorate the organ functionality.

Tubulointerstitial fibrosis is the hallmark of CKD. In contrast to AKI, where the tubular cell regeneration process is left with no fibrotic lesions, chronic injury leads to an irreversible fibrosis and stiffening of the renal tissue. Data has shown that the degree of fibrosis correlates with the impaired excretory function, suggesting fibrosis as an important therapeutic target [22]. The loss of tubular epithelial cells, the rarefication of the peritubular microvasculature and the accumulation of ECM are histopathological features, which contribute to the irreversible progression and worsening of CKD [118, 119]. Unfortunately, no effective anti-fibrotic therapies have been yet developed for clinical use [120]. Figure 8 shows a schematic representation of the development of renal interstitial fibrosis upon chronic kidney injury.

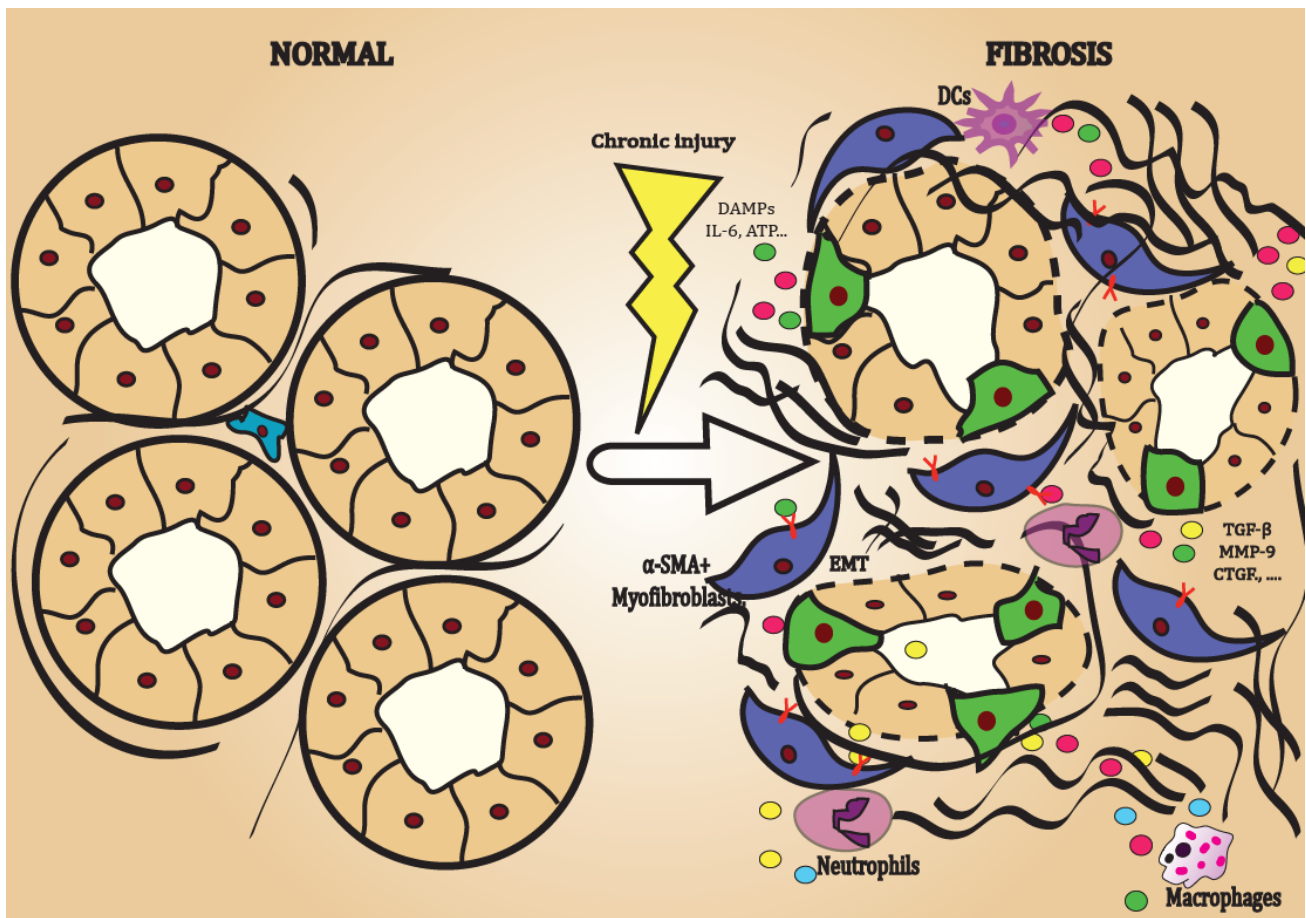


Figure 8: Renal interstitial fibrosis. Schematic representation of the tubular interstitial space and development of fibrosis. Chronic injury leads to tubular cell damage, which releases DAMPs and activates the immune system, releasing further profibrotic cytokines. DAMPs and profibrotic cytokines activate resident fibroblasts into myofibroblasts. Damaged tubular cells and disrupted basement membrane induce EMT. Fibroblast accumulation and activation enhances ECM deposition and fibrosis. Abb: α -SMA: alpha smooth muscle actin, EMT: epithelial to mesenchymal transition, TGF- β : transformig growth factor beta, MMP-9: matrix metalloproteinase 9.

1.4.1 Biomolecular basis of mesenchymal healing and fibrosis: TGF- β signaling

Previously, I have described how fibroblasts and matrix deposition can lead to tissue fibrosis. But what are the molecular mechanisms behind this process? Upon injury, TGF- β and other cytokines are released from innate immune cells including monocytes, macrophages, DCs, and epithelial cells within the wounded tissue. ECM-producing fibroblasts activate and respond immediately to re-establish tissue stability. It is known that TGF- β is the most potent profibrotic cytokine released during wound healing, as found in hypertrophic scars of the skin, which showed very high concentrations of the cytokine [121, 122]. Other cytokines as CTGF, CCN2, ED-A fibronectin also

contribute to this process, compared to IFN γ and prostaglandin E₂ (PGE₂), which normally have a proinflammatory response, but interestingly also an anti-fibrotic function [123, 124].

TGF- β belongs to a family of proteins contributing to diverse functions in the organism including embryonic development, wound healing, tissue homeostasis, chemotaxis and cell cycle control. The TGF- β superfamily is responsible for regulation, differentiation and apoptosis of epithelial and hematopoietic cells. The following cytokines belong to the TGF- β superfamily: **bone marrow stimulating proteins (BMPs)**, known for their influence on cartilage and bone induction; **GFs**, **anti-müller hormones (AMH)** and TGF- β itself (including TGF- β 1, TGF- β 2 and TGF- β 3, being type 1 the most representative). This family is known to inhibit the proliferation of most cells (e.g. inflammatory cells), inducing apoptosis in epithelial cells, and interestingly stimulating the proliferation of mesenchymal cells [125]. These effects of TGF- β have been evaluated several times. An experiment with mice lacking TGF- β 1 showed impaired last-stage wound repair and decreased epithelialization and collagen deposition compared to wild type mice. Deficiency of TGF- β in mice was lethal due to the wasting syndrome, a generalized inflammatory response associated with tissue necrosis, organ failure and death [126].

TGF- β in its inactive form is found constitutively expressed in the ECS. This latent precursor is bound by a disulfide bridge to a protein called **latent TGF- β binding protein (LTBP)**. In this way, TGF- β is incapable of binding to its receptor, thus preventing its uncontrolled activation [127]. Cytokines like MMP-9 [128], TSP-1 (**thrombospondin-1**) [129], integrin α - β and other mediators like ROS and low pH of the ECS, can activate TGF- β through proteolytic cleavage of the TGF- β -LTBP complex. Active TGF- β binds to the transmembrane receptor TGF- β receptor II (T β RII), a serine/threonine kinase that recruits the transmembrane receptor TGF- β receptor I (T β RI), which subsequently leads to R-SMADs (**receptor regulated SMADs**) phosphorylation, specifically SMAD2 and SMAD3 [130-132]. SMADs are homologous proteins of both *Drosophila* MAD proteins (**mothers against decapentaplegic homolog**) and the *Caenorhabditis* protein SMA (**small body size**) [133]. They are a group of globulated proteins with different functions involving the regulation of the TGF- β signaling pathway and gene transcription. SMAD1, SMAD2, SMAD3 and SMAD5 are the main regulators of TGF- β signaling, while SMAD4 is considered a common-mediator SMAD. SMAD6 and SMAD7 have been shown to have an inhibitory role on the SMAD2/3 complex. Phosphorylation of SMAD2 and 3 builds a complex with co-SMAD (SMAD4), subsequently binding with other co-transcriptional factors to regulate gene expression. SMAD1, SMAD5, and SMAD9 are

stimulated by BMP-7, an antifibrotic cytokine [134]. Other signaling pathways also participate in TGF- β signaling, e.g. the RAS/MER/ERK signaling pathway has been shown to influence SMADs in epithelial cells by inhibiting SMAD3, thus diminishing the response to TGF- β 1 [135]. Figure 9 shows a simplified schematic of TGF- β signaling. In spite of the intensive studies regarding TGF- β , contradictory results still emerge among scholars, e.g. one study showed T β RII null mice had more renal interstitial fibrosis and collagen deposition, compared to wild type mice after UUO. The contradictory results of TGF- β rely mostly on its dose dependent activity [136].

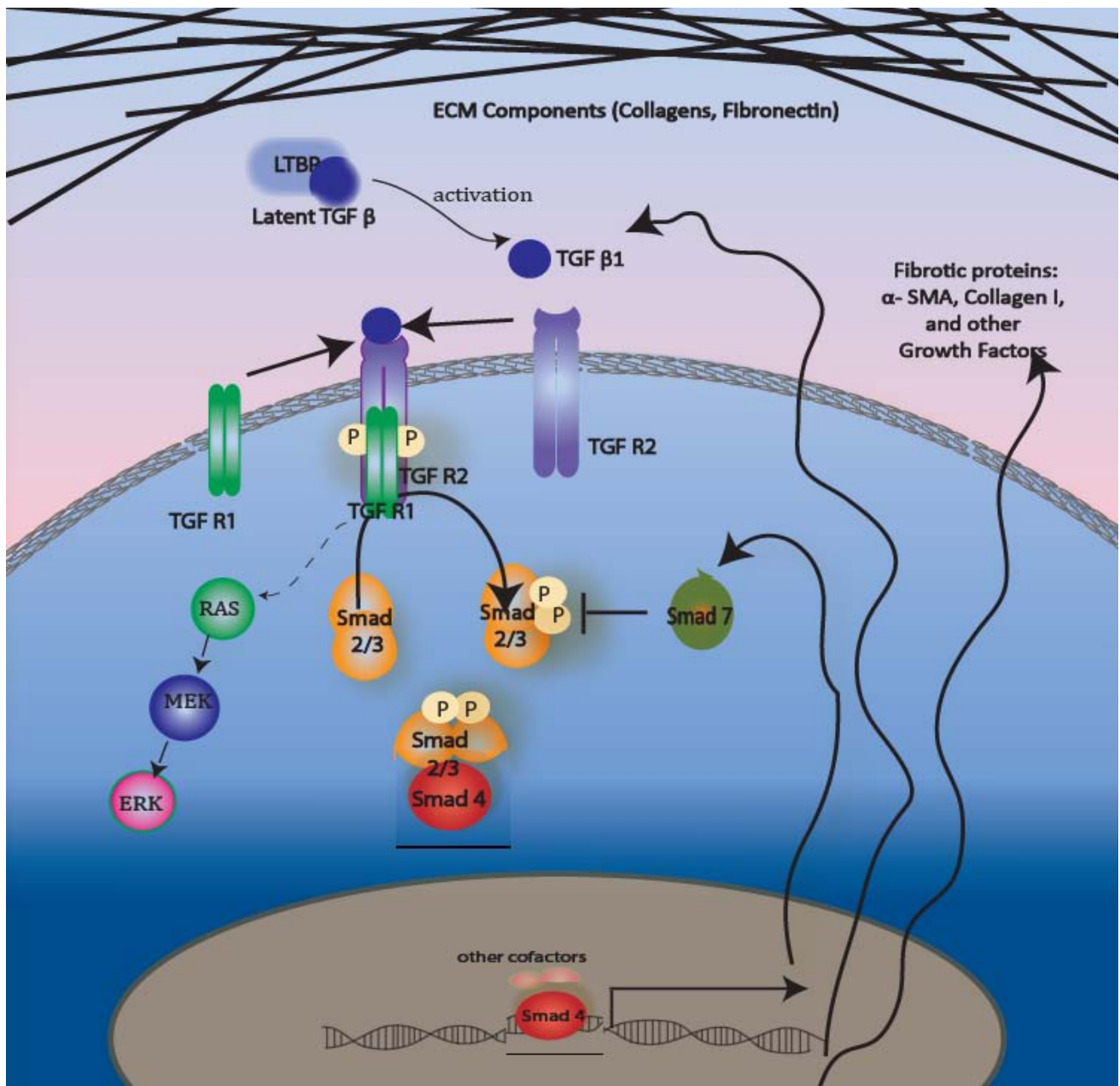


Figure 9: TGF- β 1 signaling pathway. Schematic representation of the TGF- β signaling pathway: Latent TGF- β is constitutively expressed in ECM. After activation, TGF- β is released, binding TGF-R2 who undergoes oligomerization and recruits TGF-R1. The activated receptor phosphorylates Smad2/3 complex, which then binds Smad4. Smad 4 together with other cofactors induces gene transcription of several profibrotic (α SMA, collagen I & -III, fibronectin) and anti-fibrotic genes including Smad7, which inhibits Smad2/3 phosphorylation. TGF-R1 and TGF-R2 complex activation additionally induces RAS/MEK/ERK signaling. Abb.: TGF- β : transforming growth factor β , α SMA: alpha smooth muscle actin.

1.5 The NLRP3 inflammasome in kidney diseases

Most kidney diseases leading to ESRD are glomerular, non-microbial pathologies and result in renal interstitial inflammation, which is the hallmark feature of kidney diseases. PRRs have been demonstrated to contribute significantly to this process. However, evidence about the role of the NLRP3 inflammasome during kidney diseases is limited. Under normal conditions, the human brain, spleen and testis express more NLRP3 than the kidney. Contrary to humans, expression of NLRP3 in mice is significantly higher in the spleen and kidney compared to other organs [137]. In healthy kidneys, the inflammasome components NLRP3 and ASC are highly expressed in resident macrophages, DCs and tubular cells, compared to the glomerular cells [138]. Other studies have suggested inflammasome components NLRP3, ASC and Casp-1 are also expressed in mouse podocytes [139, 140]. Patients with IgA-nephropathy showed increased NLRP3 expression in glomerular cells compared to healthy kidneys, but still significantly less compared to tubular epithelial cells in humans [141]. Nevertheless, the expression of NLRP3 in renal interstitial fibroblasts has not been determined. Studies involving resident fibroblasts from the heart and gingival fibroblast evidenced the expression of NLRP3 [142, 143]. However, not all these cells have proved to have a functional NLRP3 inflammasome with concomitant production of the cytokines IL-1 β and IL-18, as seen in tubular epithelial cells, which express NLRP3 but not the active forms of these cytokines [138]. The next paragraphs describe important findings on the role of the NLRP3 inflammasome in acute and chronic kidney diseases.

1.5.1 Inflammasome in AKI and CKD pathology

Several DAMPs are known to activate the NLRP3 inflammasome. AKI generally presents with acute tubular necrosis releasing DAMPs that worsen the renal injury. Several mouse models of AKI including ischemia reperfusion injury (IRI) with post-ischemic tubular necrosis [144, 145] and toxic (cisplatin-induced) tubular injury [146, 147] have shown increased levels of IL-1 β and IL-18 in kidneys of mice post-AKI. In humans, biopsies of critically ill patients with AKI showed also increased levels of IL-18 [148]. Crystal-induced AKI was also proven to be mediated through the NLRP3 inflammasome. Herein, *Nlrp-3*-, *Asc*-, *Casp-1*- and *IL-1 β* -deficient mice were significantly protected from calcium oxalate-induced AKI, compared to the wild type mice. But the study suggested that these results were mainly due to the diminished inflammatory response, i.e. reduced DCs and macrophages infiltration into the renal interstitium, and not due to renal parenchymal cells that underwent necrosis upon crystal exposure, without IL-1 β production [64]. Moreover, the NLRP3

inflammasome plays a central role in the development of uric acid-induced nephropathy, gout and hyperuricemia-induced progression of diabetic nephropathy [149, 150]. But the interaction between crystals and the receptor itself remain uncertain. It is clear that reduction of the intracellular K^+ concentration is highly associated with crystal-mediated inflammasome activation [143, 188]. MSU crystals trigger the release of Na^+ following phagocytosis, resulting in osmolarity changes within the cell, thus inducing water influx and dilution of the intracellular K^+ concentration [189].

The importance of the NLRP-3 inflammasome has been also shown in CKD animal models. A streptozotocin (STZ)-induced diabetic nephropathy model demonstrated the contribution of NLRP3 in non-myeloid cells of the kidney (such as intra-glomerular endothelial cells and podocytes), with the aggravation of diabetic nephropathy in mice [151]. Other studies using a UUO model showed significant protection from renal injury in purinergic receptor-7 ($P2_{X7}$)-deficient mice compared to wild type mice [151]. In general, the protection observed in CKD models involving reduced inflammasome activity was associated with a reduced inflammatory component in CKD. A direct relationship between the NLRP3 inflammasome and the development of aberrant fibrosis in CKD is still not well defined.

1.5.2 Inflammasome-independent NLRP3 signaling in kidney disease

Muruve et al. suggested that the NLRP3 inflammasome as well as the cytokines IL-1 β and IL-18 contribute to renal injury and progression of CKD in the UUO mouse model [152]. In this study, *Nlrp-3*-deficient mice were significantly protected from renal injury upon UUO and this protection correlated with a diminished Casp-1 activation and reduced maturation of IL-1 β and IL-18 [152]. The next study performed by the same group showed primary tubular epithelial cells (pTECs) following stimulation with TGF- β 1 were unable to release IL-1 β *in vitro* despite the increased expression of NLRP3 [138]. Also, EMT was associated with this process. These results suggested an inflammasome-independent role in TECs during renal fibrogenesis [138]. One possible explanation for this might be an interaction between TGF- β 1 downstream signaling and the inflammasome component NLRP3 in TECs. Additionally, SMAD2 phosphorylation was diminished in *Nlrp-3*-deficient TECs stimulated with TGF- β 1, suggesting that NLRP3 enhances TGF- β 1 signaling, in an inflammasome-independent manner [138].

Furthermore, a study involving *Nlrp-3*-, *Asc*-, *Il-1R*-deficient and *Il-18*-deficient mice with an *lpr/lpr* background (a mild phenotype of spontaneous lupus-like autoimmunity) showed contradictory results [153]. Lack of Il-1R and Il-18 did not affect the phenotype, whereas mice lacking NLRP3 and ASC showed a massive lymphoproliferation and severe lupus nephritis, which was absent in *lpr/lpr*

controls. The increased DC and macrophage activation, as well as elevated expression of proinflammatory mediators and expansion of T- and B-cell subsets in *Nlrp-3*- and *Asc*-deficient mice suggested an immunosuppressive effect of NLRP3 and ASC [153]. This highlights a possible role for NLRP3 and ASC in TGF- β 1 signaling. Further experiments corroborated these results showing a significant suppression of TGF- β 1 target genes and SMAD2 phosphorylation in both mutant mouse strains, suggesting an important role of NLRP3 and ASC in SMAD2 phosphorylation and thus TGF- β 1 signaling.

1.6 Mouse models of CKD

Several mouse models have been established for studying CKD. Generally, *in vivo* models are advantageous as they allow an accurate approach as they mimic the different disease mechanisms and pathophysiology, enable the focused study of genetic implications and give the investigator liberty for experimental planning and design. However, *in vivo* models in rodents and other species do not reflect with precision the human disease and its consequences, mostly due to the marked genetic differences between species. In this study, we focused on a CKD model, which would specifically replicate the tubulointerstitial fibrosis and which would closely mimic the human disease complications. The preferred models for our target were the UUO and the oxalate-induced nephropathy model. Table 6 summarizes the most frequently used mouse CKD models based on the underlying pathology [154].

Table 6: Mouse models of CKD, classified by pathology

| Pathology | Model | Mechanism |
|-----------------------|---------------------------------------|----------------------------------|
| Glomerulonephritis | Lupus nephritis | Immune complex GN |
| | Anti-GBM-nephritis | Autoimmune-mediated GN |
| Glomerulosclerosis | Aging | Spontaneous podocyte loss |
| | PAN/adriamycin nephropathies | Toxic podocyte loss |
| | 5/6 nephrectomy | Surgical nephron reduction |
| Interstitial fibrosis | Unilateral ureteral obstruction (UUO) | Obstructive nephropathy |
| | Oxalate nephropathy | Crystal and direct tubular toxin |
| | AAN (aristocholeic acid nephropathy) | Toxic nephron loss |
| | Cyclosporin A nephropathy | Vasoconstriction and ischemia |

Adapted from Yang, H.C., et al.[154] Abb.: GS: glomerulosclerosis, GN: glomerulonephritis, GBM: glomerular basement membrane; PAN: puromycin aminonucleoside; UUO: unilateral ureteral obstruction.

Unilateral Ureteral Obstruction model: Obstructive nephropathy is a common cause of acute or chronic kidney diseases. It leads to urine stasis and elevation of the pressure in the urinary tract. Causes of urinary tract obstruction may be congenital or acquired due to intrinsic or extrinsic factors. One common cause of urinary tract obstruction in children is the vesicoureteral reflux, mostly found in infants due to misplacement of the ureter in the bladder. Patients with unilateral vesicoureteral reflux manifest repeated urinary tract infections but no functional impairment. On the contrary, bilateral vesicoureteral reflux may lead to ESRD if not treated [155]. Acquired defects are very common in adults, mostly as a result of kidney stones, infections and trauma, tumors of the urinary tract and side-tissues or retroperitoneal fibrosis.

The increased hydrostatic pressure upon the collecting duct system and subsequent elevated tubular pressure leads to tubular dilation and dysfunction. When the elevated hydrostatic pressure reaches the glomerular space, GFR declines until ceasing completely. Additionally, tubular malfunction leads to natriuresis and polyuria. Increased PGE₂, ANP and particularly angiotensin II aggravate this scenario by inducing more profibrotic cytokines. Meanwhile, the renal interstitium becomes edematous and infiltrated with mononuclear inflammatory cells, which upon progression activate interstitial fibroblasts, increasing ECM production resulting in tubulointerstitial fibrosis and atrophy of the papilla, medulla and cortex [3, 156]. Azotemia and other consequences of CKD do not develop upon unilateral obstruction; these patients may present with hypertension, usually a consequence of RAAS over-activation by the obstructed kidney.

Urinary tract obstruction induced by ligating one of the mouse ureters (Figure 10) results in tubulointerstitial inflammation and fibrosis. The rapid disease development, simple and economic surgical requirements make it an optimal model for studying renal interstitial fibrosis, which explains why it is so widely used in the scientific community [157]. Unfortunately, this model does not mirror human CKD because it does not show alterations of kidney function parameters in blood and urine with the systemic consequences of the disease.

Chronic oxalate nephropathy model: Oxalate is a metabolic end product in humans. Normally, 40 to 50 mg of oxalate are excreted in the urine every day. Elevated levels of urine oxalate lead to super-saturation and production of intrarenal crystals and kidney stones [158]. Three main causes of oxalate-induced kidney injury in humans are known: (1) primary hyperoxaluria (type 1 and type 2), a rare autosomal recessive disease that presents already in childhood with recurrent formation of calcium oxalate stones and when not discovered can quickly lead to ESRD; (2) dietary hyperoxaluria, which represents the most frequent form of hyperoxaluria in humans; and (3) enteric

hyperoxaluria, as a result of the fatty acid malabsorption due to e.g. bariatric surgery, and Chron's disease involving small intestines or pancreatic insufficiency. Under normal conditions, insoluble calcium oxalate is excreted with the stool. Decreased absorption of fatty acids from the intestinal lumen sequesters calcium. This stops binding of oxalate to calcium and therefore, increases its solubility and intestinal absorption [159]. Furthermore, acute oxalosis due to ethylene glycol poisoning can induce AKI as a consequence of the widespread intrarenal crystal deposition [160].

Unlike many other crystal nephropathies which involve localized crystallization in the renal pelvis (kidney stone formation) or in the collecting duct system and renal medulla like MSU crystals, calcium oxalate (in mice) and cysteine (in humans) crystallization can be found diffusely in the renal interstitium and inside the tubular lumen, affecting the whole kidney parenchyma [161]. Urine, with its high osmolarity and pH variations, boosts crystallization of the filtered oxalate. Different mechanisms for the tubular cell injury have been proposed: (1) the activation of the immune system upon crystals inducing the infiltration of inflammatory cells and production of proinflammatory cytokines and chemokines and the concomitant obstruction of the tubules pose as an indirect mechanism for tubular cell injury. (2) Crystals are cytotoxic and induce upon direct contact oxidative stress and tubular cell death, which will, in turn, activate the immune system and enhance renal inflammation. The continuous renal inflammation and tubular damage lead to tubular atrophy and activation of resident fibroblasts, promoting ECM production and renal interstitial fibrosis [161, 162].

Two models of hyperoxaluria have been developed in mice: an acute and a chronic model. In the acute model, hyperoxaluria is induced by intraperitoneal injection of 100 mg/kg sodium-oxalate and 3% sodium-oxalate in drinking water, leading to a marked kidney injury within 24 hours [64, 163]. In order to imitate hyperoxaluria-induced CKD in humans, mice were fed a high oxalate diet prepared by adding high-soluble sodium-oxalate to a virtually calcium-free diet for up to 14 days. Blood and urine were analyzed throughout the experiment and kidneys harvested after sacrifice.

Indeed, a recent study by *Knauf et al.* observed that a high oxalate and calcium-free diet in C57BL/6 mice resulted in elevated serum and urine oxalate concentrations, increased intrarenal crystal deposition and severe damage of the tubular cell architecture, leading to renal inflammation and interstitial fibrosis, and thus mimicking CKD [164].

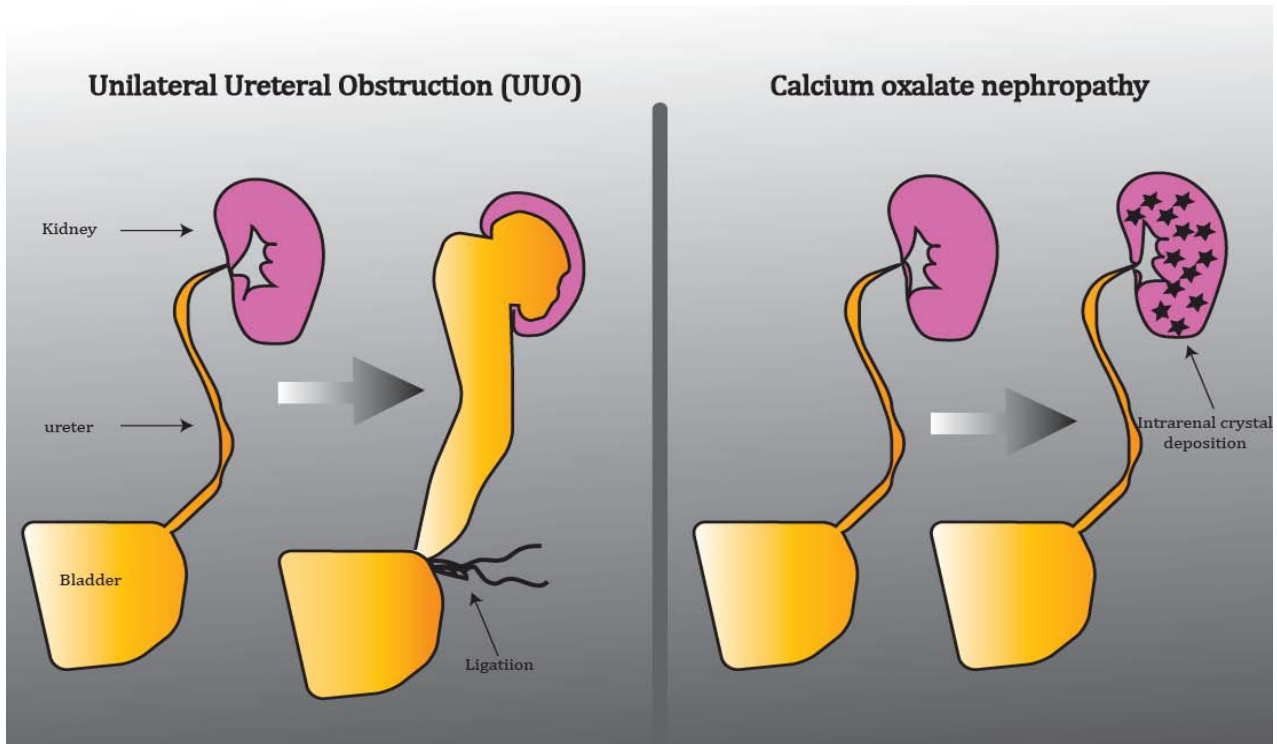


Figure 10: Implemented mouse models of CKD. Schematic anatomical representation of the applied mouse models of CKD. Left: Unilateral ureteral obstruction displays ligation of the ureter with urine stasis in distal, proximal ureter and renal pelvis. Right: High soluble oxalate diet results in diffused crystal deposition in the kidney parenchyma.

1.7 Hypothesis

Based on the published literature, we hypothesized that the inflammasome component NLRP3 drives renal fibrogenesis in CKD by augmenting TGF- β receptor signaling and not only via Casp-1-mediated IL-1 β release.

Accordingly, the objectives of this study were:

1. Assessment of the NLRP3 inflammasome-dependent and -independent signaling during UUO.
2. Assessment of the NLRP3 inflammasome-dependent and -independent signaling during hyperoxaluria-induced nephrocalcinosis and CKD.
3. Assessment of the NLRP3 inflammasome-dependent and -independent signaling in murine fibroblasts and the influence on their proliferation and their capacity to produce ECM.

2. Materials and Methods

2.1 Materials

Table 7: Instruments and Devices

| Instrument | Designation | Manufacturer |
|------------------------------------|--|--------------------------------------|
| Balance | Analytic balance BP 110 S | Sartorius, Göttingen, DE |
| | Mettler PJ 3000 | Mettler-Toledo, Greifensee, CH |
| Centrifuges | Centrifuge 5415 C | Eppendorf, Hamburg, DE |
| | Centrifuge 5418 C | Eppendorf, Hamburg, DE |
| | Heraeus, Minifuge T | VWR Internation, Darmstadt, DE |
| | Heraeus, Sepatech Biofugue A | Heraeus Sepatech, Osterode, DE |
| | Universal 16 | Hettich, Bäch, CH |
| Microscopes | Light microscope Leitz DM II | Leica Microsystems, Solms, DE |
| | Libra 120 | Carl-Zeiss AG, Oberkochen, DE |
| | CCD-Camera | Tröndle, Moorenweis, DE |
| | Light microscope Zeiss | Carl-Zeiss AG, Oberkochen, DE |
| | AxioPlan 2 | Carl-Zeiss AG, Oberkochen, DE |
| | Axiocam HR | Carl-Zeiss AG, Oberkochen, DE |
| Microscope imaging | Cell P software | Olympus, Hamburg, DE |
| Fluorescence microscope | Leica DC 300 F | Leica Microsystems, Cambridge, UK |
| | Olympus BX50 | Olympus Microscopy, Hamburg, DE |
| Cell Culture | | |
| Cell incubator | Heracell Type B5060 EC-CO2 | Heraeus Sepatech, Osterode, DE |
| Cell counting chamber | Neubauer cell counting chamber | Roth, Karlsruhe, DE |
| Workbench | Sterile card hood class II, type A/B3 | The Baker Company, Stanford, ME, USA |
| UV-light | | Bachofer, Reutlingen, DE |
| ELISA | | |
| ELISA reader | Tecan, GENios Plus | Tecan, Crailsheim, DE |
| ELISA plate washer | Microplate washer ELx50 | Biotek, Bad Friedrichshall, DE |
| Real-Time PCR | | |
| Nano drop | Spectrophotometer | PEQLAB Biotech., Erlangen, DE |
| Light Cycler 480 | Real-time PCR system | Roche, Basel, CH |
| Light Cycler 480 | Multiwell-plate 96 | Roche, Basel, CH |
| Western Blot | | |
| Gel electrophoresis chamber | Gel electrophoresis chamber | PeqLab Biotech., Erlangen, DE |
| X-ray developer | X-ray developer machine | AGFA, Köln, DE |
| Blotting System | Semi-dry blotting system | BioRad, München, DE |
| SDS-gel electrophoresis chamber | Mini VE, vertical electrophoresis system | Amersham Bioscience, Glattbrugg, CH |
| Voltage source SDS-electrophoresis | Power PAC 3000 | BioRad, München, DE |

| Instrument | Designation | Manufacturer |
|----------------------|--|---|
| Other Devices | | |
| Tissue homogenizer | Ultra Turrax T 25 | IKA GmbH, Staufen, DE |
| Microtome | Microtome HM 340 E | Microm, Heidelberg, DE |
| Cryomicrotome | Cryostat RM 2155 | Leica Microsystems, Bensheim, DE |
| | Cryostat CM 3000 | Leica Microsystems, Bensheim, DE |
| pH meter | pH meter WTW | WTW GmbH, Weilheim, DE |
| Thermomixer | Thermomixer 5436 | Eppendorf AG, Hamburg, DE |
| | Thermocycler UNO II | Biometra, Göttingen, DE |
| Vortex mixer | Vortex Genie 2tm | Bender & Hobein, Zürich, CH |
| Workbench | Sterile workbench Microflow, biological safety cabinet class II | Nunc GmbH, Wiesbaden, DE |
| Rotary mixer | Heavy duty rotator | Bachofer Laboratoriumsgeräte, Reutlingen, DE |
| Roller mixer | Stuart roller mixer SRT6d | Bibby Scientific, Stone, UK |
| Water bath | Water bath HI 1210 | Leica Microsystems, Bensheim, DE |
| Pipette Aids | | |
| Manual dispenser | Multipipette Plus | Eppendorf AG, Hamburg, DE |
| Manual pipette aid | Research Plus 30 – 300 µl | Eppendorf AG, Hamburg, DE |
| | Pipetman 2, 10, 20, 100, 200, 1000 µl | Gilson, Middleton, WI, US |
| | Pipetus classic | Hirschmann Laborgeräte, Eberstadt, DE |

Table 8: Disposable instruments

| Instrument | Designation | Manufacturer |
|------------------------|--|---|
| Eppendorf tubes | 1.5, 2, 15, 50 ml | TPP Trasadingen, CH |
| Falcon tubes | 15, 50 ml | BD, Heidelberg, DE |
| Serological pipettes | 5, 10, 25 ml | BD Heidelberg, DE |
| Pipettes | Pipettes Pipetman | Gilson, Middleton, WI, USA |
| Pipette tips | 1-1000 µl type Gilson Pipette tips ep T.I.P.S | Peske, Aindling-Arnhofen, DE Eppendorf AG, Hamburg, DE |
| Embedding cassettes | Embedding cassettes “Biopsy” | ISOLAB, Wertheim, DE |
| X-ray films | BioMax XAR Film Kodak | Sigma Aldrich, Deisenhofen |
| Syringes | Diskardit II 1 ml, 2 ml, 5 ml | BD, Fraga, ES |
| Tweezers | Sterile tweezers | Angiokard Medizintechnik GmbH & Co. KG, Freiburg, DE |
| Pre-separation filters | MACS pre-separation filter 100 µm Cell strainer 70 µm | Miltenyi Biotec, Bergisch Gladbach, DE BD Falcon, Franklin Lakes, US |
| Filter systems | Vacuum filtration system 150 ml, 500 ml | TPP; Trasadingen, CH |
| Filter paper | Whatman paper | Sigma Aldrich, Deisenhofen, DE |
| Cell culture plates | 6-, 12-, 96-well plate | TPP, Trasadingen, CH |
| ELISA 96-well plate | NUNC Immuno-plate F96, Maxisorp | Thermo Scientific, Waltham, US |
| Cell scraper | Cell scraper 24 cm | TPP, Trasadingen, CH |
| Western blot membrane | Immobilon P transfer membrane 0,45 µm pore size | Miltenyi Biotec, Bergisch Gladbach, DE |
| Needles | Needles | BD, Drogheda, IE |
| Microscope slides | Super frost r Plus | Menzel-Gläser, Braunschweig, DE |
| Tissue culture dishes | Ø100 mm, Ø150 mm | TPP, Trasadingen, CH |
| Ultra-cut | | Leica Microsysteme, Wetzlar, DE |

Table 9: Chemicals, kits, reagents and solutions

| Product | Designation | Manufacturer |
|---------------------------|---|--|
| Cell Culture | | |
| Antibiotics | Penicillin-streptomycin | PAA Laboratories, Pasching, AT |
| Fetal bovine serum (FBS) | Fetal bovine serum | Biochrom KG, Berlin, DE |
| Cell detachment | Trypsin/EDTA (1x) | PAA Laboratories GmbH, Cölbe, DE |
| Cell buffer & media | Dulbecco's phosphate buffered saline 1x (PBS) | PAA Laboratories GmbH, Cölbe, DE |
| | Dulbecco's modified eagle medium (DMEM) | Biochrom KG, Berlin, DE |
| Cell freezing | Dimethyl sulfoxide (DMSO) | Merck, Darmstadt, DE |
| MTT Assay | | |
| Cell proliferation assay | Cell titer 96 A Queous | Promega GmbH, Mannheim, DE |
| Real-Time PCR | | |
| RNA isolation kit | Ambion Pure Link RNA Mini Kit | Life technologies, GmbH, Darmstadt, DE |
| Reverse transcription | Acrylamide | Ambion, Darmstadt, DE |
| | Hexanucleotide | Roche, Mannheim, DE |
| | dNTPs (25 mM) | GE Healthcare, München, DE |
| | RNAsin | Promega, Mannheim, DE |
| | DTT (0,1 M) | Invitrogen, Karlsruhe, DE |
| | Strand buffer (5x) | Invitrogen, Karlsruhe, DE |
| | Superscript II | Invitrogen, Karlsruhe, DE |
| | RNase free spray | Gene Choice, Frederick, US |
| | SYBR Green dye | Applied Biosystems, Norwalk, US |
| | Taq DNA Polymerase | New England Biolabs, Ipswich, US |
| | PE buffer (10x) | Finnzymes, Espoo, FIN |
| dNTPs (1,25mM) | Metabion, Martinsried, DE | |
| MgCl ₂ (25 mM) | Fermentas, St.LeonRot, DE | |
| ELISA | | |
| ELISA kit | OptEIA mouse IL-1 β kit | Bd; Franklin Lakes, US |
| ELISA coating | Poly-L-Lysine | Cultrex, Trevigen, Gaithersburg, US |
| ELISA signal detection | OptEIA | BD, Fraga, ES |

Abb: dNTPs: nucleosid triphosphate, RNAsin: ribonuclease inhibitor, DTT: dithiothreitol, RNase: ribonuclease, MgCl: magnesium chloride, DMEM: Dulbecco's modified eagle medium, DMSO: Dimethyl sulfoxide, PBS: Dubelcco's phosphate buffered saline, EDTA: Ethylenediaminetetraacetic acid, ELISA: enzyme-linked immunosorbent assay

| | | |
|------------------------------|---|---------------------------------------|
| Western blot | | |
| RIPA buffer | Radio immunoprecipitation assay buffer | Sigma-Aldrich, St.Louis, USA |
| Protease inhibitor | Complete protease inhibitor tablets | Roche, Mannheim, DE |
| Tris | Trisaminomethane | Rot, Karlsruhe, DE |
| Blocking solution | Skin milk powder | Merck, Darmstadt, DE |
| SDS | Sodium dodecyl sulfate | BioRad, München, DE |
| Tween 20 | Polysorbate 20 | Sigma-Aldrich, Steinheim, DE |
| APS | 10% ammonium persulfate | BioRad, München, DE |
| Acrylamide | 30% acrylamide | Carl Roth GmbH, Karlsruhe, DE |
| Protein assay | Bio-Rad protein assay | BioRAD, München, DE |
| Blocking solution | | Roche, Mannheim, DE |
| Bromophenol blue | | Merck, Darmstadt, DE |
| TEMED | Tetramethylethylenediamine | BioRad, München, DE |
| Marker (proteins) | Lane marker non-reducing sample buffer (5x) | Thermo Scientific, Rockford, US |
| Miscellaneous | | |
| Acetone | | Merck, Darmstadt, DE |
| Lysis buffer | Ammonium chloride | Merck, Darmstadt, DE |
| EDTA | Ethylenediaminetetraacetic | Calbiochem, San Diego, US |
| Eosin | | Sigma, Deisenhofen, DE |
| Ethanol | | Merck, Darmstadt, DE |
| Formalin | | Merck, Darmstadt, DE |
| Hydroxyethyl cellulose | | Sigma-Aldrich, Steinheim, DE |
| Hydrogen chloride | | Merck, Darmstadt, DE |
| Isopropanol | | Merck, Darmstadt, DE |
| Calcium chloride | | Merck, Darmstadt, DE |
| Calcium dihydrogen phosphate | | Merck, Darmstadt, DE |
| Calcium hydroxide | | Merck, Darmstadt, DE |
| β -mercaptoethanol | | Roth, Karlsruhe, DE |
| Sodium acetate | | Merck, Darmstadt, DE |
| Sodium chloride | | Merck, Darmstadt, DE |
| Sodium citrate | | Merck, Darmstadt, DE |
| Triton X | Tetramethylbutylphenyl-polyethylene glycol | Fluka, Chemie AG, Buchs, CH |
| Tissue fixation | Solution of formaldehyde 18% | Thermo Fisher Scientific, Waltham, US |
| Tissue mobilization | RNA later | Qiagen GmbH, Hilden, DE |

Abb: EDTA: Ethylenediaminetetraacetic acid, RNA: ribonucleic acid

Table 10: Buffers

| Experiment | Buffer | Composition |
|---------------------|-----------------------------|--|
| ELISA | | |
| | Sodium bicarbonate (0,05 M) | 2.1g NaHCO 2.645g Na ₂ CO ₃ in 500 ml H ₂ O |
| | PBS (10x) | 80.0 g NaCl 11.6 g Na ₂ HPO ₄ 2.0 g KH ₂ PO ₄ 2.0 g KCl in 1 L H ₂ O (ph:7.0) |
| | Tris NaCl (10x) | Tris: 60.57 g NaCl: 81.8 g all in 1 L H ₂ O (pH:7.0) |
| | Sulfuric acid | H ₂ SO ₄ |
| Western blot | | |
| | TBS | 50 mM tris 150 mM NaCl (pH 7.6) |
| | TBS-T Running buffer | 0.1% Tween-20 in TBS 3 g tris 14.4 g glycine 0.5 g SDS In 1000 ml dd H ₂ O (pH 8.3) |
| | Transfer buffer | 1.5 g tris 7.2 g glycine in 500 ml dd H ₂ O |
| | Separating buffer | 18.2 g tris (1.5 mM) 0.4 g SDS In 1000 ml dd H ₂ O (pH: 8.8) |
| | Collecting buffer | 6.05 g tris (0.5 mM) 0.4 g SDS in 100 ml dd H ₂ O (pH 6.8) |

Abb: Tris (hydroxyethyl) aminomethane and sodium chloride , TBS: Tris-buffered saline , TBS-T: Tris-buffered saline plus Tween-20 ,SDS: Sodium dodecyl sulfate ,ddH₂O: distilled water, PBS: Phosphate buffered saline.

Table 11: PCR Primer sequences

| Gene | Forward | Reverse |
|--------------------------------|--------------------------------|-------------------------------|
| <i>18 S</i> | 5'-GCAATTATTCCCATGAACG-3' | 5'-AGGGCCTCACTAAACCATCC-3' |
| <i>Acta 2</i> | 5'-ACTGGGACGACATGGAAAAG-3' | 5'-GTTCAAGTGGTGCCTCTGTCA-3' |
| <i>Asc</i> | 5'-GAGCAGCTGCAAACGACTAA-3' | 5'-GCTGGTCCACAAAGTGTCT-3' |
| <i>Casp1</i> | 5'-TCAGCTCCATCAGCTGAAAC-3' | 5'-TGGAAATGTGCCATCTTCTTT-3' |
| <i>Ccl2</i> | 5'-CCTGCTGTTACAGTTGCC-3' | 5'-ATTGGGATCATCTTGCTGGT-3' |
| <i>Col 1a1</i> | 5'-ACATGTTTCAGCTTTGTGGACC-3' | 5'-TAGGCCATTGTGTATGCAGC-3' |
| <i>Col 4a1</i> | 5'-GTCTGGCTTCTGCTGCTCTT-3' | CACATTTTCCACAGCCAGAG-3' |
| <i>Ctgf</i> | 5'-AGCTGACCTGGAGGAAAACA-3' | 5'-CCGCAGAACTTAGCCCTGTA-3' |
| <i>Cxcl 2</i> | 5'-CGGTCAAAAAGTTTGCCTTG-3' | 5'-TCCAGGTCAGTTAGCCTTGC-3' |
| <i>E-cadh</i> | 5'-GAGGTCTACACCTTCCCGGT-3' | 5'-CCACTTTGAATCGGGAGTCT-3' |
| <i>Fib1</i> | 5'-GGAGTGGCACTGTCAACCTC-3' | 5'-ACTGGATGGGGTGGGAAT-3' |
| <i>Fsp1</i> | 5'-CAGCACTTCCTCTCTTGG-3' | 5'-TTTGTGGAAGGTGGACACAA-3' |
| <i>α-Gst</i> | 5'-CAATGGCCGGGAAGCCCGTG-3' | 5'-CTTCAAACCTCCACCCCTGCTGC-3' |
| <i>Il-1β</i> | 5'-TTCCTTGTGCAAGTGTCTGAAG-3' | 5'-CACTGTCAAAGGTGGCATT-3' |
| <i>Il-18</i> | 5'-CCAAATCAGTTCCTCTTGGC-3' | 5'-GGCCAAAGTTGTCTGATTCC-3' |
| <i>Il-1r</i> | 5'-TGAGGAGGCAGTTTTTCGTTT-3' | 5'-GAGCCCCAGTAGCAGTTCA-3' |
| <i>Il-6</i> | 5'-TGATGCACTTGCAGAAAACA-3' | 5'-ACCAGAGGAAATTTCAATAGGC-3' |
| <i>Kim-1</i> | 5'-TGGTTGCCTTCCGTGTCTCT-3' | 5'-TCAGCTCGGGAATGCACAA-3' |
| <i>Lfabp</i> | 5'-AGGCAATAGGTCTGCCCCGAGGAC-3' | 5'-CCAGTTCGCACTCCTCCCCCA-3' |
| <i>Mmp9</i> | 5'-TTGACAGCGACAAGAAGTGG-3' | 5'-GCCATTCACGTCGTCTTAT-3' |
| <i>Nlrp-3</i> | 5'-AGAAGAGACCACGGCAGAAG-3' | 5'-CCTTGGACCAGGTTCAAGTGT-3' |
| <i>Pdgf</i> | 5'-ATGCAACGGCTCGTTTTAGTC-3' | 5'-CGGAGTCGCAAAGTGTCC-3' |
| <i>Smad 2</i> | 5'-ATGTCGTCCATCTTGCCATTC-3' | 5'-AACCGTCCTGTTTTCTTTAGCTT-3' |
| <i>Smad 3</i> | 5'-AGGGGCTCCCTCACGTTATC-3' | 5'-CATGGCCCGTAATTCATGGTG-3' |
| <i>Smad 4</i> | 5'-ACACCAACAAGTAACGATGCC-3' | 5'-GCAAAGGTTTCACTTTCCCCA-3' |
| <i>Tgfβ1</i> | 5'-GGAGAGCCCTGGATAACCAAC-3' | 5'-CAACCCAGGTCCTTCCTAAA-3' |
| <i>Tgfr1</i> | 5'-GCTCCTCATCGTGTGGTG-3' | 5'-CAGTGACTGAGACAAAGCAAAGA-3' |
| <i>Tgfr2</i> | 5'-AGTCGGATGTGGAAATGGAA-3' | 5'-ACAGCTGTGGAAGCTTGACC-3' |
| <i>Vegf</i> | 5'-GTACCTCCACCATGCCAAGT-3' | 5'-TCGCTGGTAGACATCCATGA-3' |
| <i>Vimentin</i> | 5'-AGAGAGAGGAAGCCGAAAGC-3' | 5'-TCCACTTTCGTTCAAGGTC-3' |

Table 12: Antibodies for immunofluorescence, immunohistology and western blotting

| Method | Name | Manufacturer |
|---------------------------|---|--|
| Immunohistology | CD3+ | Serotec, Oxford, UK |
| | Collagen 1 | Cell Signaling, Danvers, MA, USA |
| | F4/80 | Serotec, Oxford, UK |
| | α -SMA | Cell Signaling, Danvers, MA, USA |
| | Anti-mouse IgG | Caltag Laboratories, Burlingame, CA, USA |
| Immunofluorescence | Anti-mouse α -SMA | Dako GmbH, Hamburg, DE |
| Western blot | HRP-linked anti-rabbit secondary antibody | Cell Signaling, Danvers, MA, USA |
| | HRP-linked anti-mouse secondary antibody | Cell Signaling, Danvers, MA, USA |
| | β -actin antibody | Cell Signaling, Danvers, MA, A |
| | NLRP3 antibody | Cell Signaling, Danvers, MA, USA |
| | Smad 2/3 antibody | Cell Signaling, Danvers, MA, USA |
| | Phospho-smad2 (Ser 465/467) | Cell Signaling, Danvers, MA, USA |

Abb.: CD: Cluster of differentiation, α -SMA: alpha smooth muscle actin, HRP: horseradish peroxidase, IgG: immunoglobulin G, NLRP-3: Nod-like receptor protein 3, SMAD: small body size mothers against decapentaplegic homolog, Ser: serine.

Table 13: Stimulants and cytokines

| Method | Name | Manufacturer |
|----------------------|-------------------------------------|--|
| Cell Culture | ATP (5 mM) | Invitrogen, Eugene, USA |
| | LPS (10 ng/ml) | Invivogen, Toulouse, FR |
| | mTGF- β 1 | Cell Signaling, Danvers, MA |
| Animal models | Pan-caspase inhibitor “Z-VAD” | Invivogen, Eugene, USA |
| | IL-1 receptor antagonist “Anakinra” | Swedish Orphan Biovitrum, Stockholm, S |

Table 14: Animal experiments

| Method | Name | Manufacturer |
|--|--|---|
| Mouse Strains | C57BL/6 N | Charles River Laboratories International Inc., Sulzfeld, DE |
| | <i>Asc</i> $-/-$ (BL/6 background) | J. Tschopp (University of Lausanne, Lausanne, Switzerland). |
| | <i>Nlrp-3</i> $-/-$ (BL/6 background) | J. Tschopp (University of Lausanne, Lausanne, Switzerland). |
| Mouse handling and preservation | Macrolon Type II cages with filter cover | Bioscape, Emmendingen, D |
| | Standard chow | Sniff, Soest, Germany |

Abb.: C57BL/6: C57 black 6 N, BL/6: black 6 N, *Asc* $-/-$: Apoptosis-associated speck-like protein containing a CARD knock out mice, *Nlrp3* $-/-$: nod-like receptor protein 3 knock out mice.

2.2 Methods

2.2.1 Cell culture

Basic principles and theory of cell culture: Cell culture is a method where cells from different tissues and origins are grown in an artificial environment. Strains may be classified according to their origin and lifespan. Primary cells are isolated directly from tissue and show a limited lifespan. This thesis used isolated **p**rietary **m**ouse **e**mryonic **f**ibroblasts (pMEFs) from mouse embryos. Continuous cell lines are cell clones genetically transformed, which have a much longer lifespan than the primary cells. For this thesis, a cell line called NIH-3t3 was used. Each new batch underwent Mycoplasma contamination screening using a PCR-kit (Pan Vera, Stratagene; also see Coté, 2000).

General terms and conditions: A sterile environment was assured for the manipulation of cells. The cell culture hood was treated 10 to 15 min with UV light and cleaned with 70% Ethanol. To keep a sterile environment, laminar air-flow was used during cell handling. All other instruments were disinfected with 70% Ethanol solution prior to use. All cells were grown under standard conditions (in an incubator set at 37°C supplied with 5% CO₂/air).

Culture and passage of cells: Frozen primary cells or cell lines were cultured in 10 to 15 ml of pre-warmed (37°C) *Dulbecco's modified Eagle's* medium (DMEM), with 1% Penicillin/Streptomycin (PS) and 10% Fetal bovine serum (FBS). The medium was changed after 48 hrs. Cells were split by over 80% confluence. Detachment followed using warm trypsin/EDTA and incubation for 5 min at 37°C. After complete detachment, the warm medium was poured in order to annul the effect of the enzyme, and placed into Falcon tubes. Cells were spun at 1000 rpm, the old medium was replaced with fresh DMEM containing 10% FBS and 1% PS and then cultured in two new plates.

Cell count and vitality: Vitality of the cells was regularly checked with the light microscope. After detaching cells with Trypsin/EDTA and centrifugation at 75 rpm for 5 min, cells were diluted in 1ml DMEM and gently mixed. 10µl were taken and diluted in a falcon, which contained 1ml DMEM, giving the proportion 1 in 10. This proportion changed, depending on the pellet and the dilution needed (1:5 to 1:100). Neubauer's chamber was used for cell counting (Figure 11).

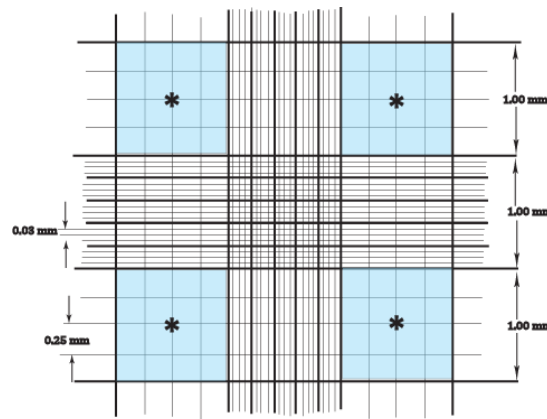


Figure 11: Neubauer cell chamber. Neubauer's cell chamber is a widely used method for cell counting. Concentrations between 250,000 cells/ml and 2.5 million cells/ml are usually necessary for obtaining an accurate estimation of the original concentration. Cells are counted in the blue (*) marked squares. Concentration is calculated using the following equation: $\frac{n^{\circ} \text{cells/square}}{4} \times \text{dilution} \times 1 \text{ml} \times 10^4$ respectively. Equal concentrations were plated in 6-, 8-, 12- or 96-well plates respectively.

Cryopreservation and defrosting of the cells: Healthy cells, at earlier passages were frozen for their future use. They were detached from the culture plates with Trypsin/EDTA and spun down for 3 min at 1000 rpm. The pellet was maintained on ice and carefully re-suspended in cold medium (90 % culture medium and 10 % DMSO) by mixing up with the pipette. 1.5 ml aliquots were quickly dispensed into freezing vials and stored at 4°C. Later slowly frozen at -20°C for 1 hr. and then at -80°C. For cell thawing, vials were placed in a water bath at 37°C. For culturing, cells were dispensed in 5 ml of warmed DMEM and spun down at 1000 rpm for 5 to 7 min. The cell pellet was re-suspended in fresh medium and transferred to 100 mm² culture plates.

2.2.1.1. Stimulation of NIH-3t3 cells and primary mouse embryonic fibroblasts

NIH-3t3 cells and pMEFs were plated in 6-, 8- or 12-well plates with a maximum concentration of 0.3×10^6 (NIH-3t3) and 0.5×10^6 (pMEFs) cells per well. After 24 hrs, cells were stimulated with different cytokines or other non-protein stimulators according to the experimental design. NIH-3t3 cells were stimulated with mouse TGF-β1 at different concentrations (10, 50 and 100 ng/ml) and for various time points (0, 6, 12, 24 and 48 hrs) in order to optimize the results of following experiments. Other experiments required co-stimulation with LPS (100 ng/ml) and/or ATP (5 mM). PMEFs from WT and *Nlrp-3*-deficient mice were also stimulated with mouse TGF-β1 (optimized concentration: 10 ng/ml), LPS (100 ng/ml) and/or ATP (5 mM) according to the experimental design.

2.2.1.2 Isolation of primary mouse embryonic fibroblasts

12.5 to 13 days pregnant C57 black 6 (C57BL/6 N) female mice from WT and *Nlrp-3*-deficient mice were sacrificed for the posterior isolation of pMEFs. Approximately 8 to 10 mouse embryos were extracted from each mouse. Directly after extraction, embryos were placed in PBS and dissected with sterilized scissors, scalpel and dissecting forceps. The inner-organs were extracted. The skeleton was minced and soaked in warmed DMEM. Minced pieces were then placed in 20 ml falcon tubes with trypsin and kept at 37° C for 15 min. Under the sterile laminar flow hood, trypsinized tissue was soaked and filtered through a 100 µm cell filter in DMEM, placed into 50 ml Falcons, and spun for 5 min at 1000 rpm. The supernatant was removed, pellet re-suspended in 10 to 50 ml fresh DMEM with 10% FCS and 1% PS, and plated on 100 mm² culture dishes. After 48 to 72 hrs cells viability was checked under a light microscope and debris was removed. Fresh DMEM was changed every 48 hrs. After achieving 80% confluence (2 to 5 days after), cells were split as previously described.

2.2.2 Cell viability assay

Basic principles and theory: Cell viability assay or MTT assay is a method used to quantify proliferation and viability of cells in response to an external stimulus. It is based on the chemical reaction of its yellow compound *MTT* (3-[4,5-dimethylthiazol-2-yl]-2,5-diphenyltetrazolium bromide) tetrazolium, which is reduced in presence of NADH or NADPH to formazan (Figure 12). This reaction is produced by dehydrogenase enzymes, which generate reducing equivalents. The equivalents NADH and NADPH can only be produced by metabolic activity and thus living cells. The purple/blue intracellular formazan can be solubilized and measured with spectrophotometric devices by the changes in the light absorbance of the wells. The absorbance increases proportionally to the produced formazan, which mirrors the proliferation status of the cells.

Procedure: Cells, NIH-3T3 fibroblasts and pMEFs, were plated in a 96-well cell proliferation plates at a concentration of approx.10000 cells/well. After 24 hrs, the medium was changed to plain DMEM with 1% PS, and without FCS in order to avoid its influence on the cell growth rate and enhance synchronization of their proliferation. Mouse TGF-β1 and LPS were added to the wells as determined in the experimental design. Pure DMEM was used as a negative control. After 24 to 48 hrs, 15 µl of MTT dye were added to the samples (in the dark) and left for 4 to 6 hrs wrapped in an aluminum cover to avoid light. 75 µl of detergent solution were then added to stop the reaction. After 24 hrs in the dark, data were analyzed with the ELISA Reader with an absorbance filter of 490 nm wavelength.

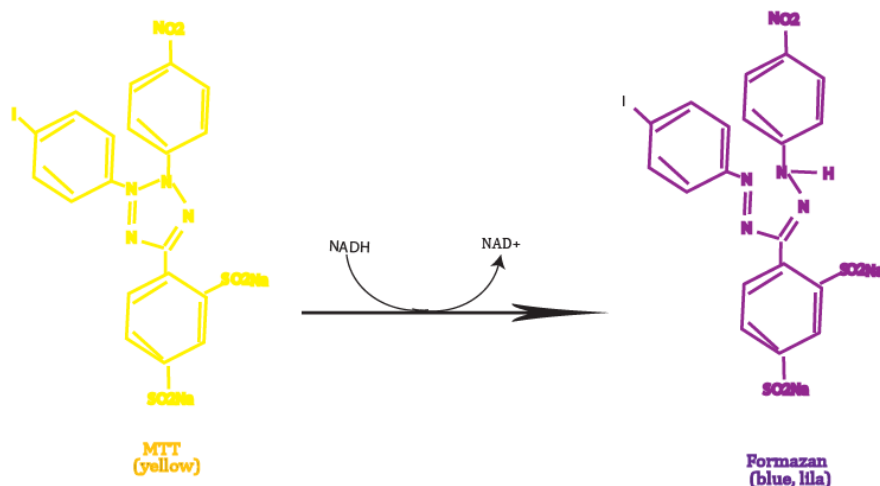


Figure 12: MTT chemical reaction. The yellow MTT (3-(4,5-Dimethylthiazol-2-yl)-2,5-diphenyltetrazolium bromide) tetrazolium is reduced by living cells by NADH which transfers the electrons to the MTT turning into Formazan, which has a stable blue color. Adapted from [165].

2.2.3 Biomolecular methods: Gene expression and quantification

Generalities: For the detection and quantification of genes (DNA, RNA) a PCR (**P**olymerase **C**hain **R**eaction) or RT-qPCR (**R**eal **T**ime quantitative **P**olymerase **C**hain **R**eaction) is needed. These require different steps. For the RNA expression analyses following steps are required:

1. RNA isolation
2. RNA quantification and purity check
3. cDNA preparation
4. RT-qPCR

2.2.3.1. RNA isolation

RNA was isolated from tissues (kidneys from C57BL/6 mice from WT, *Nlrp-3*-deficient and *Asc*-deficient mice) and cells (NIH-3t3 cell line and pMEFs) with the RNA isolation kit Ambion Pure as instructed by the kit's protocol. Kidneys were placed in 600 μ l lysis buffer (containing 1% β -mercaptoethanol) and homogenized for approx. 60-80 seconds in total and then spun at 6000 rpm for 5 min. For RNA isolation from cells, 500 μ l lysis buffer (containing 1% β -mercaptoethanol) were used. Cells were spun at 6000 rpm for 5 min. Hereinafter same protocol was used for both tissue and cells. Meanwhile, an equal amount of volume was prepared in another tube with 70% ethanol. Supernatant from homogenized tissue was gently mixed and transferred into the 70% ethanol

column. Centrifugation at 11000 rpm followed for 15-30 sec. Remaining ethanol was removed and 350 µl of wash buffer I were added to the columns. Samples were spun at 11000 rpm for 15-30 sec two times in a row. 500 µl wash buffer II were then added into the columns and spun at 11000 rpm for 15-30 sec three times in a row. Samples were then spun at 11000 rpm for 1 min and columns were placed into new elution tubes. Here, 35 µl of RNase free water were added to the samples and incubated for 1min at room temperature (RT). Samples were spun at 11000 rpm at last for 1 min and placed on ice.

2.2.3.2. RNA quantification and purity check

Using the NanoDrop spectrophotometer, isolation purity and quantity were checked. 2 µl were taken from each sample and loaded on the measuring surface. Absorbance was measured at the desired wavelength, determining RNA concentration in each sample. From the determined concentration, we calculated the necessary amount (in µl) needed for the extraction of 1µg RNA per sample. Furthermore, absorbance ratio 260/280 nm was used for RNA purity-check. Values around 2.0 (+/- 0.2) were rated as pure [166].

2.2.3.3. cDNA preparation

Reverse transcription is the process used for producing complementary DNA from extracted RNA. For this, the enzyme reverse transcriptase (Superscript) is needed. Samples were separated into two groups, with and without Superscript, the latter used as a control. For each sample we placed 1 µg of sample RNA together with RNase free water, and a “Premix”, containing 9 µl of buffer 1 , 2 µl 1 M dithiothreitol (DTT), 0.9 µl 25 mM of nucleoside triphosphates (dNTPs), 1 µl ribonuclease inhibitors (RNasin), 0.5 µl acrylamide, and 0.5 µl hexamer in a new Eppendorf vial. The amount of RNase free water was given complementarily to the amount of sample RNA, in order to achieve 16.5 µl per sample. Finally, Superscript was added to the samples together with the 6.9 µl of premix and were spun at 42°C for 90 min. Synthesized cDNA was either directly used, or kept at -80°C.

2.2.3.4. Real Time-PCR

Basic principles and theory of the Polymerase chain reaction: PCR is a method used to localize, analyze and compare the gene expression at DNA or RNA level of different genotypes based on the cell’s natural method for duplication of its genetic material. A DNA-fragment (or template) from cells or tissue; a heat-stable DNA polymerase (Taq-Polymerase), primers (forward and reverse), nucleotides or dNTPs, specific buffers and MgCl₂ are the necessary components to reproduce this

reaction. It undergoes 3 steps: (1) denaturation, where double strand DNA separates after heating at 95°C; (2) annealing, where the respective primers bind to the DNA strands and (3) extension, where heat-stable DNA polymerases (Taq-polymerase from the bacteria *Thermus aquaticus*), which works at a temperature of about 70-72° C, will attach the correspondent nucleotides of the DNA strand and reflect the genetic material. This process will repeat till completing approx. 30 to 45 cycles, amplifying the DNA with a factor 2^{20} to 2^{40} [167].

The gene amplification rate undergoes three phases: (1) An exponential phase, where for each cycle an exact duplication of the product takes place; (2) a linear phase, where the reaction slows down due to the consumption its components (dNTPs) and (3) a plateau phase, where the reaction is completely stopped and no other products are formed. This is the phase where the amplified DNA is detected in agarose gel.

Real-Time quantification PCR: Unlike PCR, qPCR or RT-qPCR has the advantage of not only detecting the desired gene-template but also quantifying the concentration of the targeted DNA in a sample. The other advantage of the qPCR relies on the time-point of DNA detection. A PCR will show the detected DNA at the end of the reaction. The q-PCR in change uses fluorescent substances which bind the target DNA strands while amplifying them, resulting in an increased emission of fluorescence. This fluorescence is directly proportional to the expression of the target DNA. Higher expressed genes will be easier for the Taq-polymerase to detect, leading to an earlier appearance of fluorescence. The so-called C_t or C_p value (Cycle threshold) represents the achievement of a defined threshold (threshold of how many cycles were achieved until that point) and reflects a significant change in fluorescence emission compared to the background fluorescence. The number of cycles needed to reach this specific threshold level is inversely correlated to the amount of nucleic acid that was in the original sample; i.e. the lower the C_p value, the more target DNA is present in the sample. This value is always found in the exponential phase of amplification [168].

Procedure: Light Cycler 480 Real-time PCR Systems (Roche, Basel, CH) was used for RT-PCR. The prepared cDNA samples were diluted in a 1:10 ratio with RNase free water. 2 µl were taken from this dilution and placed in microwells of a 96 multiwell plate, together with 10 µl of SYBR-Green mastermix, 0.6 µl of forward and reverse primers of the desired genes respectively, 0.16 µl of TaqMan polymerase and 6.64 µl of distilled water. Plates were sealed with a plastic film and placed in the Light Cycler 480. C_p values were given after 95 min running program (Figure 13).

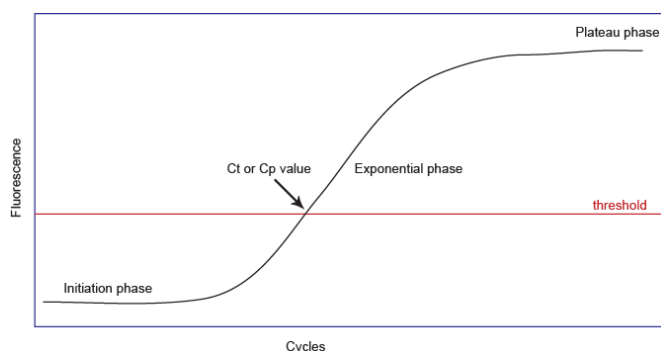


Figure 13: Cp value in RT-PCR. Schematic representation of the amplification curve in RT-PCR: After the initiation phase, luminescence rises until arriving the threshold (Ct or Cp value), reflecting a significant change in fluorescence. The number of cycles needed for the threshold is inversely correlated to the amount of nucleic acid in the sample.

2.2.4 Immunological Methods

2.2.4.1. Immunofluorescence cell staining

Immunofluorescence staining was used to evidence different target proteins in cells after stimulation with mouse TGF- β 1. PMEFs were plated in a 4 well chamber slide at a concentration of 5000 cells per well in DMEM together with 10% FCS and 1% PS. After 24 hrs, medium was changed to plane DMEM which included mouse TGF- β 1. For cell fixation and permeabilization, medium was removed and 500 μ l of acetone were added per well and then kept at -20° C for 10 min. Wells were then blocked with 5% BSA for 3 hrs at 25° C. Incubation with primary antibody (1/100 in PBS plus 5% BSA) followed for 2 hrs at 25° C. A rabbit anti-mouse (1/10000) antibody was used as secondary antibody [169]. Fluorescence was assessed using a fluorescence microscope (Leica DC 300 F, Cambridge, UK) and then quantified using analysis software Image J.

2.2.4.2. Enzyme-linked immunosorbent assay:

Basic principles and theory: The enzyme-linked immunosorbent assay or ELISA is a technique used for the detection of proteins, antigens, and other biomolecules from serum, plasma, cell culture supernatants and other substances. Many techniques can be found to perform this experiment. In this particular case, we used the so-called “sandwich” ELISA, in which 2 antibodies are used for the detection of our target protein. In it, the first antibody (capture antibody) will fix the target protein to the plate and later a second antibody (detection antibody) linked to an enzyme (in this case horseradish peroxidase or HRP) will attach on the surface of the first antibody. A substrate (here: Streptavidin-horseradish peroxidase conjugate or SA_v-HRP) will react with the HRP enzyme producing luminescence. The amount of color produced is quantified by measuring the absorbance with a spectrophotometer. Figure 14 shows a schematic representation of the ELISA “sandwich”.

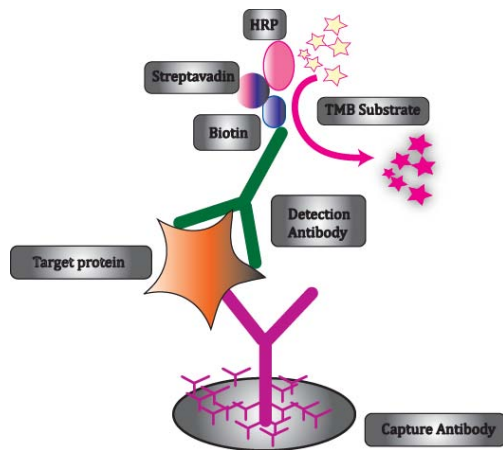


Figure 14: ELISA sandwich. A capture antibody coats the plate to further bind the target protein. A detection antibody linked to HRP binds specifically to the targeted protein, which after addition of Streptavidin-HRP reacts with the enzyme, producing luminescence. Abb.: HRP: horseradish peroxidase.

Procedure: We used OptEIA's set for mouse IL-1 β ELISA for the detection of IL-1 β in supernatants from NIH-3t3 and pMEFs after 24 hrs of stimulation with LPS (100 ng/ml) and ATP (5 mM). ELISA's 96 well plate was coated with 100 μ l of capture antibody, diluted in coating buffer, sealed and incubated overnight at 4 $^{\circ}$ C. Wells were then aspirated and washed 3 times with 300 μ l wash buffer per well using ELISA's microplate washer. In order to remove any residual buffer, the plate was inverted and blotted on absorbent paper. 200 μ l of assay diluents were added per well and incubated it at RT for 1 hr. Aspiration and washing step were repeated three times. Standards (used for determining concentration gradient) and sample dilutions were placed on ice. 100 μ l of each standard, sample, and control were pipetted and incubated at RT for 2 hrs. Aspiration and washing steps were repeated five times. 100 μ l of detection antibody were then added and diluted in assay diluent to each well, then incubated for 1 hr at RT. Aspiration and washing step were again repeated five times. New 100 μ l of enzyme reagent were diluted in assay diluent and added to each well. After 30 min of incubation at RT, aspiration and washing followed, now seven times. 100 μ l of substrate solution were added to each well and incubated for 30 min (unsealed) at RT in the dark. In order to stop the reaction, other 50 μ l of stop solution were added to each well. Results were quantified with the ELISA Reader at an absorbance of 450 nm within 30 min after stopping the reaction [170].

Analysis: Standards defined different concentrations, which were used to build a linear function. This function was then used to calculate the concentration values in the samples. Blanks were subtracted from the standards.

2.2.4.3. Western Blot

Basic Principles of western blotting: Western blot is a technique researchers use to evidence the presence and amount of a desired protein in cells, tissue, serum or other substances. Four basic steps are essential in this process:

1. Isolation of proteins from cells or tissue
2. Protein estimation using Bradford's Assay
3. Separation of proteins with gel electrophoresis (SDS – PAGE)
4. “Blotting”: Transfer of proteins to a solid support (PVDF membrane)
5. Detection of the targeted protein with antibodies and developing

Protein isolation: The technique used for extraction of proteins from cells and tissue followed basic principles with minor differences:

From Tissue: Kidneys from sacrificed mice were carefully extracted. After thawing, or directly after sacrifice, tissues were placed in 1.5 ml Eppendorf tubes containing 520 µl of lysis buffer (composed of 500 µl RIPA Buffer and 20 µl protease inhibitor in a 25 to 1 ratio. The protease inhibitor stock tablet was previously prepared and diluted in 2 ml water. For identifying phosphorylated proteins, a phosphatase inhibitor was added to the mixture in a 4 to 1 ratio. This inhibitor was used to prevent the lysis of the phosphate-bindings. Samples were kept on ice during this step to avoid protein denaturation and were later homogenized using blade homogenizer for 30 sec.

From Cells: Media was extracted from previously stimulated cells and then washed with PBS. Wells were then placed on ice and lysis buffer was added in the same amount and proportions as described above. Cells were detached with a 24 cm cell scraper and gently mixed with a pipette. The supernatant was placed into 1.5 ml Eppendorf tubes and later homogenized as described above. Following homogenization, samples from both tissue and cells were kept at 4° C for 2 hrs on a rotor. Afterwards, they were spun at 12000 rpm for 20 min at 4° C. The remaining supernatants, which contained the protein fraction, were collected and placed in 1.5 ml Eppendorf tubes.

Protein estimation - Bradford's assay - and Sample preparation: The amount of protein collected from the samples always depends on quality and amount of the extracted tissue or cells. The determination and equalization of protein concentration in samples are essential for the posterior comparison between them. Bradford's assay was used for analysis of protein concentration. It uses Coomassie Brilliant Blue G-250 dye, which binds to proteins and by doing so turns into its stable

blue form. The concentration can be measured with a spectrophotometer at 595 nm absorbance filter [171].

Samples and standards were placed in a 96 well plate. Bovine serum albumin (BSA) was used for as a control. BSA was diluted with water at different concentrations, forming a linear function, which served as a reference for the samples. We took 1 μl of each sample and diluted it in 9 μl of water. At the end, Coomassie Brilliant Blue was given to the standards, samples and blanks. After 10 min incubation at RT, absorbance was measured with Elisa reader and a 590 nm absorbance filter. Using the function derived from standards, protein concentration was determined. For the gel electrophoresis, equal amounts of protein were needed from the samples (60 to 100 μg protein per column). The amount of solution needed per sample; in order to get 60 μg protein for each column, was calculated using the following equation:

$$N1 \times V1 = N2 \times V2$$

This applies in our experiment as followed:

$$\text{Sample concentration} \left(\frac{\text{mg}}{\text{ml}} \right) \times V \mu\text{l} = \text{Desired protein concentration} \left(\frac{\text{mg}}{\text{ml}} \right) \times 100 \mu\text{l}$$

With ***V = volume of sample needed.*** The needed volume of water to dilute the samples will then result from:

$$100 \mu\text{l} - V\mu\text{l} = \text{Volume} (\mu\text{l}) \text{ of Water necessary for dilution}$$

Finally, 25 μl of 4X loading buffer (100 mM Tris-HCl, 4% SDS, 20% glycerol and 0.2% bromophenol blue) were added to each sample. SDS (sodium dodecyl sulfate) was used to line up proteins and impart a negative charge. This allows proteins to separate only by size. Samples were then boiled at 95°C for 5 min in order to denature the higher order structure and ensuring that the negative charge of amino acids is not neutralized.

Gel Electrophoresis (SDS–PAGE) and semi-dry transfer

Gel Electrophoresis: This method is used to separate molecules (DNA, RNA or proteins) by size. Here, molecules travel through a polyacrylamide gel from the cathode to the anode. Here, acrylamide is used to determine the pore size. The smaller the protein, the more acrylamide was needed.

SDS-gel preparation: Two types of gel were prepared: one *stacking gel* used to place the samples and order them in a line (less amount of acrylamide), and a *separating gel* (with a higher amount of acrylamide) used for the actual separation of the molecules. Table 10 above lists the ingredients of both gels. The gel was placed after solidification in the electrophoresis chamber, together with the

running buffer, which was added until stacking gel was covered. 10 to 20 μl of each sample were loaded in the stacking gel. The previously added bromophenol blue allowed tracking of the proteins during the electrophoresis. Lane non-reducing protein marker was placed in the first well and served as a reference to protein size. Samples ran for 30 min at a lower voltage (100 V) in the *stacking gel* and higher voltage (140 V) in the *separating gel* during 60 min.

“Blotting”-transfer to the PDVF membrane-: Blotting refers to the transfer of molecules from a membrane to a solid support. In this case, a semidry transfer was used as pictured below (Figure 15):

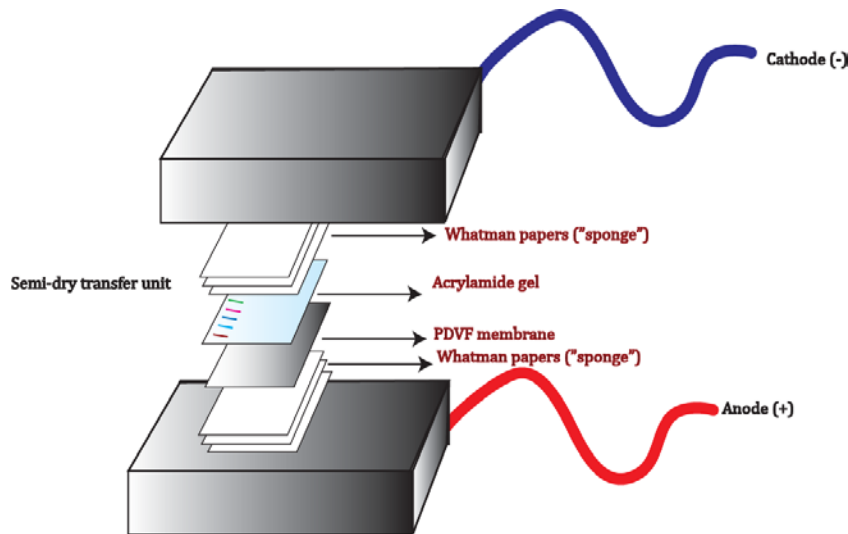


Figure 15: “Blotting” or semidry transfer. The separated proteins are transferred to a PDVF membrane. Transfer buffer is carefully removed from Whatman paper. On top follows the PDVF membrane and subsequently the gel with the separated proteins. After a new piece of transfer buffer-soaked Whatman paper, the semidry transfer unit is closed. The “transfer-sandwich” ran for 120 min at 25 V. Abb: PDVF: polyvinylidene difluoride.

Whatman paper was used as “sponge” after being soaked in transfer buffer. Polyvinylidene difluoride membrane (PDVF-membrane) was soaked in methanol for its activation and then placed in transfer buffer. Each step required removal of excess liquid, giving it its “semi-dry” character. The “transfer-sandwich” was placed in a semi-dry transfer unit, which ran for 120 min at 25 V. After transfer, the gel was discarded and the membrane was washed with TBS-T (preparation see table 10).

Detection of targeted protein and developing: In order to avoid a non-specific binding of the antibodies to the membrane, blocking for 60 min at RT with 5% milk in Tris-buffered saline (20mM Tris-HCl, 150 mM NaCl and 0,1% Tween 20) was performed. Incubation of the primary antibody followed overnight at 4° C on a roller-mixer. Next day, after washing several times with TBS-T, the membrane was incubated with the respective secondary antibodies in 5% milk Tris-buffered saline. Washing with TBS-T was repeated in order to prepare the PDVF membrane for developing. Signals were visualized by an enhanced chemiluminescence system (ECL) using an x-ray developer. β -actin was used as a control in all experiments [172].

2.2.5 Animal experiments

2.2.5.1. General terms and conditions

Mouse handling and preservation: C57BL/6 N WT mice were purchased from Charles River Laboratories, Sulzfeld, DE. *Nlrp-3*- and *Asc*-deficient mice (with BL/6 background) were obtained from J. Tschoop (University of Lausanne, Lausanne, Switzerland). Mice were housed in filter-top cages with unlimited access to food and water. Cages, nest lets, food and water were sterilized before use. A maximum of five mice were kept in cages with a 12 hr light-dark cycle. The mouse housing status corresponded with the “specific pathogen-free” guidelines. Mouse handling was performed in sterile banks (except for sacrifice). All experimental procedures were approved by the local government authorities.

General guidelines for surgery: For every surgical procedure, general terms and conditions described by the guidelines and suggestions of local government authorities were to be followed. The special permit by the Regierung von Oberbayern was a prerequisite for performing any surgical procedure.

Organ extraction and preservation: Kidneys were extracted from mice after sacrifice by cervical dislocation, then placed in PBS and cut with a scalpel in three parts for subsequent analysis. The first third was left in liquid nitrogen for cryopreservation. The second third was placed in histological cassettes with 1.8% formalin and after 24 hrs embedded in paraffin blocks for histopathological analysis. The third part was preserved at -20° C for RNA analysis.

2.2.5.2. Animal Models:

Chronic oxalate nephropathy: The description and purposes of this model are discussed in the previous chapter. For this model, we used male 8-12 week old gender-matched C57BL/6 N WT (n = 4), *Nlrp-3*- (n = 4), *Asc*-deficient (n = 4), vehicle- (n = 4) and anakinra-treated (n =4) mice, who received a high soluble oxalate diet which was prepared by adding 50 µmol/g sodium oxalate to a calcium-free standard diet. Oxalate- and calcium-free control diet was given for three days before switching to high soluble oxalate diet. The anakinra-treated mice group received intraperitoneal injections of anakinra in a dose of 5 mg/kg/ day for 14 days. Urine and plasma samples were collected at different time points prior to sacrifice. After 14 days mice receiving an oxalate-rich diet were sacrificed. Kidneys were extracted for analysis. All animal experiments were performed in accordance with the European protection law of animal welfare and with approval by the local government authorities Regierung von Oberbayern (reference number: 55.2-1-54-2532-189-2015).

Unilateral ureteral obstruction: 8 to 12 week old C57BL/6N WT (n = 7), *Nlrp-3*- (n = 6), *Asc*-deficient (n = 6) and zVAD-treated (n = 6) mice were housed under the previously described conditions. The general guidelines for surgery were stringently followed for the UUO surgery (including pre- and post-surgery procedures). Mouse body temperature was adjusted by placing the mouse on a HEKA breeding device. The breeder's temperature was settled at 37° C, the heating plates at 42° C. Narcosis and analgesia were performed as described by the general guidelines for mouse surgery. Mice were immediately placed in the breeder after anesthesia, kept for 10 min and then strapped to the plate. Shaving of the area of the incision with the razor blade followed after disinfection of the fur with ethanol. After cutting the skin with a scalpel, a cutaneous layer was separated from muscles and peritoneum with forceps. The peritoneal cavity was opened to find the bladder. After carefully positioning the bladder outside the body with the large forceps, a mucous layer around the bladder was removed. Ureters were to be found caudal to the bladder. A 5-0 (Ethibond) non-absorbable suture was used to ligate the left ureter with 2 double knots. The bladder was then repositioned in the peritoneal cavity. Muscles were then sutured with 5-0 (Vicryl) suture followed by the skin with (Ethibond-double knots). All events during and after surgery were carefully documented. Distress and pain score were registered regularly. After 10 days, mice were sacrificed by cervical dislocation and both kidneys (ligated and not) were harvested for analysis. All animal experiments were performed in accordance with the European protection law of animal welfare and with approval by the local government authorities Regierung von Oberbayern.

2.2.5.3 Urinary creatinine, plasma creatinine and plasma BUN

Urinary creatinine and plasma creatinine levels were measured using Jaffe's enzymatic reaction with the Creatinine FS kit. Urine samples were diluted 10 times with distilled water, whereas plasma samples were used undiluted. Different dilutions of the standard were prepared using the stock provided with the kit. Working mono-reagent was prepared by mixing 4 parts of reagent 1 (R1) and 1 part of reagent 2 (R2) provided within the kit. Then, 10µl of each of the diluted samples and standards were added to a 96 well plate with a flat bottom. The mono-reagent (200µl) was added to each well and the reaction mixture was incubated for one minute before measuring the absorbance at 492 nm immediately after and 1 (A1) and 2 (A2) min of addition using ELISA reader. The change in absorbance (ΔA) was calculated as:

$$\Delta A = [(A2 - A1) \text{ sample or standard}] - [(A2 - A1) \text{ blank}]$$

Creatinine was calculated as:

$$\text{Creatinine (mg/dl)} = \Delta A \text{ sample} / \Delta A \text{ standard} * \text{Concentration of standard (mg/dl)}$$

Plasma BUN levels were measured using a Urea FS kit. Different dilutions of the standard were prepared using the stock provided with the kit. Working mono-reagent was prepared by mixing 4 parts of reagent 1 (R1) and 1 part of reagent 2 (R2) provided with the kit. Then, 2 µl of each of the sample and standards were added to a 96 well plate. The mono-reagent (200 µl) was added to each well and the reaction mixture was incubated for one minute before measuring the absorbance at 360 nm immediately after and 1 (A1) and 2 (A2) min of addition using ELISA plate reader.

The change in absorbance (ΔA) was calculated as:

$$\Delta A = [(A1 - A2) \text{ sample or standard}] - [(A1 - A2) \text{ blank}]$$

And BUN content of samples was calculated as [173]:

$$\text{BUN (mg/dl)} = \Delta A \text{ sample} / \Delta A \text{ standard} * \text{Concentration of standard (mg/dl)} * 0.467$$

2.2.6 Histological pathological staining and evaluation

Kidney tissues were preserved as described above. After paraffin embedment, 2 µm thick sections were cut with the cryomicrotome Cryostat RM 2155 and placed with ammonium persulfate on microscope slides. After drying for 12 hrs at 37°C, xylene and ethanol were added for de-paraffinization and rehydration of the samples and then washed with PBS.

Periodic Acid-Schiff: Re-hydrated sections were incubated in periodic acid (2% in distilled water) and washed with distilled water. Then, sections were incubated with Schiff solution for 20 min at RT. After washing with tap water, samples were stained with hematoxylin for 2 min. Sections were then washed with tap water and 90% ethanol before drying with closure coverslips.

Immunostaining: For immunostaining, rehydrated sections were incubated in H₂O₂ and methanol (20 ml of 30% H₂O₂ in 180 ml of methanol) for 20 min in the dark and then washed with PBS. Sections were dipped in antigen unmasking solution (3 ml of antigen unmasking solution together with 300 ml of distilled water) and cooked in the microwave for a total of 10 min, with continuous water check over time. They were then cooled at RT for 20 min and washed with PBS. Sections were then incubated with Avidin (Vector for blocking endogenous biotin) followed by an incubation with biotin. Slides were then washed with PBS prior to incubation with primary antibodies. The primarily used antibodies are listed in Table 12. Negative controls were performed for each staining by incubating with a respective isotype antibody instead of primary antibody. Incubation with primary

antibody was performed either for 1 hr at RT or overnight at 40° C in a wet chamber. They were then washed with PBS. Slides were incubated with biotinylated secondary antibodies (1:300, dilution in PBS) for 30 min and then washed with PBS. Substrate solution (ABC solution, Vector) was added and sections were incubated for 30 min at RT in a wet chamber. After washing with PBS and Tris, sections were stained for DAB by counterstaining with methyl green (Fluka). Posteriorly they were washed with alcohol (96%) to remove excess stain and xylene. Sections were dried and mounted with Vecta Mount (Vector).

Pizzolato's staining: Calcium-oxalate deposition in kidney sections was visualized with Pizzolato's staining. Kidney sections were placed in paraffin, then deparaffinized and rehydrated with distilled water. Silver nitrate hydrogen peroxide solution was poured onto slides and subsequently placed under a 60 Watt light bulb for 30 min. After careful washing with distilled water, slides were counter-stained for 5 min. Repeated washing with distilled water followed. Finally, 95% alcohol, 100% alcohol and xylene were used for dehydration.

2.2.6.1 Histopathological evaluation and scoring

PAS: Histopathological evaluation of mouse kidneys was assessed by using a tubular injury score. This semi-quantitative scoring evaluated the percentage of tubular dilation, cast formation, flattening of the tubular cells and denudation of the renal tubules with or without loss of brush border (loss of tubular cells from basal membrane), having for each point a minimum (0 pts) and maximum (5 pts) as described in table 15. Kidney sections were evaluated using a light microscope Leica DII. Quantification is expressed as mean \pm SEM [174].

Table 15: Tubular injury score for evaluation of kidney injury

| Score | Estimated damage | Estimated Percentage |
|-------|------------------|----------------------|
| 0 | None | 0% |
| 1 | Very mild | <10% |
| 2 | Mild | 11% - 40% |
| 3 | Significant | 41% - 60% |
| 4 | Severe | 61% - 79% |
| 5 | Very severe | >80% |

Adapted from [173]

Alfa-SMA and collagen I: Interstitial fibrosis was assessed by quantification of α -SMA and collagen I positivity per kidney section. Kidney sections were evaluated using light microscope Leitz I and photographed. Image J software was used for quantification analysis of positive areas from kidney sections. Data are presented as mean \pm SEM %/area [175].

Crystal deposition: Calcium-oxalate crystal deposition was assessed using Pizzolato's staining. Kidney sections were evaluated using light microscope Leitz I and photographed. Quantification analysis of calcium-oxalate positivity was assessed using Image J software. Data are presented as mean \pm SEM %/area.

CD3 +: CD3 antibody was used for assessment of the expression of the T-cell receptor complex (TCR). Kidney sections were analyzed using light microscope Leitz I and photographed. CD3 positivity was counted in each kidney section and then a mean was calculated for each kidney. Results are presented as mean \pm SEM.

F4/80 +: Immunostaining using F4/80 antibody assessed macrophage infiltration per kidney section. Slides were evaluated with a light microscope Leitz I and subsequently photographed. F4/80 positivity was assessed using Image J software. Results are presented as mean \pm SEM %/area.

2.2.7 Statistical analysis

All the results are shown in column bar graphs and represent the means of each group with their correspondent standard errors of the mean (SEM). For determining statistical differences between groups unpaired student's T-test and one-way ANOVA were used. P-values are shown as follows: * $p < 0.05$; ** $p < 0.01$; *** $p < 0.001$.

3. Results

3.1 *In vivo* studies

3.1.1 Unilateral ureteral obstruction model

CKD is associated with abnormalities of kidney function and structure [4] and its progression correlates with the amount of interstitial inflammation and fibrosis [176]. The UUO animal model is often used for studying renal inflammation and interstitial fibrosis. To address the potential role of NLRP3 and ASC in the development of renal interstitial fibrosis *in vivo*, UUO surgery was performed in age and gender-matched C57BL/6 WT, *Nlrp-3*- and *Asc*-deficient mice and sacrificed after 10 days.

3.1.1.1 NLRP3 inflammasome axis is up-regulated in C57BL/6 mice upon UUO.

Muruve et al. previously suggested that the NLRP3 inflammasome is activated in mice after UUO surgery [152]. We corroborated these observations by measuring mRNA expression levels of the NLRP3 inflammasome related genes *Nlrp-3*, *Asc* and *Casp-1*, and the proinflammatory cytokines *pro-IL-1 β* and *pro-IL-18* in kidneys of WT mice after UUO compared to control mice. mRNA expression levels of *Nlrp-3*, *Asc* and *Casp-1* were significantly higher in WT mice after UUO compared to control mice (Figure 16). Similarly, expression levels of the pro-inflammatory cytokines *pro-IL-1 β* and *pro-IL-18* showed a significant increase in WT mice after UUO compared to control mice. These findings suggest that the *Nlrp-3*-*IL-1 β* -axis was up-regulated in mice after UUO surgery.

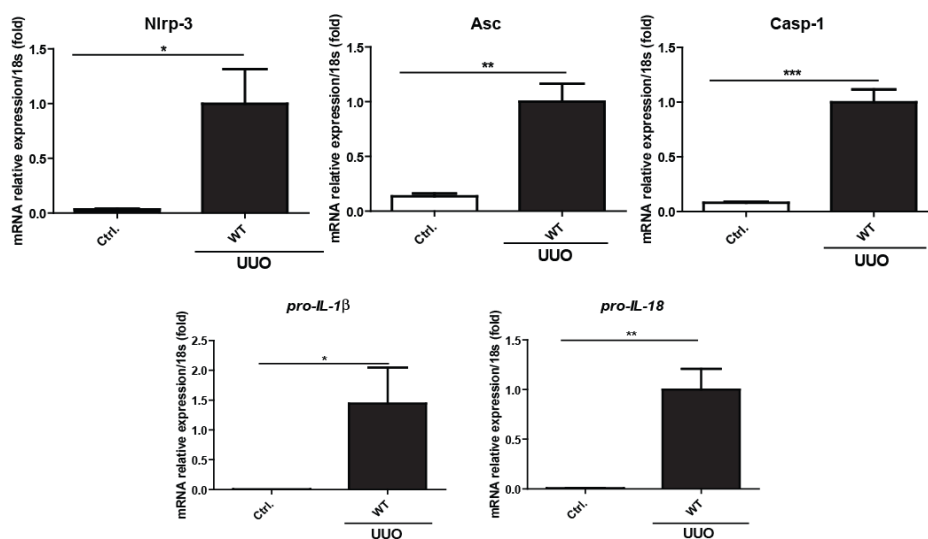


Figure 16: UUO involves up-regulation of NLRP-3 inflammasome associated genes. WT C57BL/6 mice (n = 7) underwent UUO surgery and were sacrificed at day 10. Graphs show mRNA expression levels of inflammasome related genes *Nlrp-3*, *Asc*, *Casp-1* and cytokines *pro-IL-1 β* and *pro-IL-18* in WT kidneys compared to control kidneys (n = 7), without UUO. Significant up-regulation of these genes is observed in mice that underwent UUO. Gene expression is shown as x-fold increase of the target gene over the 18s mRNA expression. These results represent the mean \pm SEM of one out of two independent experiments. Abb.: Ctrl: control, WT: wild type, * $p < 0.05$, ** $p < 0.01$.

3.1.1.2 *Nlrp-3*- or *Asc*-deficiency protects mice from tubular injury upon UUO

In the next series of experiments renal pathological changes were assessed in C57BL/6 WT, *Nlrp-3*- and *Asc*-deficient mice after UUO and compared to control mice without UUO. Renal injury was evaluated on PAS stained kidneys that showed a marked tubular cell flattening, atrophy and denudation in WT mouse kidneys after 10 days UUO (Figure 17 A and B). These pathological features were ameliorated in *Nlrp-3*- and *Asc*-deficient mice, which showed significant protection when assessed by tubular injury scoring (Figure 17 A and B). These findings were corroborated by estimating mRNA expression levels of the kidney injury markers *Kim-1*, *L-FABP* and π -*GST*, which were significantly less expressed in both *Nlrp-3*- and *Asc*-deficient mice compared to WT mice (Figure 17 C). Taken together, we confirm that lack of *Nlrp-3* and *Asc* in mice diminishes renal injury upon UUO.

3.1.1.3 *Nlrp-3*- or *Asc*-deficiency protects mice from renal inflammation upon UUO

Inflammation is the response of the immune system to an injurious trigger. The NLRP3 inflammasome is well-known for its crucial role in inflammatory processes. Therefore, we evaluated the inflammatory component in WT, *Nlrp-3*- and *Asc*-deficient kidneys upon UUO and compared it to control mice, without UUO. Immunostaining for the macrophage/monocyte marker F4/80 revealed an increased infiltration of these cells into the tubulointerstitial space of WT kidneys after UUO compared to controls. This expression was significantly reduced, although not abolished, in *Nlrp-3*-deficient mice compared to the WT group (Figure 18 C and D). However, this observation could not be replicated in *Asc*-deficient mice (Figure 18 C and D). An increased infiltration of CD3+ T-lymphocytes in WT mice upon UUO was observed compared to control mice as indicated by CD3 immunostaining (Figure 18 A and B). Whereas less CD3+ T-lymphocytes were found in *Nlrp-3*- and *Asc*-deficient mice as quantified in figure 18 B. Additionally, mRNA levels of the inflammatory markers CCL2 and CXCL2 were significantly increased in kidneys of WT mice compared to control mice. In *Nlrp-3*- and *Asc*-deficient mice the expression of CCL2 and CXCL2 was less but not significant compared to the WT group (Figure 18 E). Taken together, both inflammasome components NLRP-3 and ASC drive renal inflammation upon UUO.

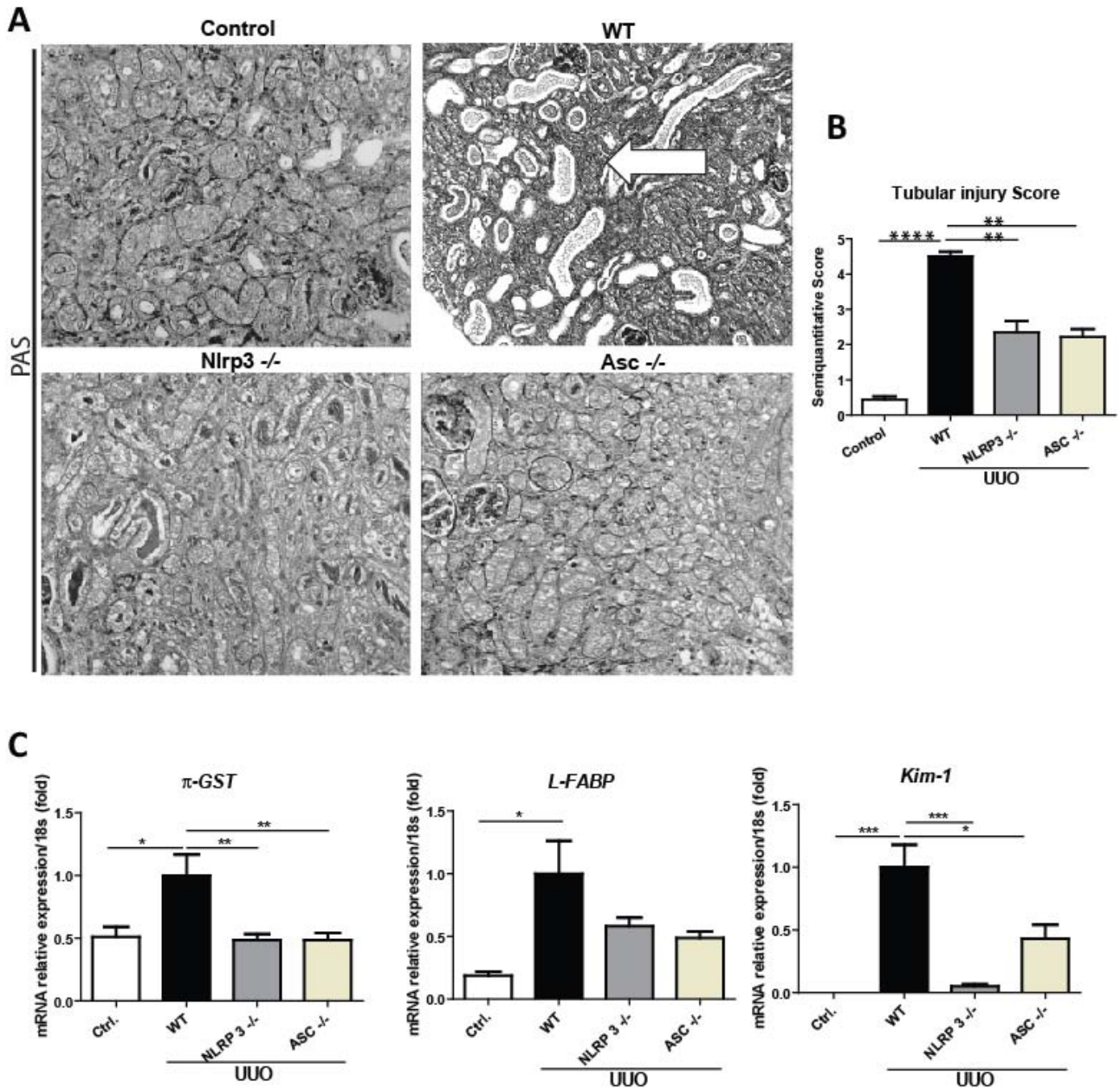


Figure 17: *Nlrp-3*- or *Asc*-deficiency protect mice from tubular injury upon UUO. C57BL/6 mice from WT (n = 7), *Nlrp-3*^{-/-} (n = 6) and *Asc*^{-/-} (n = 6) underwent UUO surgery, were sacrificed at day 10 and compared to control mice (n = 7) without UUO. (A) PAS staining of kidney sections from control, WT, *Nlrp-3*^{-/-} and *Asc*^{-/-} mouse kidneys after 10 days UUO. Arrows show dilated proximal tubules with tubular cell flattening. (B) Quantification of tubular injury after pathologic scoring showed significant less injury in *Nlrp-3*^{-/-} and *Asc*^{-/-} mouse kidneys. (C) MRNA expression levels of kidney injury markers *L-FABP*, *Kim-1* and π -*GST* in controls, WT, *Nlrp-3*^{-/-} and *Asc*^{-/-} mouse kidneys. Significant less expression of these markers is observed in *Nlrp-3*^{-/-} mouse kidneys compared to the WT. Gene expression is shown as x-fold increase of the target gene over the 18s mRNA expression. These results represent the mean \pm SEM of one out of two independent experiments. Abb.: Ctrl: control mice, WT: wild type mice, NLRP3^{-/-}: *Nlrp-3*-deficient mice, ASC^{-/-}: *Asc*-deficient mice *p<0.05, **p<0.01.

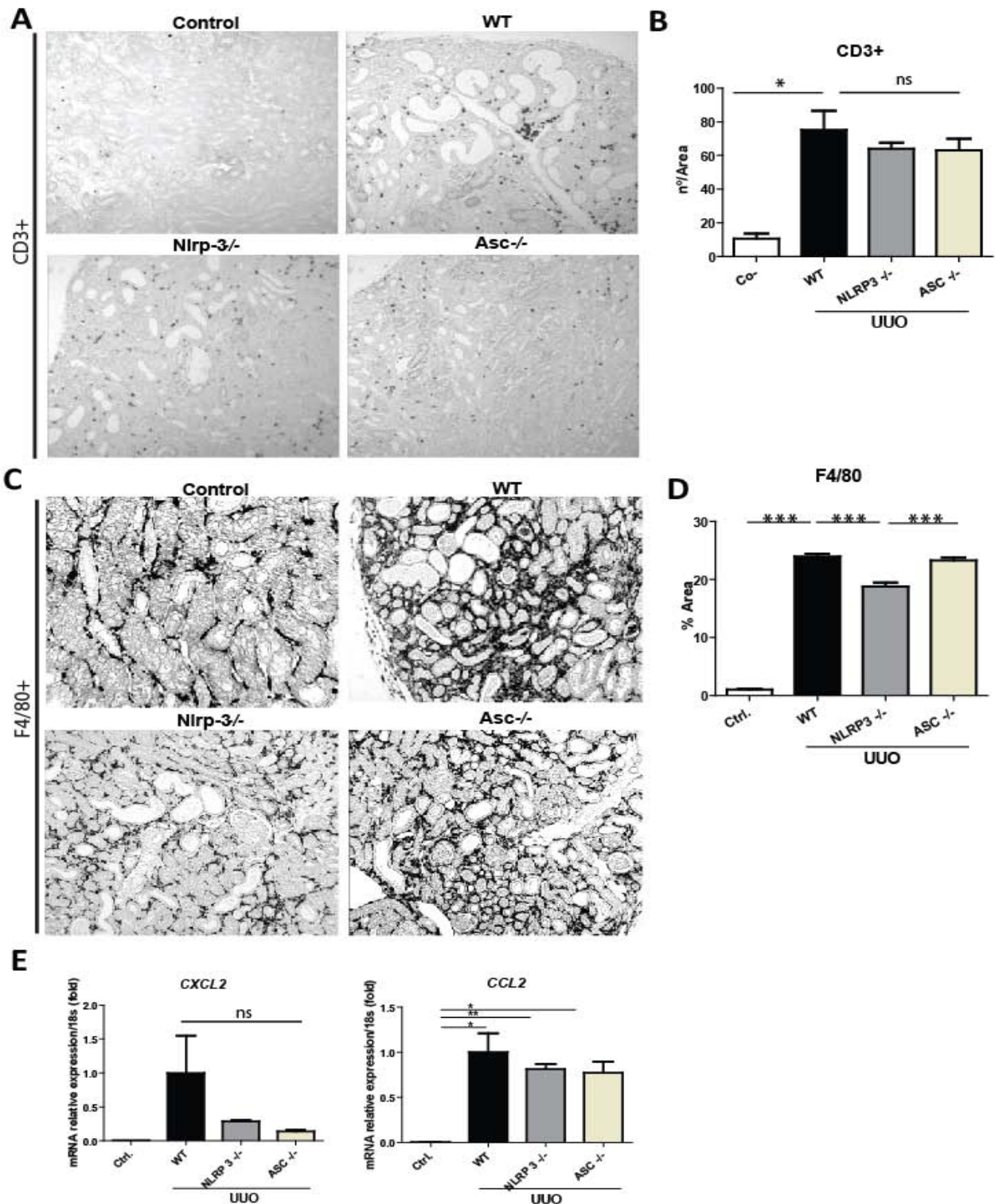


Figure 18: Renal inflammation is reduced in *Nlrp-3*- and *Asc*-deficient mice undergoing UUO. C57BL/6 mice from WT (n = 7), *Nlrp-3*^{-/-} (n = 6) and *Asc*^{-/-} (n = 6) underwent UUO surgery, were sacrificed at day 10 and compared to control mice (n = 7) without UUO. **(A)** Immunostaining of kidney sections for T_H-cell marker CD3 and **(B)** quantification analysis reveal a significantly increased expression in the WT group and a trend to less expression in the *Nlrp-3*^{-/-} and *Asc*^{-/-} group. **(C)** Immunostaining of kidney sections for macrophage marker F4/80 and **(D)** quantification analysis of F4/80 positivity reveal a significant reduction of these in *Nlrp-3*^{-/-} compared to WT mouse kidneys. This could not be shown for *Asc*^{-/-} mice. **(E)** MRNA expression levels of inflammation markers CXCL2 and CCL2 in Ctrl, WT, *Nlrp-3*^{-/-} and *Asc*^{-/-} mouse kidneys after 10 days UUO show a trend to less expression of the markers in *Nlrp-3*^{-/-} and *Asc*^{-/-} compared to the WT. Gene expression is shown as x-fold increase of the target gene over the 18s mRNA expression. These results represent the mean ± SEM of one out of two independent experiments. Abb.: Ctrl: control mice, WT: wild type mice, *Nlrp-3*^{-/-}: *Nlrp-3* deficient mice, *Asc*^{-/-}: *Asc* deficient mice *p<0.05, **p<0.01.

3.1.1.4 *Nlrp-3*- or *Asc*-deficiency protects mice from interstitial fibrosis upon UUO

The UUO model is characterized by a prominent tubulointerstitial fibrosis produced in a short period of time. In order to address the role of NLRP3 and ASC in tubulointerstitial fibrosis *in vivo*, immunostaining of the myofibroblasts marker α -SMA and ECM matrix protein collagen I was assessed in kidney sections of control, WT, *Nlrp-3*- and *Asc*-deficient mice after UUO. Quantification of immunostaining for α -SMA and quantification analyses showed a significant increase in the expression of α -SMA in the WT group after UUO compared to the controls. *Nlrp-3*^{-/-} and *Asc*^{-/-} mouse kidneys revealed significantly less interstitial deposition of α -SMA when compared to the WT group (Figure 19 A and B). These findings correlated with the increased collagen I deposition in WT mice after UUO, which was also significantly reduced in *Nlrp-3*^{-/-} and *Asc*-deficient mice (Figure 19 C), as quantified in figure 19 D. Thus, we conclude that NLRP3 and ASC augment renal fibrogenesis upon UUO.

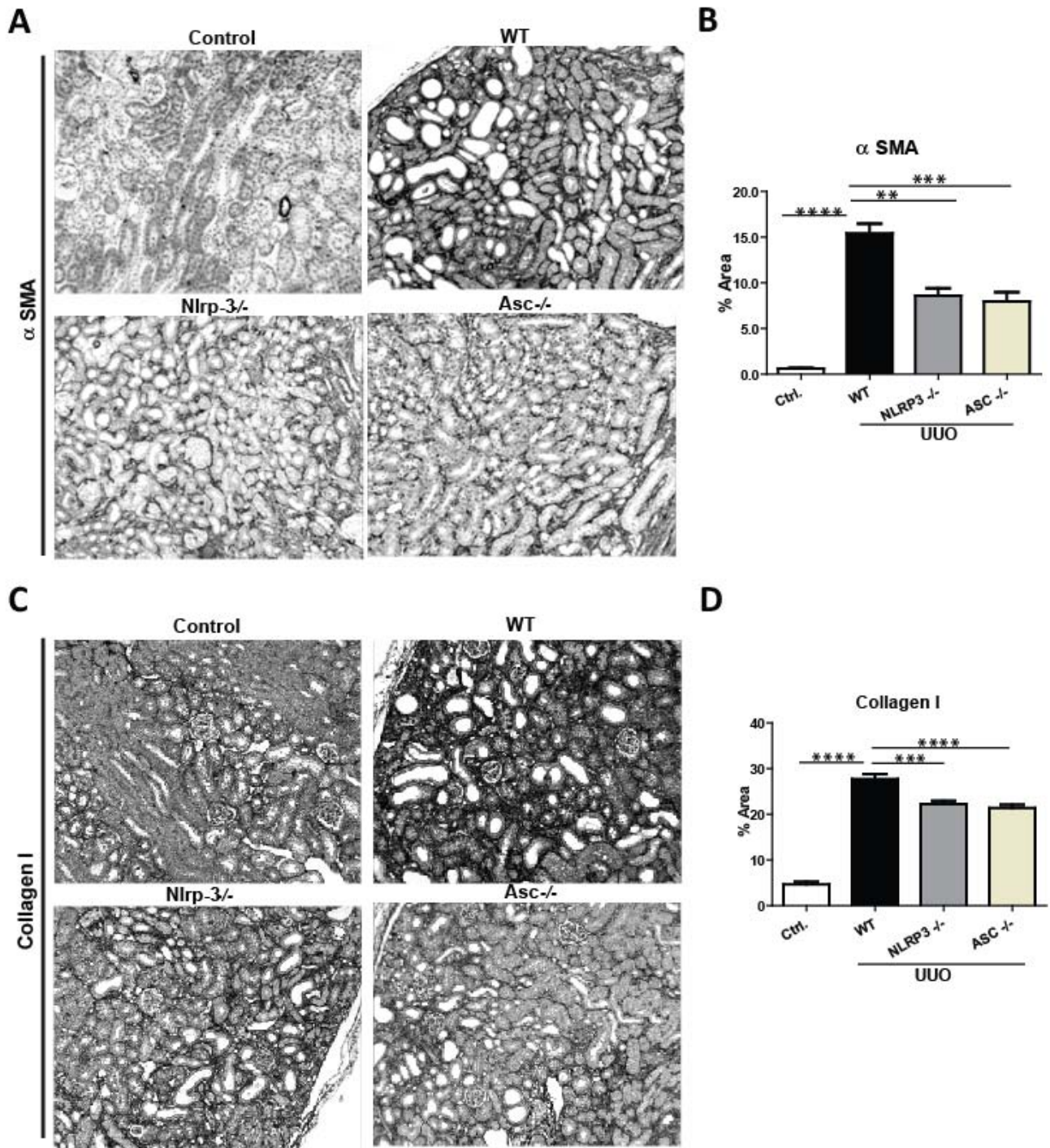


Figure 19: *Nlrp-3* or *Asc* deficiency protects mice from tubulointerstitial fibrosis after UUO. C57BL/6 mice from WT (n = 7), *Nlrp-3*^{-/-} (n = 6) and *Asc*^{-/-} (n = 6) underwent UUO surgery, were sacrificed at day 10 and compared to control mice (n = 7) without UUO. (A) Immunohistochemistry of myofibroblast marker α -SMA and (B) quantification analysis of the α -SMA positive areas in kidney sections after UUO (results in mean % area \pm SEM). (C) Immunohistochemistry of fibrosis marker collagen I and (D) quantification of collagen I positive areas in kidney sections after UUO (results in mean % area \pm SEM). Significant less expression of both fibrosis markers in *Nlrp-3*^{-/-} and *Asc*^{-/-} mice is shown compared to WT kidneys after UUO surgery. These results represent the mean \pm SEM of one out of two independent experiments. Abb.: Ctrl: control mice, WT: wild type mice, *Nlrp-3*^{-/-}: *Nlrp-3* deficient mice, *Asc*^{-/-}: *Asc* deficient mice, *p < 0.05, **p < 0.01.

3.1.1.5 Caspase inhibition only partially improves renal injury and inflammation upon UUO

We have previously demonstrated that *Nlrp-3*- or *Asc*-deficiency protects mice from renal injury, inflammation and tubulointerstitial fibrosis upon UUO. Whether this effect relies on the NLRP3-Casp-1-dependent reduced IL-1 β secretion was not assured. A recent study suggested a Casp-1-independent role of NLRP3 in tubular epithelial cells [138]. To address the role of Casp-1 in renal injury, inflammation and interstitial fibrosis, in particular on inflammasome-activation and cleavage of IL-1 β , 2 mg/kg/day of the pan-caspase inhibitor zVAD were given by intraperitoneal injection to C57BL/6 mice, starting with treatment from day -1 prior to UUO surgery until sacrifice on day 10. PAS stainings of control, WT and zVAD-treated mice revealed increased tubular injury in WT and zVAD treated mice compared to the controls after UUO (Figure 20 A). Pathological scoring showed significantly less injury in zVAD-treated mice compared to the WT group (Figure 20 C). Although this difference was considerably less than previously observed in *Nlrp-3*- and *Asc*-deficient mice when compared to the WT group as demonstrated in figure 17 A and B. mRNA expression analysis of the kidney injury markers *Kim-1*, *L-FABP* and π -*GST* revealed a significantly higher expression of these markers in both WT and zVAD-treated mice compared to the controls, with no significant difference between WT and zVAD-treated kidneys (Figure 20 B).

Furthermore, immunohistochemical analysis of the monocyte/macrophage marker F4/80 in kidney sections from WT, zVAD-treated mice and controls, demonstrated a significantly reduced infiltration of macrophages in zVAD-treated mice compared to the WT group (Figure 21 A and C). This was not the case for CD3⁺ T-lymphocytes, which did not show any significant difference between WT and zVAD-treated mice (Figure 21 B and D). Finally, expression profiling of the inflammation markers *pro-IL-1 β* , *pro-IL-18*, *Cxcl2* and *Ccl2* did not show any significant difference between WT and zVAD-treated mice after 10 days UUO (Figure 21 E). These findings suggest that the Casp-1-dependent IL-1 β cleavage is involved in renal injury and tubulointerstitial inflammation upon UUO. Nevertheless, these results did not show a profound protection as observed in *Nlrp-3*- and *Asc*-deficient mice, suggesting a role of NLRP3 and ASC beyond Casp-1-mediated IL-1 β cleavage in renal injury and inflammation upon UUO.

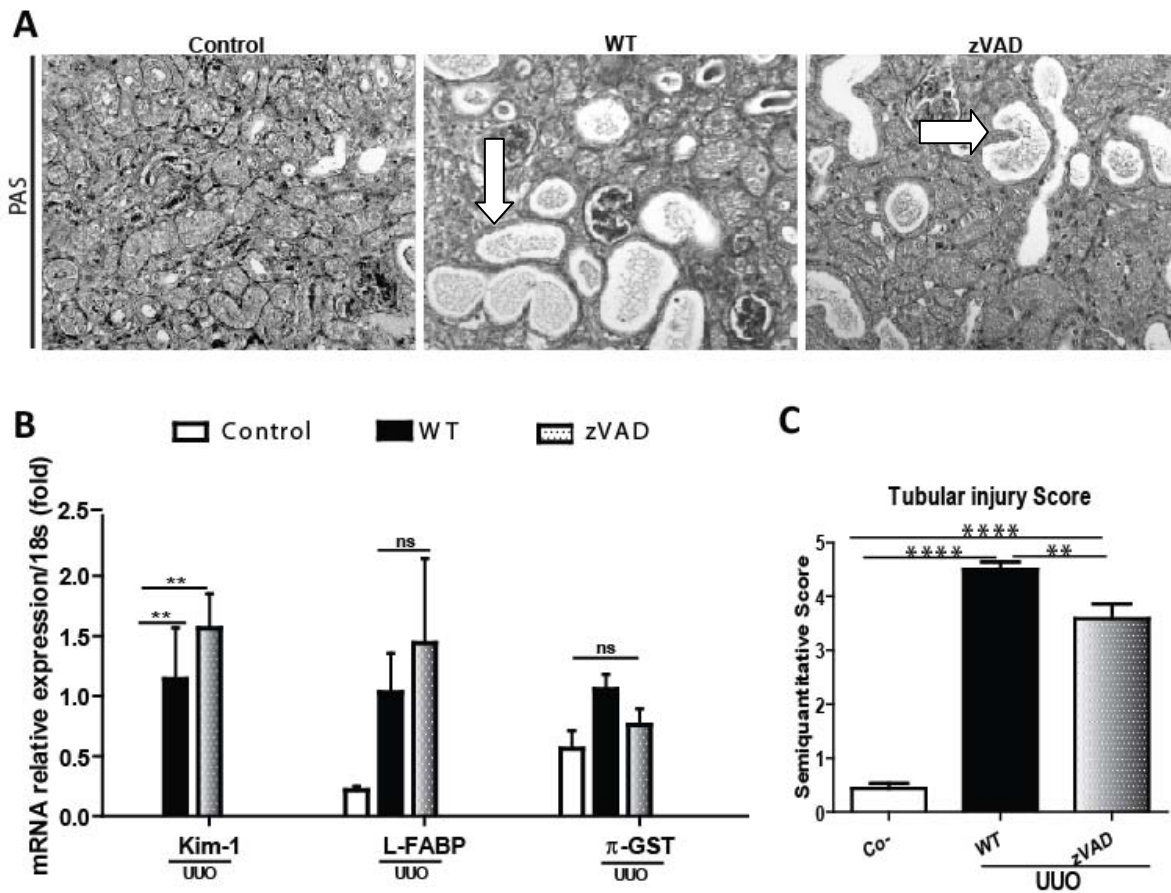


Figure 20: Caspase inhibition only partially protects mice after UUO. C57BL/6 mice from WT (n = 7) and zVAD-treated (n = 7) mice underwent UUO surgery and were sacrificed at day 10. Kidney sections of mice without UUO (n = 7) were used as control. (A) PAS-staining from WT, zVAD-treated and control kidneys after 10 days UUO. Arrows point at dilated and injured tubules. (B) MRNA expression of *Kim-1*, *L-FABP* and *π -GST* was quantified with RT-PCR and compared to control mice. Here, no significant differences are observed between WT and the zVAD-treated group. Gene expression is shown as x-fold increase of the target gene over the 18s mRNA expression. (C) Tubular injury score analysis of mouse kidneys upon 10 days UUO compared to controls (in Mean \pm SEM). Significant differences are observed between the zVAD-treated and WT group. These results represent one out of two independent experiments. Abb.: Ctrl: control mice, WT: wild type mice, zVAD: treatment with pan Caspase inhibitor zVAD. *p<0.05, **p<0.01.

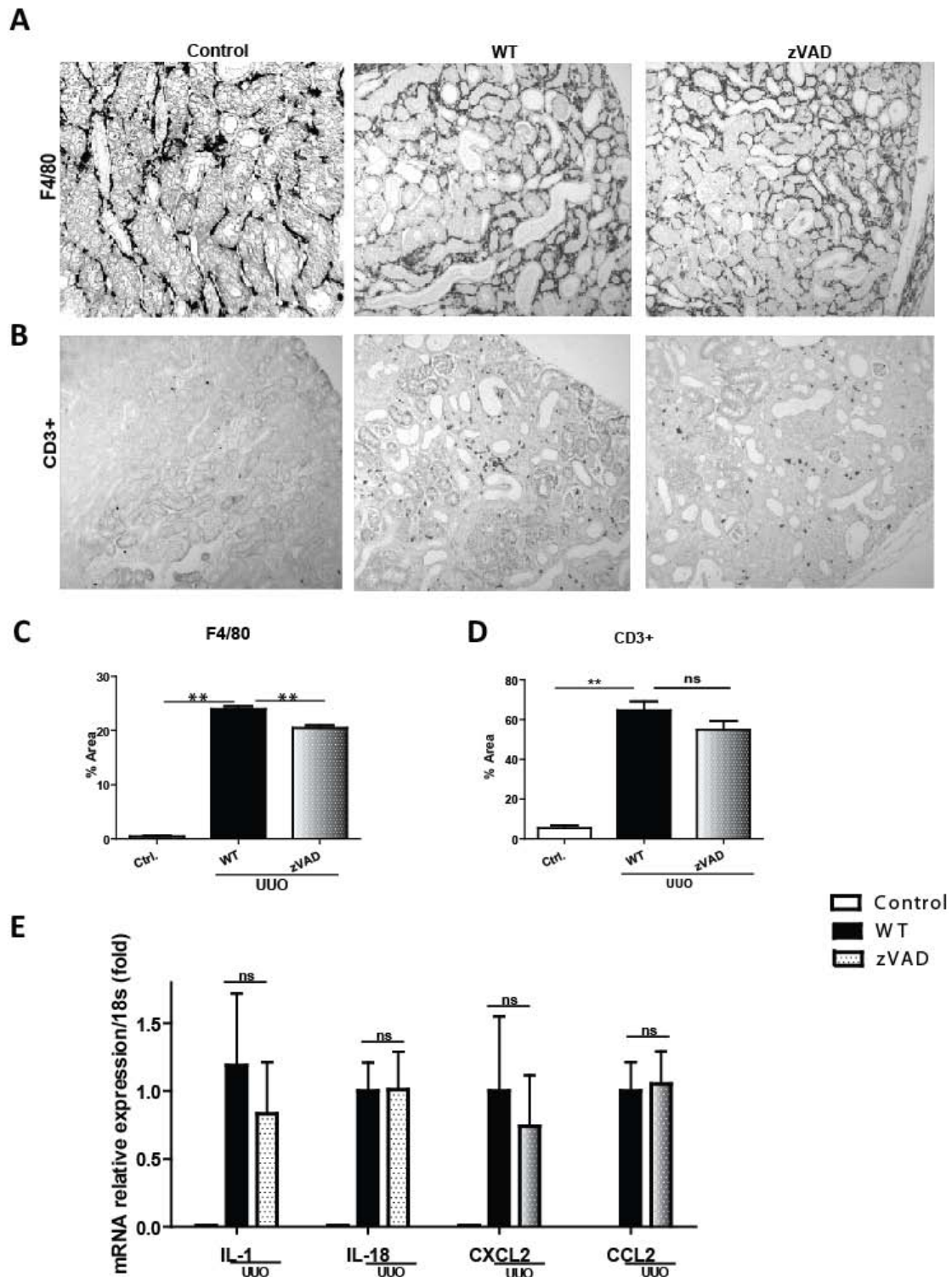


Figure 21: Caspase inhibition reduces renal inflammation after UUO. C57BL/6 mice from WT (n = 7) and zVAD-treated (n = 7) mice underwent UUO surgery and were sacrificed at day 10. Kidney sections of mice without UUO (n = 7) were used as control. **(A)** Immunohistochemistry of macrophage/monocyte marker F4/80 in WT, zVAD-treated and control kidneys. **(B)** Immunohistochemistry of T-lymphocyte marker CD3+ in WT, zVAD-treated and control kidneys. **(C)** Quantification of F4/80 positivity in kidney sections (results in mean % area \pm SEM). Significantly less positivity of F4/80 in zVAD-treated mice compared to WT. **(D)** Quantification analysis of CD3 positivity in kidney sections (results in mean % area \pm SEM). Here, no significant differences are observed between groups after UUO. **(E)** MRNA expression of proinflammatory cytokines *pro-IL-1 β* , *pro-IL-18*, and inflammation markers *Cxcl2* and *Ccl2* in kidneys of WT and zVAD-treated mice after 10 days UUO show no significant difference between groups. Gene expression is shown as x-fold increase of the target gene over the 18s mRNA expression. These results represent the mean \pm SEM of one out of two independent experiments. Abb.: Ctrl: control mice, WT: wild type mice, zVAD: treatment with pan-caspase inhibitor zVAD. ns: not significant. * $p < 0.05$, ** $p < 0.01$.

3.2.1.4 Caspase inhibition ameliorates, but does not protect mice from tubulointerstitial fibrosis after UUO

Next, we evaluated whether Casp-1-inhibition and therefore, the inability of the NLRP3 inflammasome to release active IL-1 β resulted in the reduction of renal interstitial fibrosis upon UUO. To address this, immunohistochemistry of the myofibroblasts marker α -SMA and the ECM protein collagen I was evaluated in kidney sections of WT and zVAD-treated mice after 10 days UUO (Figure 22 A-C). Quantification of α -SMA positivity revealed a significantly reduced expression of α -SMA in zVAD-treated mice compared to the WT group (Figure 22 C left). However, the collagen I stainings showed no significant difference between the WT and zVAD-treated mice (Figures 22 C right). Although Casp-1 inhibition with zVAD showed some level of reduction in immunohistochemical α -SMA expression, this was not as pronounced as in *Nlrp-3*- and *Asc*-deficient mice, as shown in figure 19. Western blot analysis of α -SMA protein expression revealed significantly less expression of α -SMA in the kidneys of *Nlrp-3*-deficient mice compared to the WT and the zVAD-treated group (Figure 22 D and F). Finally, mRNA expression profiling of the fibrotic markers *α -SMA*, *collagen I*, *vimentin*, *CTGF* and *VEGF* in kidneys of zVAD-treated and WT mice revealed no significant difference between these two groups (Figure 22 E). Taken together, our results suggest that Casp-1 inhibition ameliorates renal interstitial fibrosis upon UUO, but to a less extent compared to the protective effect observed in *Nlrp-3*-deficient mice. These observations suggest an additional inflammasome-independent role for NLRP3 in the development of renal interstitial fibrosis upon UUO.

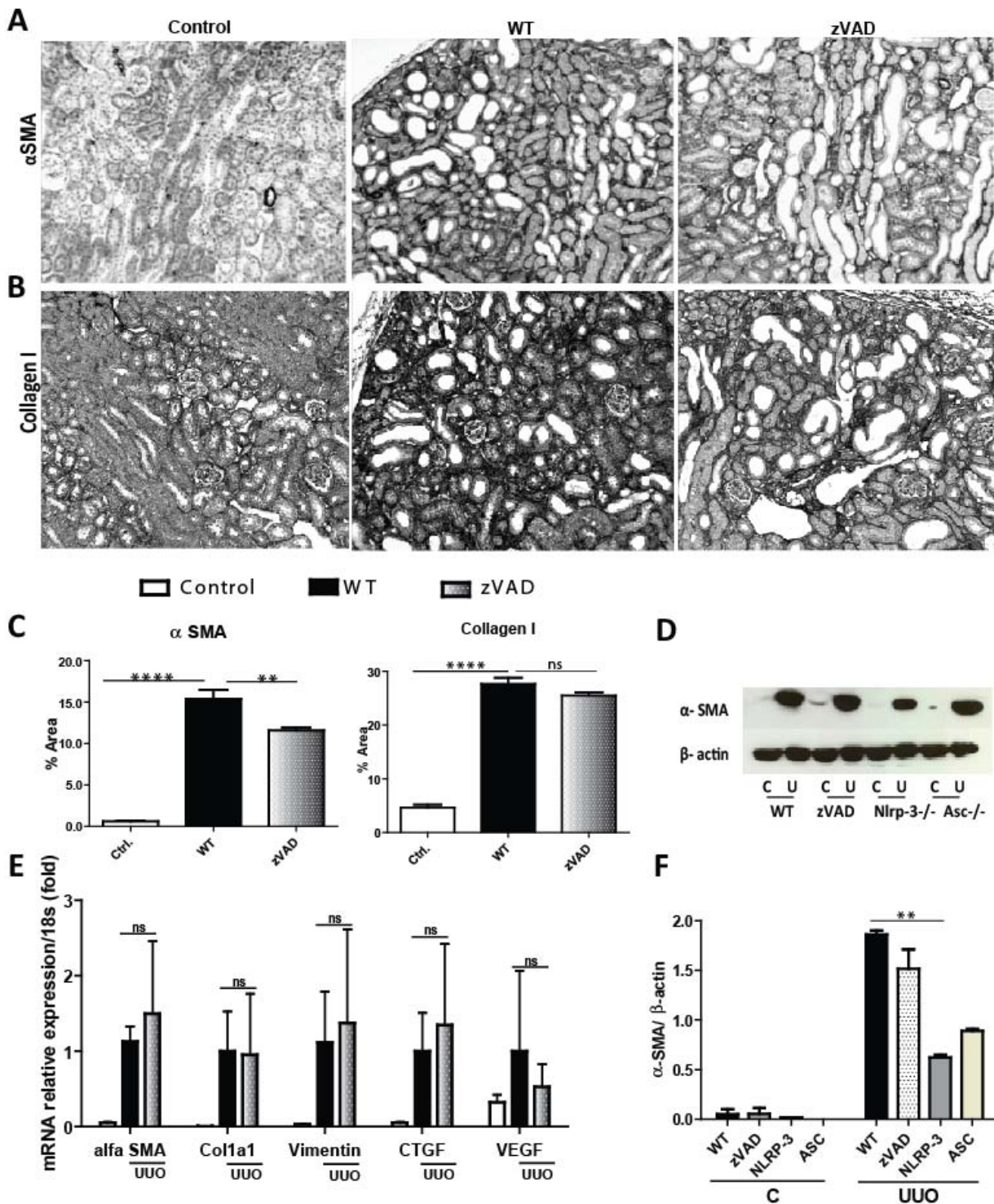


Figure 22: Caspase 1 inhibition ameliorates, but does not protect mice from tubulointerstitial fibrosis after UUU. C57BL/6 mice from WT (n = 7) and zVAD-treated (n = 7) mice underwent UUU surgery and were sacrificed at day 10. Kidney sections of mice without UUU (n = 7) were used as control. (A) Immunohistochemistry of myofibroblast marker α -SMA and (B) collagen I. (C) Quantification analyses of the α -SMA and collagen I positive areas in kidney sections after UUU (results in mean area % \pm SEM). No significant difference is observed between the WT and zVAD-treated group. (D) Western blot analysis of α -SMA expression in WT, zVAD-treated, *Nlrp-3*^{-/-} and *Asc*^{-/-} mouse kidneys. (E) Quantification analysis reveals significant less expression of the protein in the *Nlrp-3*^{-/-} and *Asc*^{-/-} group. (F) MRNA expression levels of profibrotic markers α -SMA, *coll1a1*, *vimentin*, *CTGF* and *VEGF* reveals no significant difference between WT and zVAD-treated groups. Gene expression is shown as x-fold increase of the target gene over the 18s mRNA expression. These results represent one out of two independent experiments. Abb.: C: contra lateral, U: UUU, Ctrl: control mice, WT: wild type mice, zVAD: treatment with pan-caspase inhibitor zVAD. *p<0.05, **p<0.01.

3.1.1.6 NLRP3, but not Casp-1, modulates TGF- β 1 signaling

The above-described results suggest an inflammasome-independent role for NLRP3 in renal interstitial fibrosis. It is known that the leading mechanism for the development of renal interstitial fibrosis involves TGF- β 1 signaling and that the expression of several fibrotic markers is enhanced upon secretion of TGF- β 1 [120]. One possible explanation for the protection from renal interstitial fibrosis in *Nlrp-3*-deficient mice could be an interaction between NLRP-3 and TGF- β 1 signaling. To address this, we evaluated the expression of different genes involved in TGF- β 1 signaling in kidneys of WT, *Nlrp-3*-deficient and zVAD-treated mice. The mRNA expression levels of *Tgf- β 1*, *Tgf β RI* and R-SMADs (*Smad 2* and *Smad 3*) were significantly higher in WT and zVAD-treated mice after UUO compared to the controls. No difference, however, was noted between WT and zVAD-treated mice. The lack of *Nlrp-3* resulted in a decrease in mRNA expression of these genes compared to the WT and zVAD-treated group, although no significance was observed (Figure 23 A).

We then hypothesized that the inflammasome component NLRP-3 might have a direct relation with TGF- β 1 signaling. This has been suggested in other studies from our group [153]. Western blot analysis of SMAD 2/3 and phosphorylated SMAD 2 in WT, zVAD-treated and *Nlrp-3*-deficient mouse kidneys were performed. WT, zVAD-treated and *Nlrp-3*-deficient mouse kidneys revealed no difference in protein expression of SMAD 2/3 after UUO surgery. Nevertheless, protein expression of phosphorylated SMAD 2 was significantly reduced in *Nlrp-3*-deficient mice compared to the WT and zVAD-treated groups (Figures 23 B-D). These results suggest that NLRP-3, and not the NLRP-3 inflammasome activation, regulates SMAD 2 phosphorylation in mice after 10 days UUO, and therefore reducing tubulointerstitial fibrosis.

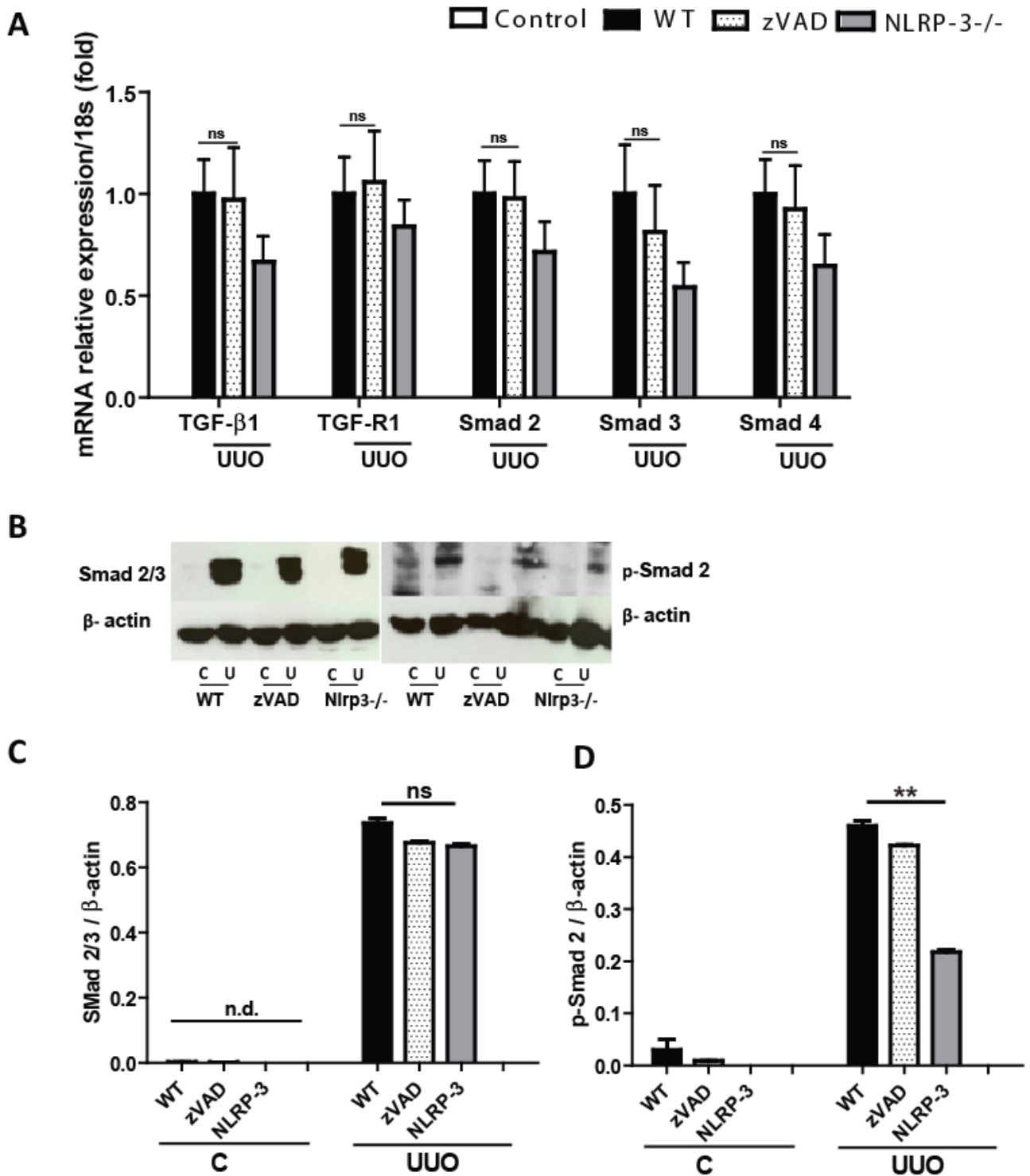


Figure 23: NLRP3 but not caspase-1 modulates TGF- β 1 signaling. C57BL/6 mice from WT (n = 7) and zVAD-treated (n = 7) mice underwent UUO surgery and were sacrificed at day 10. Kidney sections of mice without UUO (n = 7) were used as control. (A) mRNA expression levels of *Tgf- β 1*, *Tgf β RI*, *Smad2*, *Smad 3* and *Smad 4* in kidneys in WT, zVAD-treated mice and *Nlrp3*-/- mice after 10 days UUO. Gene expression is shown as x-fold increase of the target gene over the 18s mRNA expression. (C) Western blot analysis of Smad 2/3 protein expression and phosphorylated Smad 2 in WT, zVAD-treated and *Nlrp3*-deficient mice after 10 days UUO compared with contra lateral kidneys respectively. (D) Quantification of Smad 2/3 protein expression relative to β -actin expression in western blot. (E) Quantification of phosphorylated Smad 2 protein expression relative to β -actin expression in western blot. These results represent the mean \pm SEM of one out of two independent experiments. Abb.: C: contra lateral, U: UUO, Ctrl: control mice, WT: wild type mice, zVAD: treatment with pan caspase inhibitor zVAD. *p<0.05, **p<0.01.

3.1.2 Chronic oxalate nephropathy model

The UO animal model does not mimic human chronic kidney disease, as it only assesses the renal pathological features and none of the functional abnormalities. Therefore, we designed an alternative experiment using the hyperoxaluria and nephrocalcinosis-induced CKD animal model. This model uses a high-soluble oxalate diet in mice to induce renal disease. It mirrors human CKD more closely, as it leads to structural as well as functional alterations of advanced kidney disease. Recent studies from our group demonstrated that this model is appropriate for studying CKD in C57BL/6 mice, causing also the uremic and cardiovascular complications that are observed in CKD patients [163]. The next set of experiments was performed to evaluate the role of the inflammasome components NLRP3 and ASC in the chronic oxalate diet-induced CKD murine model.

3.1.2.1 High oxalate diet-induced CKD promotes expression of inflammasome components

In order to assess inflammasome activation upon a high oxalate diet-induced CKD, we first analyzed mRNA expression levels of the inflammasome components *Nlrp-3*, *Asc*, *Casp-1* and *pro-IL-1 β* in kidneys of WT mice after 14 days of a high oxalate diet in comparison to control mice, which received a normal diet. As shown in figure 24 A the mRNA expression levels of the inflammasome components were significantly up-regulated in hyperoxaluric mice compared to control mice, suggesting an important role of the NLRP3 inflammasome in hyperoxaluria and nephrocalcinosis-induced CKD.

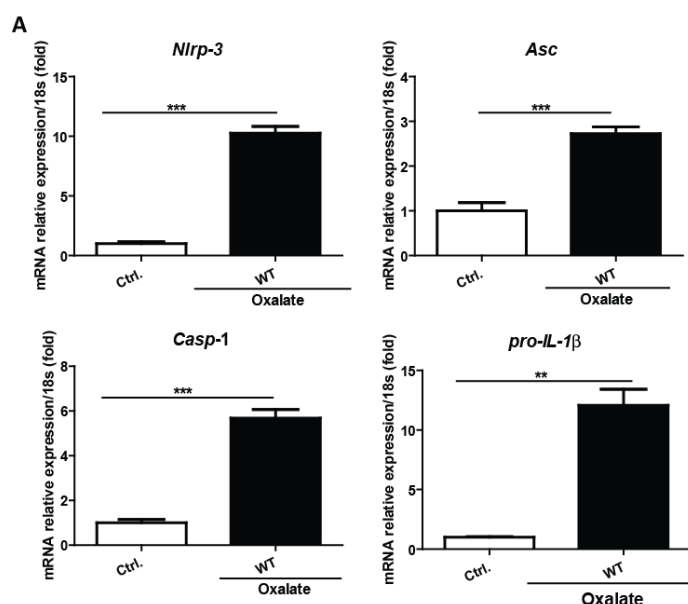


Figure 24: NLRP3-inflammasome axis is up-regulated in high-oxalate induced CKD. C57BL/6 WT mice (n = 4) were fed with a high-soluble oxalate diet for 14 days. Controls without oxalate diet (n = 4) were used as reference. (A) The mRNA expression levels of inflammasome components *Nlrp-3*, *Asc*, *Casp-1* and *pro-IL-1 β* are significantly increased in WT mice after 14 days of oxalate diet compared to control mice (without an oxalate diet). Gene expression is shown as x-fold increase of the target gene over the 18s mRNA expression. These results represent the mean \pm SEM of one out of two independent experiments. Abb.: Ctrl: control mice, WT: wild type mice, *Nlrp-3*^{-/-}: *Nlrp-3* deficient mice, *Asc*^{-/-}: *Asc* deficient mice *p<0.05, **p<0.01.

3.1.2.2 *Nlrp-3*- and *Asc*-deficient hyperoxaluric mice do not develop oxalate nephropathy

Recently published data had suggested that NLRP3 plays an important role in the development of hyperoxaluria induced CKD [177]. Nevertheless, mice lacking *Nlrp-3* were unable to develop nephrocalcinosis upon a 14-day oxalate-rich diet [177]. Our previous mRNA expression data showed that the NLRP3 inflammasome axis is up-regulated in WT mice after a 14-day high-soluble oxalate diet. To verify the role of NLRP3 and ASC in hyperoxaluria-induced CKD, age and gender-matched C57BL/6 WT, *Nlrp-3*- and *Asc*-deficient mice were fed a high-soluble oxalate diet for 14 days or received a control diet, without oxalate.

Initial assessment of the kidney function parameters plasma BUN and plasma creatinine on day 0 and day 14 (prior to sacrifice), revealed significantly higher levels in WT mice on day 14 compared to controls, whereas *Nlrp-3*- and *Asc*-deficient mice showed no elevation of these parameters. This finding was consistent with the previously published data on *Nlrp-3*-deficient mice [177] and further corroborated it for *Asc*-deficient mice (Figure 25 A). In order to exclude a possible protection of these mice due to altered intestinal oxalate absorption, oxalate concentration levels were measured in plasma and urine of WT, *Nlrp-3*- and *Asc*-deficient mice on day 0 and day 14. Quantification analysis of plasma oxalate levels showed no significant difference on day 14 between all groups with a high oxalate diet. Urinary oxalate excretion, on the other hand, was significantly higher in *Nlrp-3*-deficient mice compared to WT mice. *Asc*-deficient mice showed a similar trend as the *Nlrp-3*-deficient group, although no significant difference was achieved ($p=0,057$) (Figure 25 A). These findings suggest that there is no alteration in the intestinal oxalate intake of the mutant mouse strains. Subsequently, intrarenal crystal deposition was assessed using Pizzolato staining. Here, kidney sections of oxalate-fed WT mice revealed a marked intrarenal crystal deposition compared to the control group. Whereas *Nlrp-3*- and *Asc*-deficient mice did not display any crystal deposition (Figure 25 B and C).

Renal injury and inflammation: The level of tubular injury in mice after 14 days of a high oxalate diet was assessed using tubular injury scoring in PAS-stainings from kidney sections. WT mice presented a marked tubular injury with a significant damage of the tubular architecture compared to the control group (Figure 26 A and B). In contrast, *Nlrp-3*- and *Asc*-deficient mice were completely protected from renal injury (Figure 26 B). mRNA expression of the kidney injury marker *Kim-1* significantly increased in WT mice compared to the control group, an expression which was absent in both mutant mouse strains (Figure 26 C). Additionally, immunostainings of the macrophage/monocyte marker F4/80 and the T-lymphocyte marker CD3 showed a significant

infiltration of these cells in hyperoxaluric WT mice compared to the controls (Figure 26 D-F). No infiltration of immune cells was observed in *Nlrp-3*^{-/-} and *Asc*^{-/-} mouse kidneys.

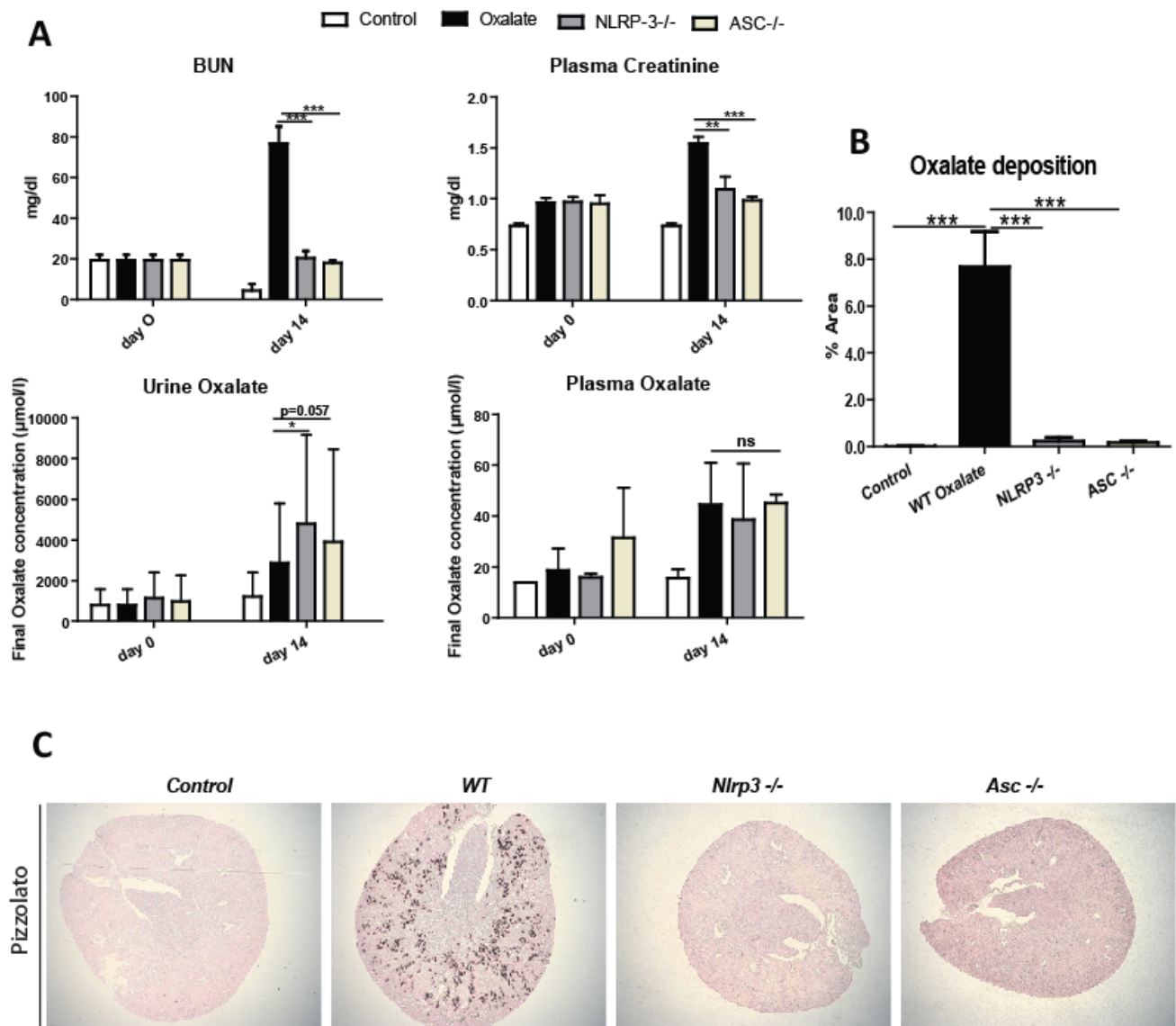


Figure 25: A high-soluble oxalate-rich diet does not induce hyperoxaluria-related CKD in mice lacking *Nlrp-3* or *Asc* despite high levels of plasma and urine oxalate. C57BL/6 mice of WT (n = 4), *Nlrp-3*^{-/-} (n = 4) and *Asc*^{-/-} (n = 4) were fed with high soluble oxalate diet for 14 days. Controls without oxalate diet (n = 4) were used as reference. **(A)** BUN (left) and Creatinine (right) in mg/ml were measured in the plasma of mice at day 0 previous to oxalate intake and day 14 (results in mean \pm SEM). **(B)** Oxalate concentration in $\mu\text{mol/l}$ was measured in plasma (left) and urine (right) of mice at day 0 previous to oxalate intake and day 14 (results in mean \pm SEM). **(C)** Crystal deposition shown with Pizzolato staining of kidney sections from mice after 14 days of high oxalate diet was compared to controls. **(D)** Quantification of crystal deposition in Pizzolato staining after 14 days oxalate diet (results in % area \pm SEM). No crystal deposition is observed in *Nlrp-3*^{-/-} and *Asc*^{-/-} mouse kidneys. These results represent one out of two independent experiments. Abb.: Ctrl: control mice, WT: wild type mice, *Nlrp-3*^{-/-}: *Nlrp-3* deficient mice, *Asc*^{-/-}: *Asc* deficient mice *p<0.05, **p<0.01.

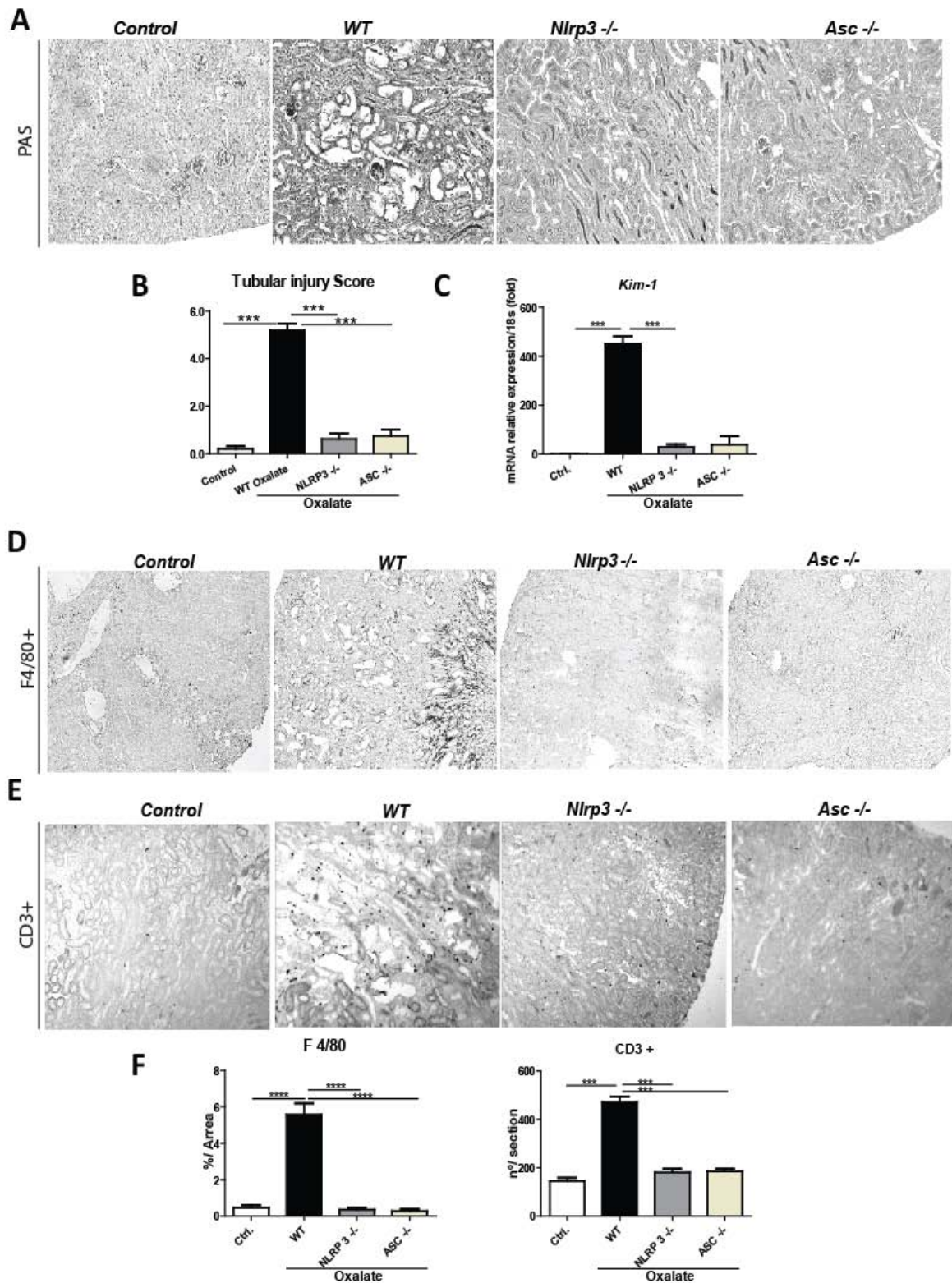


Figure 26: *Nlrp-3*- and *Asc*-deficient mice do not develop hyperoxaluria-related CKD, and hence no renal injury and inflammation. C57BL/6 mice of WT (n = 4), *Nlrp-3*^{-/-} (n = 4) and *Asc*^{-/-} (n = 4) were fed with a high-soluble oxalate diet for 14 days. Controls without oxalate diet (n = 4) were used as reference. **(A)** PAS-stainings from kidney sections of Ctrl, WT, *Nlrp-3*^{-/-} and *Asc*^{-/-} mice. **(B)** Quantification analysis using tubular injury scoring show a complete protection in *Nlrp-3*^{-/-} and *Asc*^{-/-} mice compared to WT mice. **(C)** MRNA expression levels of kidney injury marker *Kim-1* was quantified with RT-PCR. Gene expression is shown as x-fold increase of the target gene over the 18s mRNA expression. **(D)** Immunohistochemistry of monocyte/macrophage marker F/480 and **(E)** T-lymphocyte marker CD3 of kidney sections from ctrl, WT, *Nlrp-3*^{-/-} and *Asc*^{-/-}. **(F)** Quantification analysis of F/480 and CD3 positive areas respectively (results in mean area % ± SEM). These results represent the mean ± SEM of one out of two independent experiments. Abb.: Ctrl: control mice, WT: wild type mice, *Nlrp-3*^{-/-}: *Nlrp-3* deficient mice, *Asc*^{-/-}: *Asc* deficient mice. *p<0.05; **p<0.01

Interstitial fibrosis: Renal interstitial fibrosis was assessed using immunohistochemistry of α -SMA and collagen I in kidney sections of mice after 14 days of a high oxalate diet. Here, a marked deposition of these proteins was observed in the renal interstitium of WT mice compared to the controls. Whereas *Nlrp-3*- and *Asc*-deficient mice were completely protected from deposition of both matrix proteins (Figures 27 A-C). Accordingly, expression profiling of the fibrosis markers *fibronectin*, *coll1a1* and *col4a1* showed a significantly higher expression in oxalate-fed WT mice compared to controls, *Nlrp-3*^{-/-} and *Asc*^{-/-} mouse kidneys. mRNA expression of the epithelial marker *e-cadherine* was highly expressed in *Nlrp-3*-deficient mice compared to the WT mice, which correlated with the reduced tubular damage and preserved epithelial architecture (Figure 27 D).

These findings showed that hyperoxaluric mice lacking *Nlrp-3* or *Asc* do not display intrarenal calcium oxalate crystal deposition after a high-soluble oxalate diet, and consequently do not develop nephrocalcinosis-related CKD. This phenomenon was observed despite elevated plasma and urine oxalate levels in both mutant mouse strains, thus excluding an alteration in intestinal oxalate absorption.

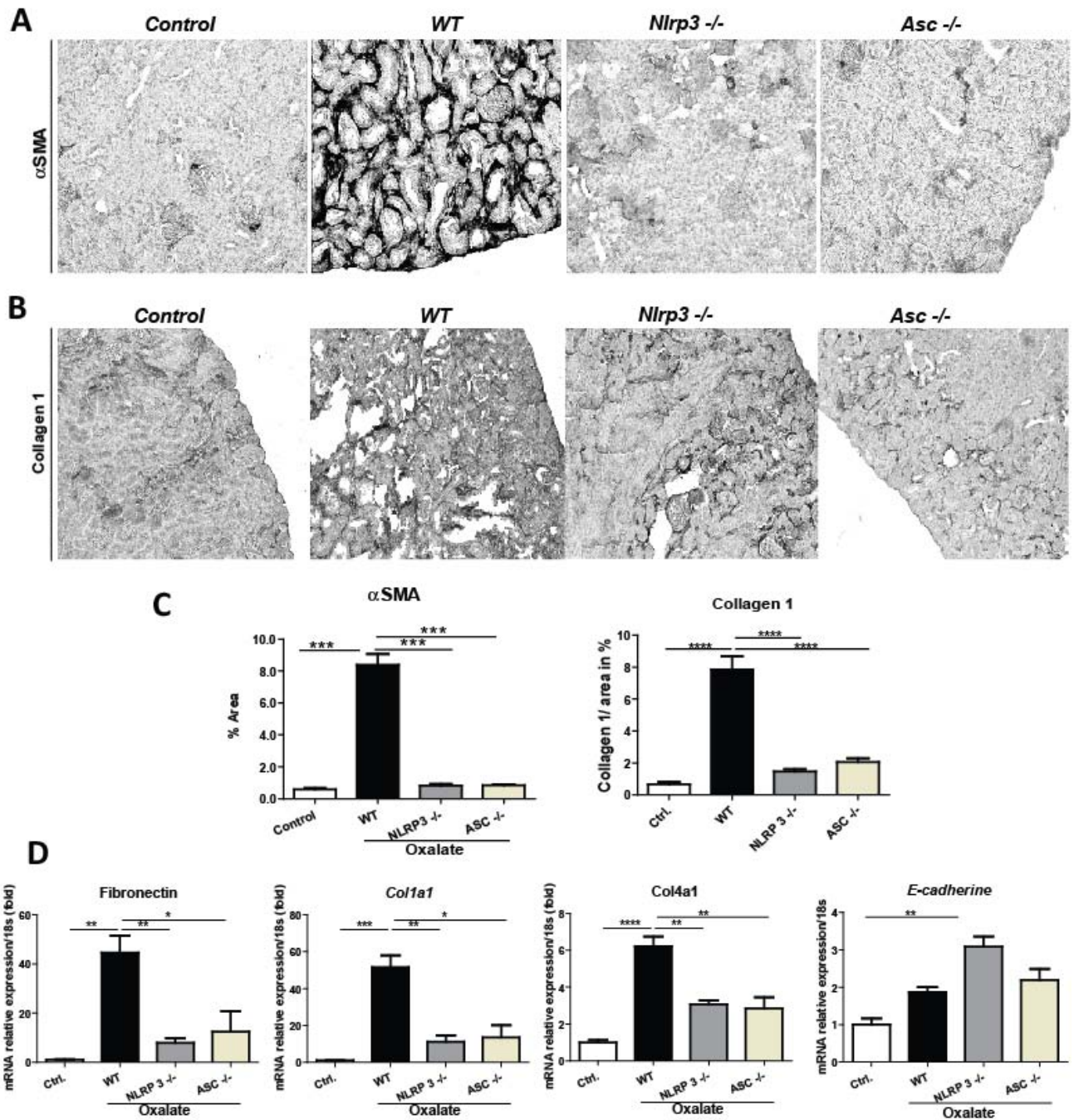


Figure 27: Mice lacking *Nlrp-3* or *Asc* do not develop hyperoxaluria-related CKD and thus, no renal tubulointerstitial fibrosis. C57BL/6 mice of WT (n = 4), *Nlrp-3^{-/-}* (n = 4) and *Asc^{-/-}* (n = 4) were fed with a high soluble oxalate diet for 14 days. Controls without oxalate diet (n = 4) were used as reference. **(A)** Immunohistochemical analysis of myofibroblasts marker α -SMA and **(B)** collagen I from kidney sections and **(C)** quantification analysis of α -SMA and collagen I positivity shows increased deposition of both proteins in WT mouse kidneys compared to controls, *Nlrp-3^{-/-}* and *Asc^{-/-}* mice. Results are shown in mean of % area \pm SEM. **(D)** MRNA expression levels of *fibronectin*, α -SMA, *coll1a1*, *col4a1*, epithelial marker *e-cadherine* were quantified with RT-PCR. Gene expression is shown as x-fold increase of the target gene over the 18s mRNA expression. These results represent the mean \pm SEM of one out of two independent experiments. Abb.: Ctrl: control mice. * $p < 0.05$, ** $p < 0.01$; *** $p < 0.001$.

3.1.2.3 Inhibition of IL-1 receptor with anakinra does not improve renal function in mice with hyperoxaluria-induced CKD

The assessment of the NLRP3 inflammasome using the hyperoxaluria and nephrocalcinosis-induced CKD mouse model in *Nlrp-3*- and *Asc*-deficient mice was limited due to the lack of intrarenal calcium oxalate crystal deposition in both mutant mouse strains. Therefore, a new experiment was designed. C57BL/6 mice were fed a high-soluble oxalate diet while receiving a treatment with the IL-1 receptor antagonist anakinra or a vehicle. This recombinant IL-1r antagonist inhibits the effects of cytokines from the IL-1 family and is extensively used therapeutically for the treatment of autoimmune diseases such as rheumatoid arthritis. In order to evaluate the role of the NLRP3 inflammasome-dependent $IL-1\beta$ activation in nephrocalcinosis-mediated CKD, C57BL/6 hyperoxaluric mice were either treated with the recombinant IL-1 receptor antagonist anakinra or a vehicle.

Initial assessment of kidney function parameters in plasma of vehicle and anakinra-treated mice showed significantly higher plasma BUN levels in anakinra-treated mice after 14 days of a high oxalate diet compared to the vehicle group. On the other hand, plasma creatinine levels in the anakinra-treated mice were slightly reduced compared to the vehicle group after 14 days of high oxalate diet (Figure 28 A). To rule out an altered intestinal oxalate intake due to anakinra treatment, plasma and urine oxalate concentrations were measured on day 0 and day 14. Plasma oxalate levels showed no significant differences between the vehicle- and anakinra-treated mice (Figure 28 B). On the other hand, urinary excretion of oxalate was significantly diminished in anakinra-treated mice compared to the vehicle group (Figure 28 B).

Subsequently, crystal deposition was assessed using Pizzolato staining in kidney sections of hyperoxaluric mice and compared to controls. Quantification analysis revealed a marked deposition of calcium oxalate crystals in kidneys of both vehicle- and anakinra-treated mice with no significant difference between the groups (Figure 28 C).

These results show that in contrast to the mutant mouse strains, IL-1 receptor inhibition does not influence intrarenal calcium oxalate crystal deposition. More importantly, these findings suggest that inhibition of IL-1 receptor does not protect mice from renal function impairment in nephrocalcinosis-induced CKD.

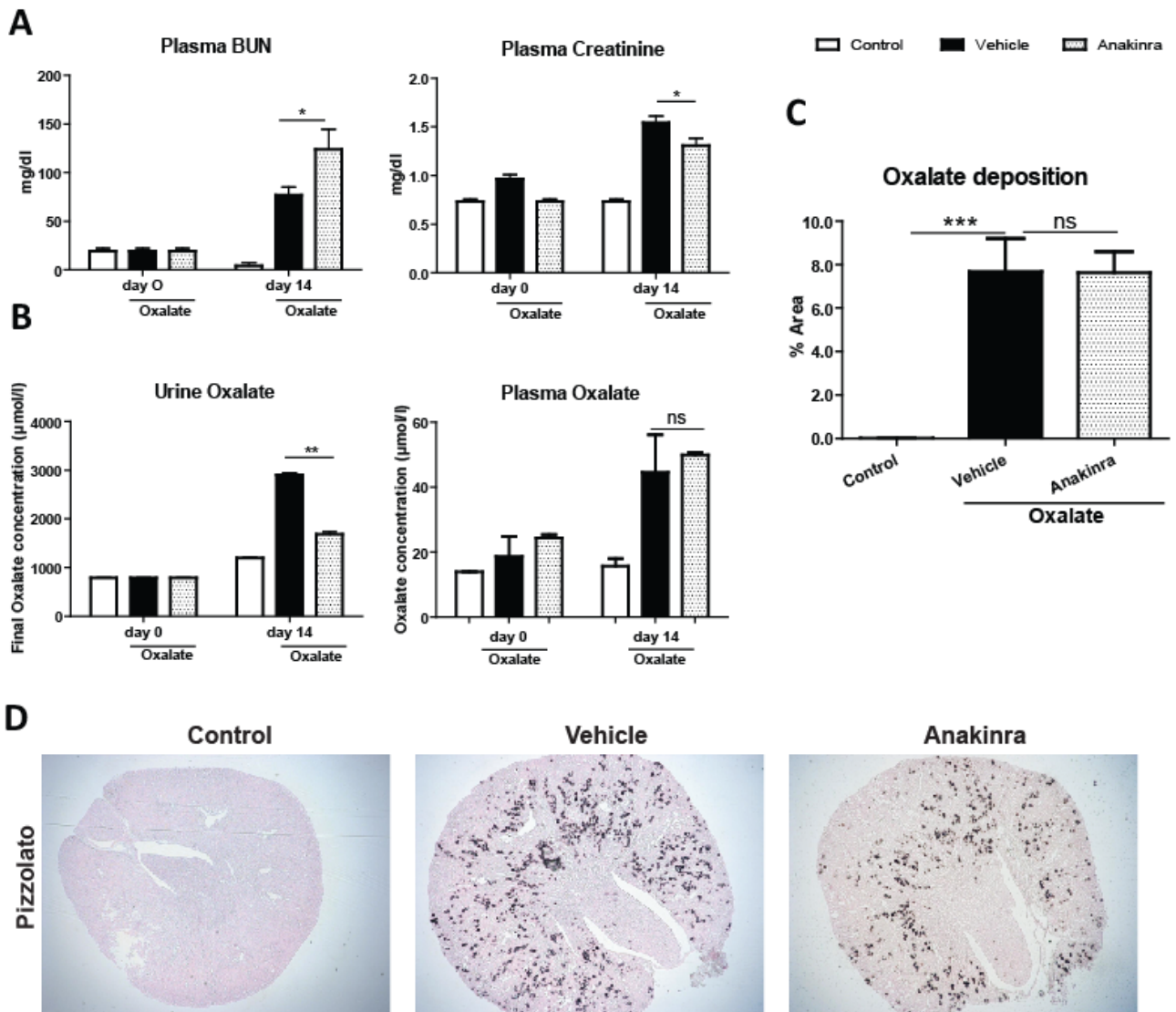


Figure 28: II-1 receptor inhibition does not protect mice from hyperoxaluria-induced CKD. C57BL/6 mice received a vehicle (n = 4) or anakinra (n = 4) treatment and were fed a high soluble oxalate diet for 14 days. Mice without oxalate diet were used as controls (n = 4). **(A)** BUN (left) and plasma creatinine (right) in mg/ml were measured in plasma of mice at day 0 previous to oxalate intake and day 14 (results in mean ± SEM). **(B)** Oxalate concentration in μmol/l was measured in plasma (left) and urine (right) of mice at day 0 previous to oxalate intake and day 14 (results in mean ± SEM). **(C)** Quantification analysis of crystal deposition in kidney sections after 14 high-soluble oxalate diet. **(D)** Pizzolato staining of kidney sections from mice after 14 days of high oxalate diet was compared to controls. These results represent the mean ± SEM of one out of two independent experiments. Abb.: Ctrl: control mice, WT: wild type mice, BUN: blood urea nitrogen *p<0.05, **p<0.01;***p<0.001

3.1.2.4 IL-1 receptor inhibition does not protect mice from kidney injury in hyperoxaluria-induced CKD

Renal pathological features were assessed in the vehicle- and anakinra-treated mice after 14 days of a high-soluble oxalate diet compared to a control diet. PAS staining of kidney sections revealed increased renal injury in both vehicle- and anakinra-treated mice compared to controls (Figure 29 A and B). Pathological scoring revealed no significant differences between the vehicle- and the anakinra-treated groups (Figure 29 B). The mRNA expression of the kidney injury marker *Kim-1* was significantly increased in both vehicle- and anakinra-treated mice compared to controls but no significant difference was evidenced between the hyperoxaluric groups (Figure 29 C). These results suggest that IL-1 receptor inhibition does not protect mice from renal injury upon hyperoxaluria and nephrocalcinosis-induced CKD.

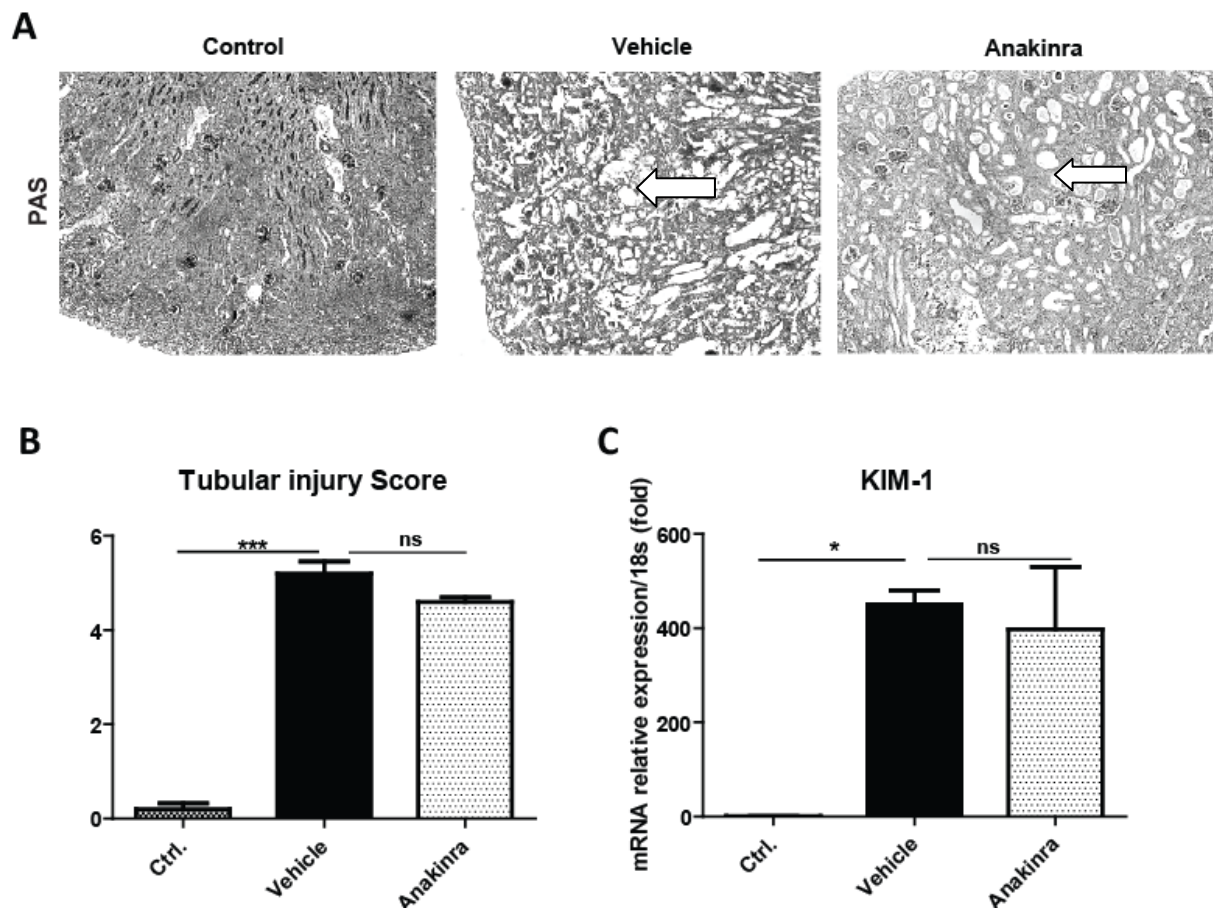


Figure 29: Anakinra treatment does not protect mice from tubular injury. C57BL/6 mice of WT (n = 4) were given a vehicle (n = 4) and anakinra (n = 4) treatment simultaneously to a high-soluble oxalate diet for 14 days. Mice without oxalate diet (n = 4) were used as controls. (A) PAS stainings of kidney sections from ctrl, vehicle- and anakinra-treated mice. Arrows indicate dilated and injured tubules. (B) Quantification analysis using tubular injury scoring of kidney sections after 14 days high-soluble oxalate diet. (C) mRNA expression level of kidney injury marker *Kim-1* was quantified using RT-PCR. Results are shown as *Kim-1* to *18s* ratio in fold increase. These results represent one out of two independent experiments. Abb.: Ctrl: control mice, WT: wild type mice, *p<0.05, **p<0.01; ***p<0.001

3.1.2.5 IL-1 receptor inhibition reduces macrophage and T_h-lymphocytes infiltration in hyperoxaluria-induced CKD, but does not protect mice from renal interstitial fibrosis.

Our previous results suggested that IL-1r inhibition does not protect mice from a high oxalate diet-induced CKD.

In order to evaluate the effects of anakinra in renal inflammation, we performed immunohistochemical analysis of the macrophage/monocyte marker F4/80 and the T_h-cell receptor marker CD3 of kidney sections. These showed less F4/80+ macrophages in anakinra-treated mice compared to the vehicle-treated mice (Figure 30 A and B). In addition, T_h-cell infiltration was reduced in anakinra-treated mice compared to vehicle-treated mice. These findings indicate that anakinra treatment reduces renal inflammation in mice upon a high oxalate diet-induced CKD.

Furthermore, renal interstitial fibrosis was assessed using immunohistochemical analysis of myofibroblasts marker α -SMA and the ECM protein collagen I. Interestingly, both anakinra- and vehicle-treated mice showed a high deposition of α -SMA and collagen I in the renal interstitium (Figure 31 A-D). Quantification analysis revealed significantly less deposition of α -SMA in anakinra-treated mice compared to the vehicle-treated mice. Collagen deposition, on the other hand, was increased in anakinra-treated mice compared to the vehicle-treated group (Figure 31 C and D). Additionally, mRNA expression profiling of the profibrotic markers *α -SMA*, *coll1a1*, *col4a1*, *fibronectin*, *FSP*, *vimentin* and the epithelial marker *e-cadherin*, did not show any significant difference in their expression levels when comparing anakinra-treated vs. vehicle-treated hyperoxaluric mice. Overall, both groups showed increased expression of these markers compared to controls. Taken together, these results indicate that IL-1 receptor blockade with anakinra reduced renal interstitial inflammation in mice with a high oxalate diet-induced CKD, but this did not prevent mice from developing a progressive renal interstitial fibrosis. The findings point to an IL-1 signaling-independent mechanism in the pathogenesis of hyperoxaluria- and nephrocalcinosis-induced CKD.

To further understand the mechanisms leading to this effect, TGF- β signaling was evaluated in hyperoxaluric mice after a 14-day high-soluble oxalate diet. The mRNA expression levels of *TGF- β 1*, *TGF-R1*, *TGF-R2*, *CTGF* and *PDGF* were assessed in anakinra- and vehicle-treated mice and revealed a significant increase in both hyperoxaluric mice compared to control mice, without any significant differences between the hyperoxaluric groups (Figure 31 F). In summary, we conclude that IL-1 β -mediated IL-1receptor signaling is not essential for the development of renal interstitial fibrosis in hyperoxaluria-induced CKD.

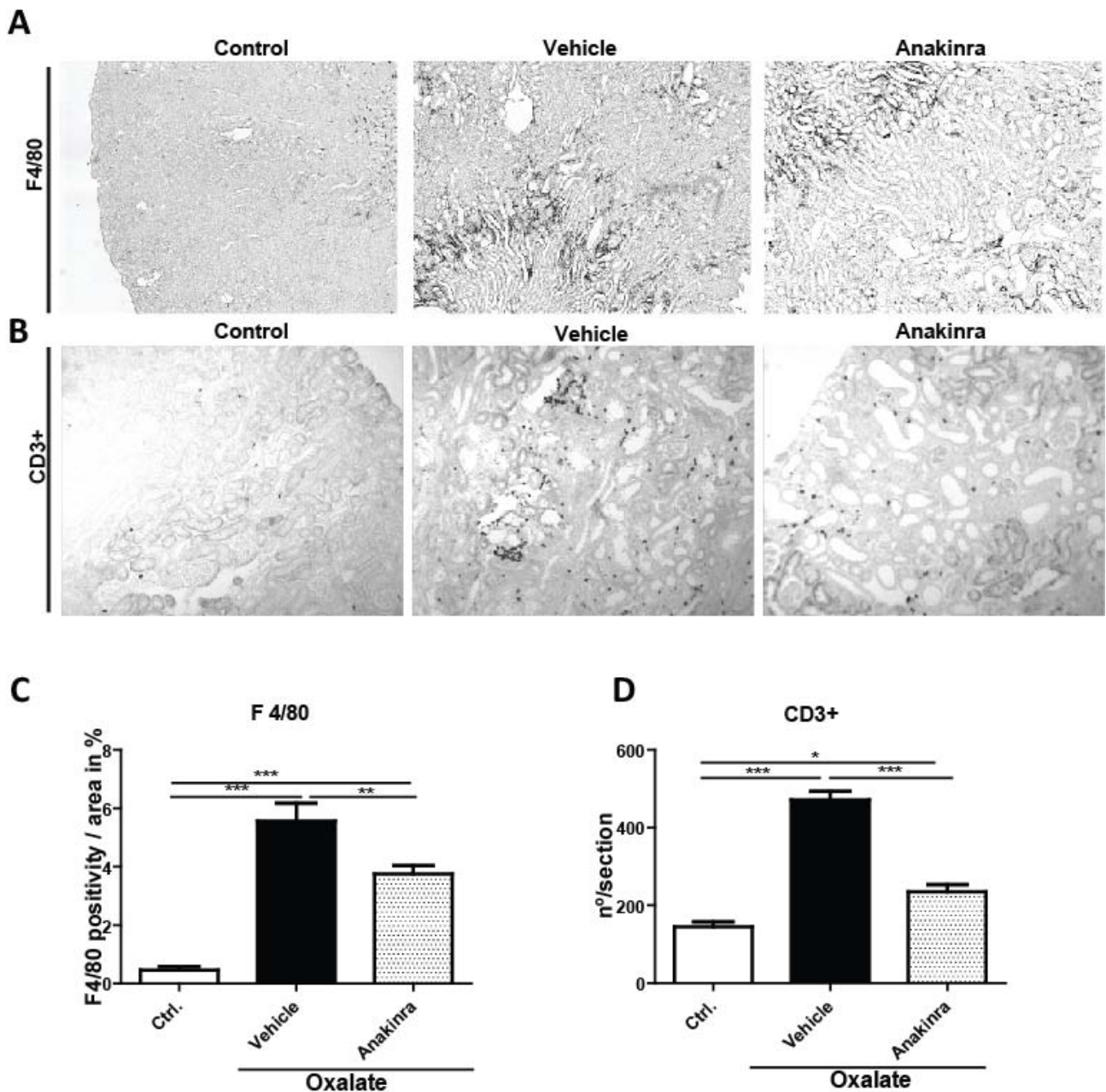


Figure 30: IL-1 receptor inhibition protects mice from renal inflammation in hyperoxaluria related CKD. C57BL/6 vehicle- (n = 4) and anakinra-treated mice (n = 4) were fed a high-soluble oxalate diet for 14 days. Mice without oxalate diet were used as controls (n = 4). **(A)** Immunohistochemical analysis of the macrophage/monocyte marker F4/80 in kidney sections and **(B)** quantification of F4/80 positivity reveals a significant reduction in macrophage deposition in the anakinra-treated group. **(C)** Immunohistochemical analysis of T-lymphocyte marker CD3 in kidney sections and **(D)** quantification of CD3 positivity (results in % area \pm SD) corroborates the previous findings. These results represent the mean \pm SEM of one out of two independent experiments. These results represent one out of two independent experiments. Abb.: Ctrl: control mice, WT: wild type mice, * $p < 0.05$, ** $p < 0.01$; *** $p < 0.001$

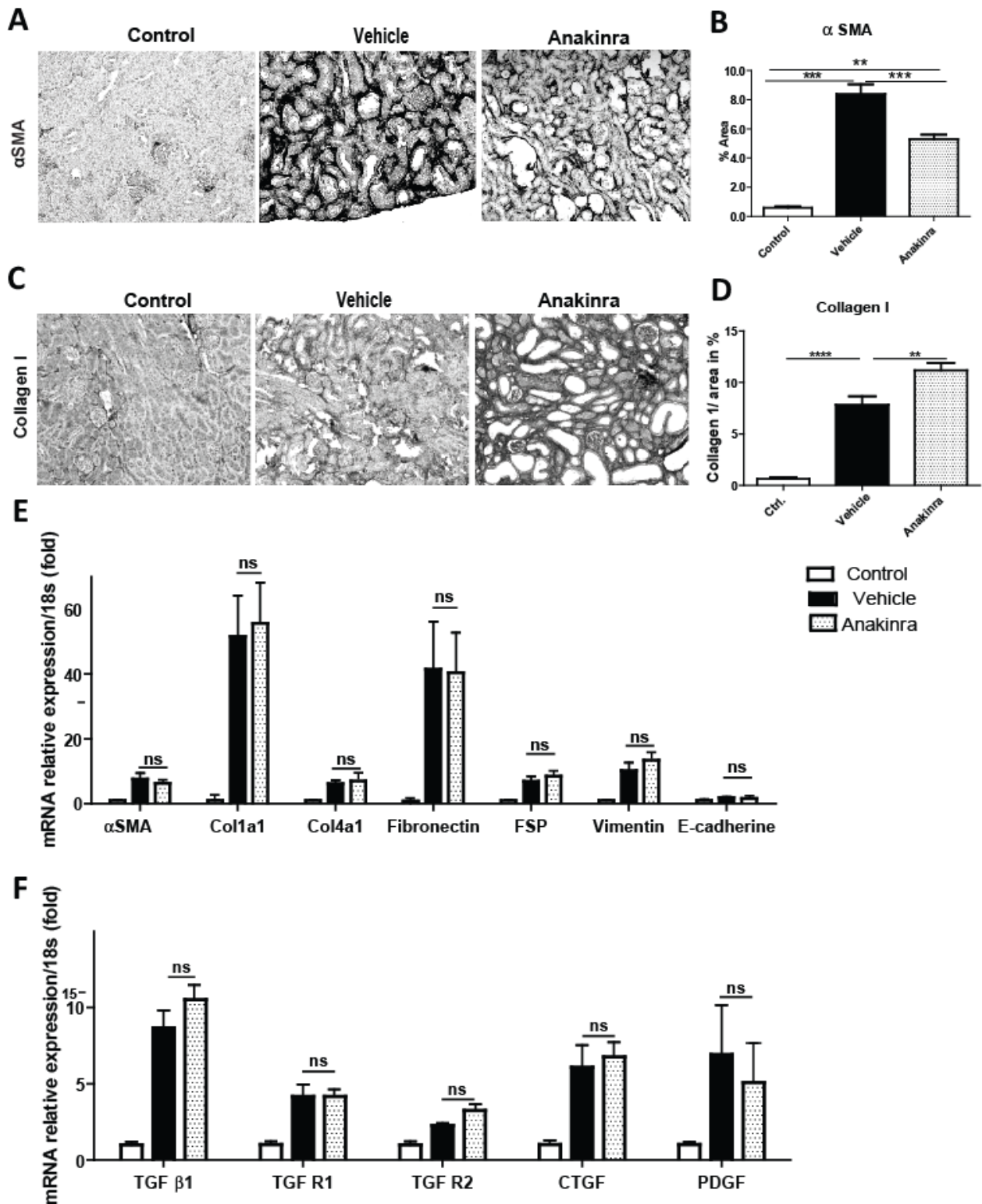


Figure 31: Il-1 receptor inhibition does not protect mice from tubulointerstitial fibrosis in hyperoxaluria-related CKD. C57BL/6 mice of vehicle- (n = 4) and anakinra-treated mice (n = 4) were fed a high soluble oxalate diet for 14 days. Mice without oxalate diet were used as controls (n = 4). (A) Immunohistochemical analysis of myofibroblasts marker α -SMA in kidney sections and (B) quantification of α -SMA positivity showed increased deposition in vehicle- and anakinra-treated mice. (C) Immunohistochemical analysis of ECM protein collagen I in kidney sections and (D) quantification of collagen I deposition show a significantly increased deposition in the anakinra-treated group. Results are shown in mean of % area \pm SEM. (E) mRNA expression levels of profibrotic markers α -SMA, *Col1a1*, *Col4a1*, *Fibronectin*, *FSP*, *Vimentin* and epithelial marker *e-cadherine* were quantified with RT-PCR. (F) MRNA expression levels of TGF- β -signaling markers *TGF- β 1*, *TGF-R1*, *TGF-R2*, *CTGF* and *PDGF* were quantified with RT-PCR. Gene expression is shown as x-fold increase of the target gene over the 18s mRNA expression. These results represent the mean \pm SEM of one out of two independent experiments. Abb.: Ctrl: control mice *p<0.05, **p<0.01, ***p<0.001 90

3.2 In vitro studies

The NLRP3 inflammasome was primarily known for its role in inflammation. Hence, current studies have mainly focused on characterizing its function in inflammatory cells such as DC's and macrophages. Our previous *in vivo* described results suggest that the NLRP3 inflammasome is also essential for the development and progression of renal fibrogenesis.

Given these observations and since fibroblasts are the main cells responsible for fibrosis, we performed several *in vitro* experiments using fibroblast (the main matrix-producing cells in fibrotic diseases) and evaluated the role of the NLRP3 inflammasome in the function of these cells.

3.2.1 NIH-3t3 fibroblast express NLRP3 and its expression augments upon stimulation with LPS and TGF- β 1

We first tested whether fibroblasts express the inflammasome component NLRP3. For this, NIH-3t3 cells were pre-treated with NLRP3 inflammasome-inducer LPS and the potent profibrotic cytokine TGF- β 1.

Western blotting and mRNA analysis of NIH-3t3 cells showed expression of *Nlrp-3* at both mRNA and protein level, which increased upon stimulation with LPS (Figure 32 A and C). Additional stimulation with mouse TGF- β 1 showed a further increase in mRNA expression of *Nlrp-3* in the NIH-3t3 cell line (Figure 32 A and B). These results demonstrated that *Nlrp-3* is expressed in LPS-stimulated NIH-3t3 cells and that this was further enhanced following TGF- β 1 stimulation.

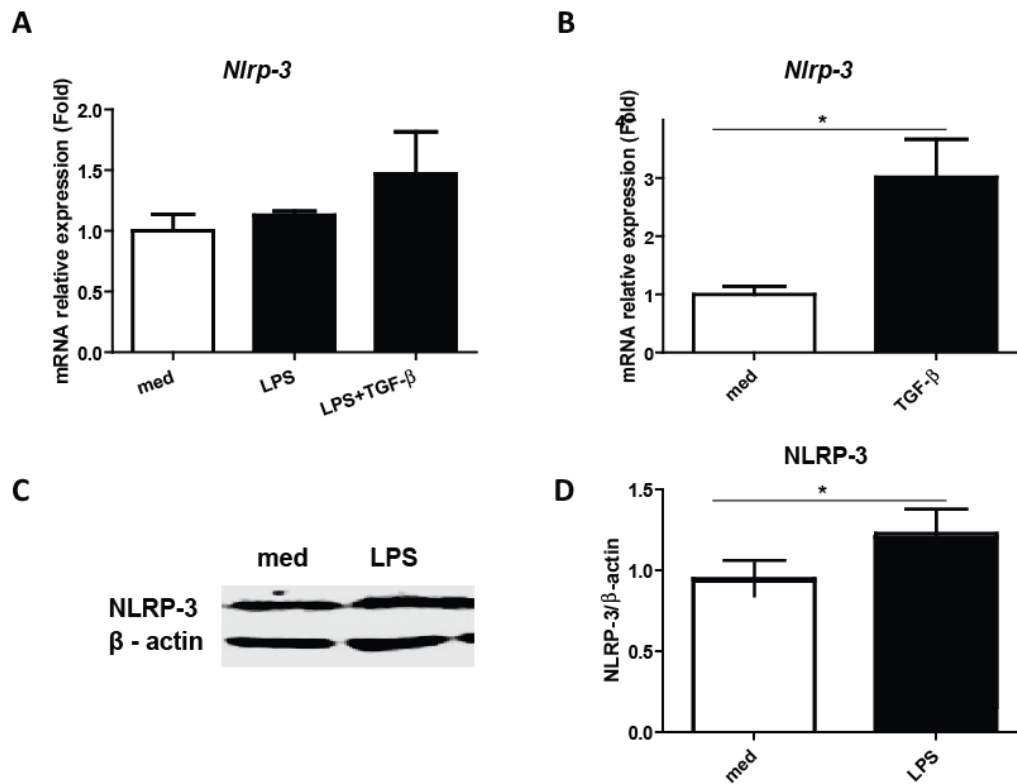


Figure 32: NIH-3t3 cells express NLRP-3 upon induction. NIH-3t3 cells were stimulated with LPS (100 ng/ml) and mTGF- β 1 (10 ng/ml) for 2 and 8 hrs respectively. **(A and B)** Total mRNA was isolated and *Nlrp-3* expression was quantified with real time polymerase chain reaction (RT-PCR). Data are expressed as *Nlrp-3/18s* ratio in fold increase. **(C)** Total protein was isolated from NIH-3t3 cells after stimulation with LPS (100 ng/ml) for 24 hrs. Nlrp-3 expression was determined by western blot analysis. β -actin was used as control. **(D)** Quantification analysis of western blotting reveals a significant increase in Nlrp-3 expression after stimulation with LPS. Results are shown as *Nlrp-3*/ β -actin ratio. These values represent one out of two independent experiments. Abb.: med: medium, LPS: lipopolysaccharide, TGF- β 1: transforming growth factor beta 1. * $p < 0.05$

3.2.2 LPS and TGF- β increased the expression of profibrotic and inflammasome genes in NIH-3t3 fibroblasts in a time-dependent manner.

Production of ECM components is the main function of fibroblasts. In order to assess whether NLRP3 is implicated in ECM production, we evaluated its expression and the expression of profibrotic markers in NIH-3t3 cells. For this, fibroblasts were stimulated with LPS and mouse TGF- β 1 simultaneously and then harvested at different time points (6, 18 and 24 hrs). mRNA expression levels of the profibrotic markers α -SMA, collagen I (*Col-1a1*), and *fibronectin* were significantly increased after 18 hrs of stimulation (Figure 33 A). This correlated with the expression of *Nlrp-3*, which also showed an expression peak after 18 hrs stimulation. However, no significant difference was achieved compared to the controls (Figure 33 B). Whereas *Asc* and *Casp-1* mRNA expression did not show the same time-dependent correlation (Figure 33 B). These results imply a positive correlation between the expression of profibrotic markers and *Nlrp-3* upon stimulation with LPS and mouse TGF- β 1 in NIH-3t3 cells.

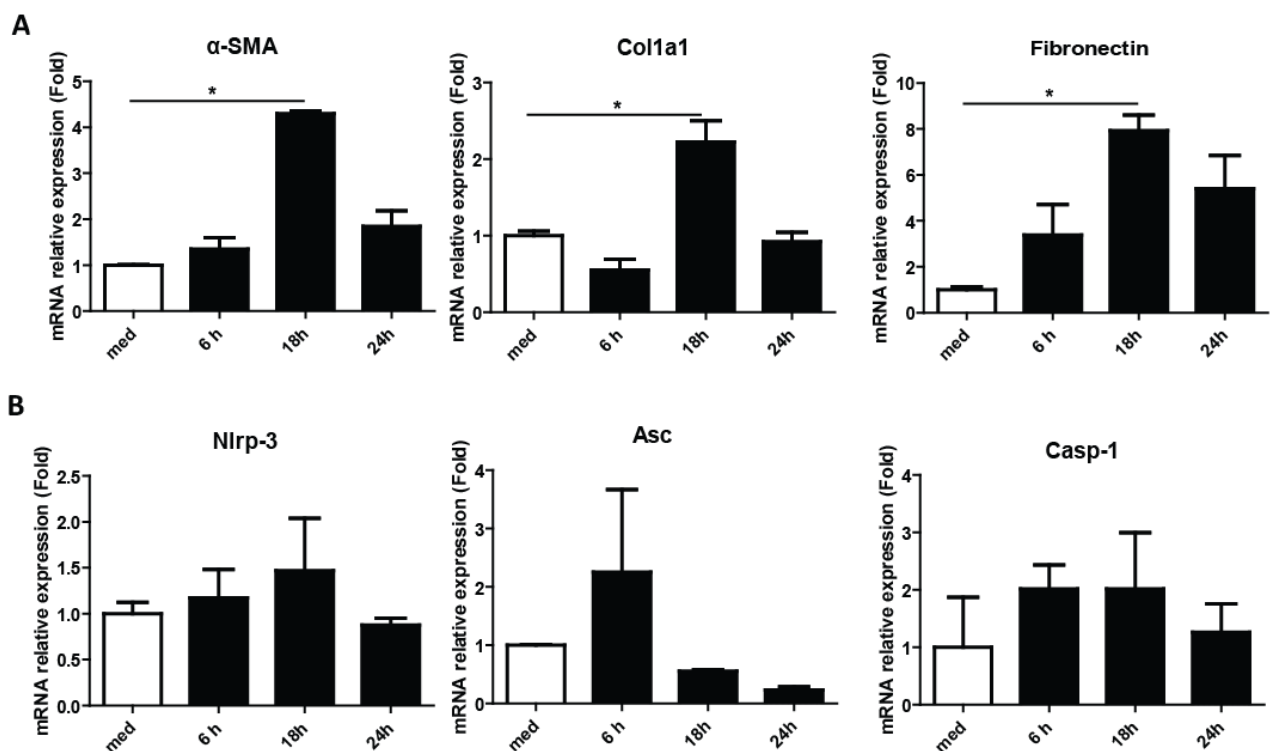


Figure 33: Profibrotic markers are expressed in a time dependent manner and correlate with the expression of inflammasome components in NIH-3t3 cells NIH-3t3 cells were incubated with DMEM medium (med) and stimulated with LPS (100 ng/ml) and mouse TGF- β 1 (10 ng/ml) for 6, 18 and 24 hrs (A) Total mRNA was isolated and quantified with RT-PCR. Expression of α -SMA, collagen I (*Col-1a1*) and fibronectin was increased after stimulation in a time dependent manner. (B) Total mRNA expression of inflammasome components *Nlrp-3*, *Asc*, and *casp-1* in NIH-3t3 cells was analyzed with RT-PCR after stimulations. Data are expressed as x-fold increase of the target gene over the 18s mRNA expression. These values represent one out of two independent experiments. Abb.: med: medium, LPS: lipopolysaccharide, TGF- β 1: transforming growth factor beta 1. * $p < 0.05$.

3.2.3 NIH-3t3 cells proliferate independently of Casp-1

Previous experiments demonstrated that the inflammasome component NLRP3 is present in NIH-3t3 cells, together with ASC and Casp-1. Additionally, expression of profibrotic markers was significantly increased after stimulation with LPS and mouse TGF- β 1, suggesting a correlation with *Nlrp-3* expression. However, whether these effects depend on inflammasome activation and Casp-1-mediated Il-1 β release is not yet clear. To address this question, the proliferation rate of native NIH-3t3 fibroblasts that were pretreated with pan-caspase inhibitor zVAD was analyzed after stimulation with LPS and mouse TGF- β 1. ZVAD is a well-known caspase inhibitor with low cell toxicity and ideal for studies investigating caspase activity in cells. Both groups were stimulated with LPS and mouse TGF- β 1 for 24 hrs and analyzed using MTT assay.

As predicted, NIH-3t3 cells showed a significant increase in their ability to proliferate upon treatment with LPS or LPS in combination with mouse TGF- β 1, which was independent of Casp-1 inhibition with zVAD. These results suggest that Casp-1 activation does not play a role in the proliferative capacity of NIH-3t3 fibroblasts (Figure 34 A).

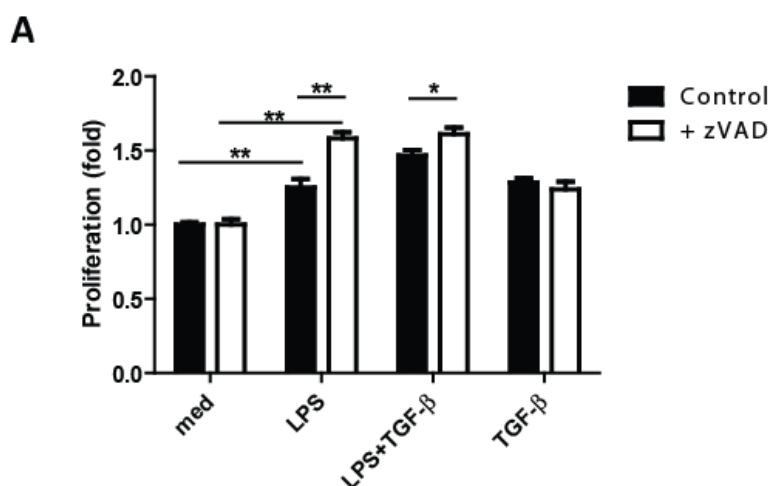


Figure 34 A: Proliferation of NIH-3t3 cells is caspase 1 independent. NIH-3t3 cells were incubated with DMEM for 24 hrs. Medium was exchanged and the zVAD pre-treated group received (30 mM) pan-caspase inhibitor zVAD. Both groups were stimulated with LPS (100 ng/ml) and/or mouse TGF- β 1 (10 ng/ml) for 24 hrs. MTT proliferation assay was performed and quantified with ELISA Reader at 490 nm. Results represent light absorbance in fold increase. Significant increase in proliferation rate was observed in both groups after stimulation with LPS or TGF- β 1. These values represent one out of two independent experiments. Abb.: med: medium, LPS: lipopolysaccharide, TGF- β 1: transforming growth factor beta. *p<0.05, **p<0.01.

3.2.4 LPS and TGF- β 1 stimulation increase *Nlrp-3* expression in primary mouse embryonic fibroblasts

To further evaluate the function of NLRP3 in cells, primary MEFs were isolated from C57Bl6 WT and *Nlrp-3*-deficient mice. mRNA expression of *Nlrp-3* was quantified in WT pMEFs, which showed a significant increase after stimulation with LPS and mouse TGF- β 1 alone or in combination (Figure 35 A). Consequently, western blot analysis revealed the presence of Nlrp-3 protein in WT pMEFs and confirmed the lack of Nlrp-3 protein in *Nlrp-3*-deficient mice. Quantification analysis of western blot studies showed a significant increase of the Nlrp-3 protein expression in WT pMEFs when primed with LPS (Figure 35 B and C). These results confirm the presence of *Nlrp-3* in pMEFs, which is also inducible upon stimulation with LPS and/or mouse TGF- β 1.

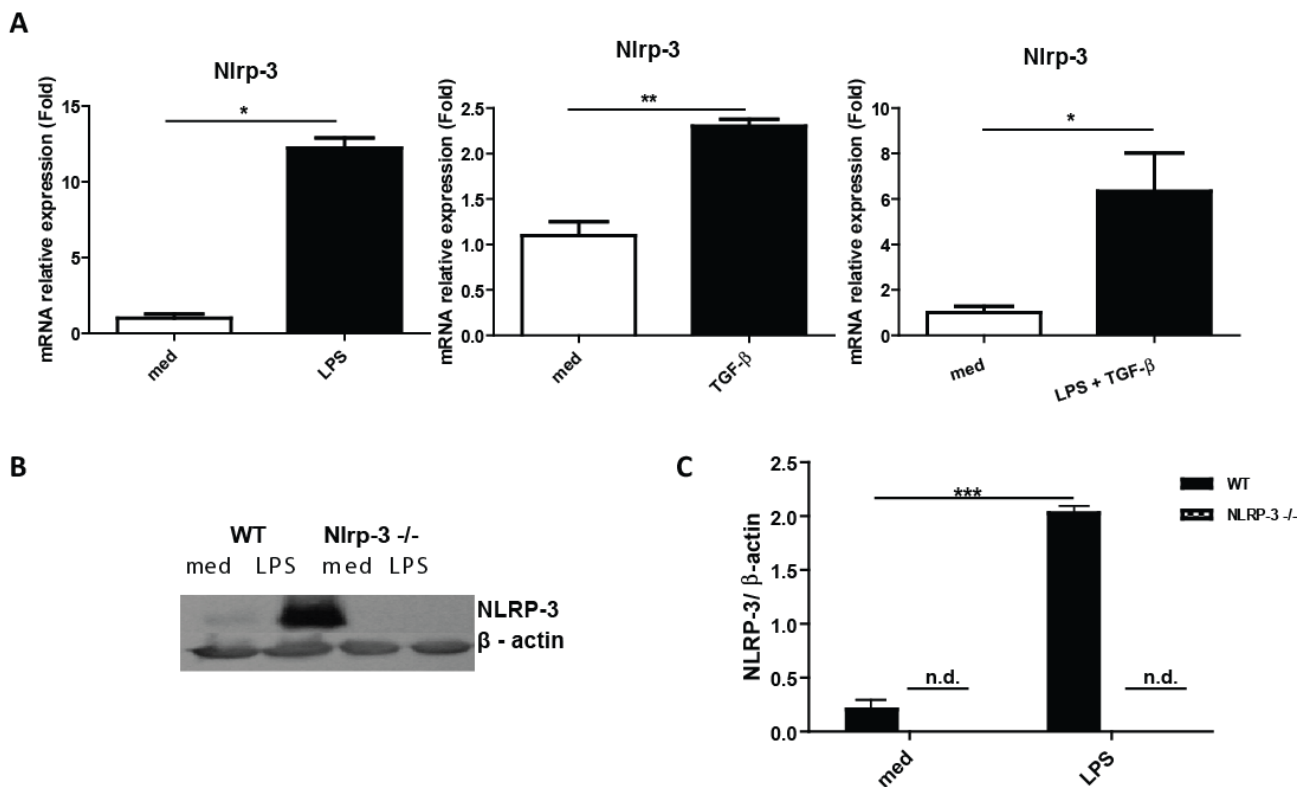


Figure 35: Expression of *Nlrp-3* in pMEFs. pMEFs were isolated from WT and *Nlrp-3*^{-/-} C57Bl6 mouse embryos at the 13th day of gestation, with posterior cultivation in DMEM for 48 hrs. (A) Total mRNA from WT pMEFs was isolated and quantified by RT-PCR after stimulation with LPS (100 ng/ml) and mouse TGF- β 1 (10 ng/ml) for 2 and 8 hrs respectively. Data are shown as *Nlrp-3/18s* ratio in fold increase. (B) Western blotting was used to show Nlrp-3 protein expression in WT and *Nlrp-3*^{-/-} pMEFs upon stimulation with LPS (100 ng/ml) for 24 hrs. (C) Quantification analysis of the western blot shows a significant increase in Nlrp-3 expression of pMEFs after stimulation with LPS. β -actin was used as a control. Results are shown as Nlrp-3/ β -actin ratio. These values represent one out of two independent experiments. Abb.: med: medium, LPS: lipopolysaccharide, TGF- β 1: transforming growth factor beta 1. β -actin: beta actin. n.d.: not detectable. * p <0.05, ** p <0.01.

3.2.5 LPS and TGF- β 1 stimulation increased profibrotic gene expression in WT pMEFs and not in *Nlrp-3*-deficient pMEFs

In order to evaluate the role of NLRP3 in pMEFs, mRNA expression levels of profibrotic markers were analyzed in WT and *Nlrp-3*-deficient pMEFs. Cells were stimulated with the inflammasome inducer LPS (signal 1) and/or activator ATP (signal 2) together with the profibrotic cytokine mouse TGF- β 1. Expression profiling of the profibrotic markers α -SMA, *coll1a1*, *col4a1* and *fibronectin* showed a significant increase in these markers after stimulation with LPS and TGF- β 1, or LPS together with ATP and TGF- β 1 in WT pMEFs. This effect was absent in pMEFs lacking *Nlrp-3* (Figure 36). In fact, *Nlrp-3*-deficient cells stimulated with LPS and mouse TGF- β 1 expressed significantly less α -SMA, *coll1a1*, *col4a1* and *fibronectin* compared to the WT group (Figure 36). Furthermore, analysis of TGF- β 1 dependent markers such as CTGF (*Ctgf*), MMP-9(*Mmp-9*) and VEGF (*Vegf*) that are crucial for fibrogenic processes, revealed a significant increase in the mRNA expression in WT pMEFs after stimulation with LPS and mouse TGF- β 1. Whereas stimulated pMEFs from the *Nlrp-3*-deficient mice did not up-regulate the mRNA expression levels of the profibrotic genes (Figure 37 A).

Further, analysis of genes involved in TGF- β 1 signaling such as TGF receptor 1 (*TGF β RI*), TGF receptor 2 (*TGF β RII*) and R-SMADs (*Smad2* and *Smad3*) showed a trend towards increased mRNA expression in WT pMEFs after stimulation with LPS and mouse TGF- β 1, unlike *Nlrp-3*-deficient pMEFs, where no such trend was observed. However, these results did not show significant differences between the phenotype groups (Figure 37 B). Expression of the inflammation markers *IL-6* and IL-1 receptor (*IL-1r*) was analyzed in WT and *Nlrp-3*-deficient pMEFs after stimulation with ATP, LPS and mouse TGF- β 1. Both *IL-6* and IL-1 receptor expression were significantly higher in stimulated WT pMEFs compared to *Nlrp-3*-deficient pMEFs (Figure 38).

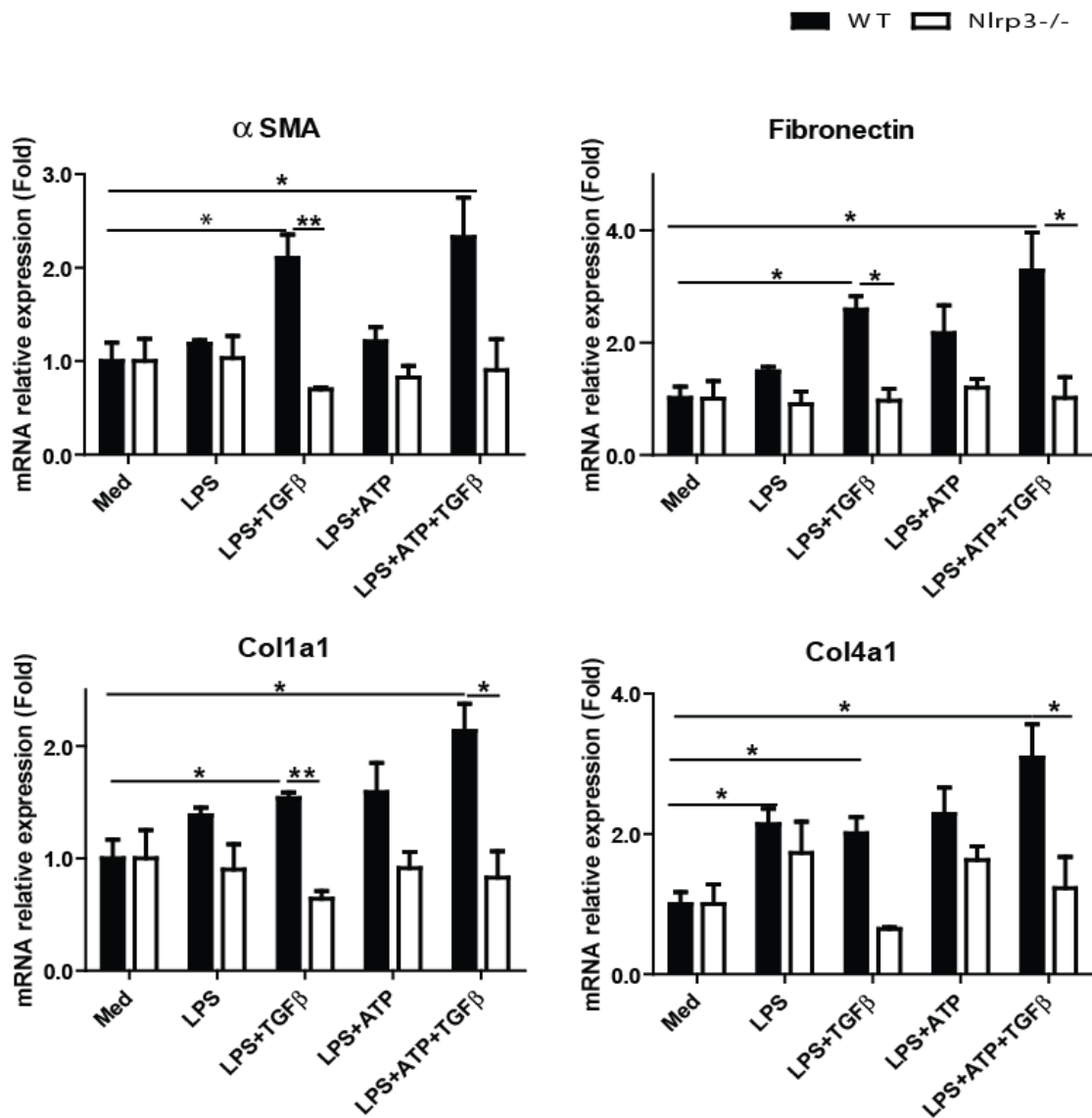


Figure 36: LPS and TGF- β 1 stimulation increases profibrotic gene expression in WT pMEFs and not in *Nlrp-3*-deficient pMEFs. pMEFs from WT and *Nlrp-3*^{-/-} mice were primed with LPS (100 ng/ml), ATP (5 mM) and mouse TGF- β 1 (10 ng/ml) for 2, 5 and 18 hrs respectively. (A) Total mRNA expression of α -SMA, fibronectin, *colla1* and *col4a1* was quantified with RT-PCR. Graphs show a significant increase in the expression of these genes after stimulation with LPS and TGF- β 1 in WT pMEFs, difference which was absent in *Nlrp3*^{-/-} pMEFs. Results are shown as x-fold increase of the target gene over the 18s mRNA expression. These values represent one out of two independent experiments. Abb.: α -SMA: α smooth muscle protein, Fib: fibronectin, *colla1*: collagen 1a1 and *col4a1*: collagen 4a1, med: medium, LPS: lipopolysaccharide, ATP: adenosinetriphosphate, TGF- β 1: transforming growth factor beta 1. *p<0.05, **p<0.01

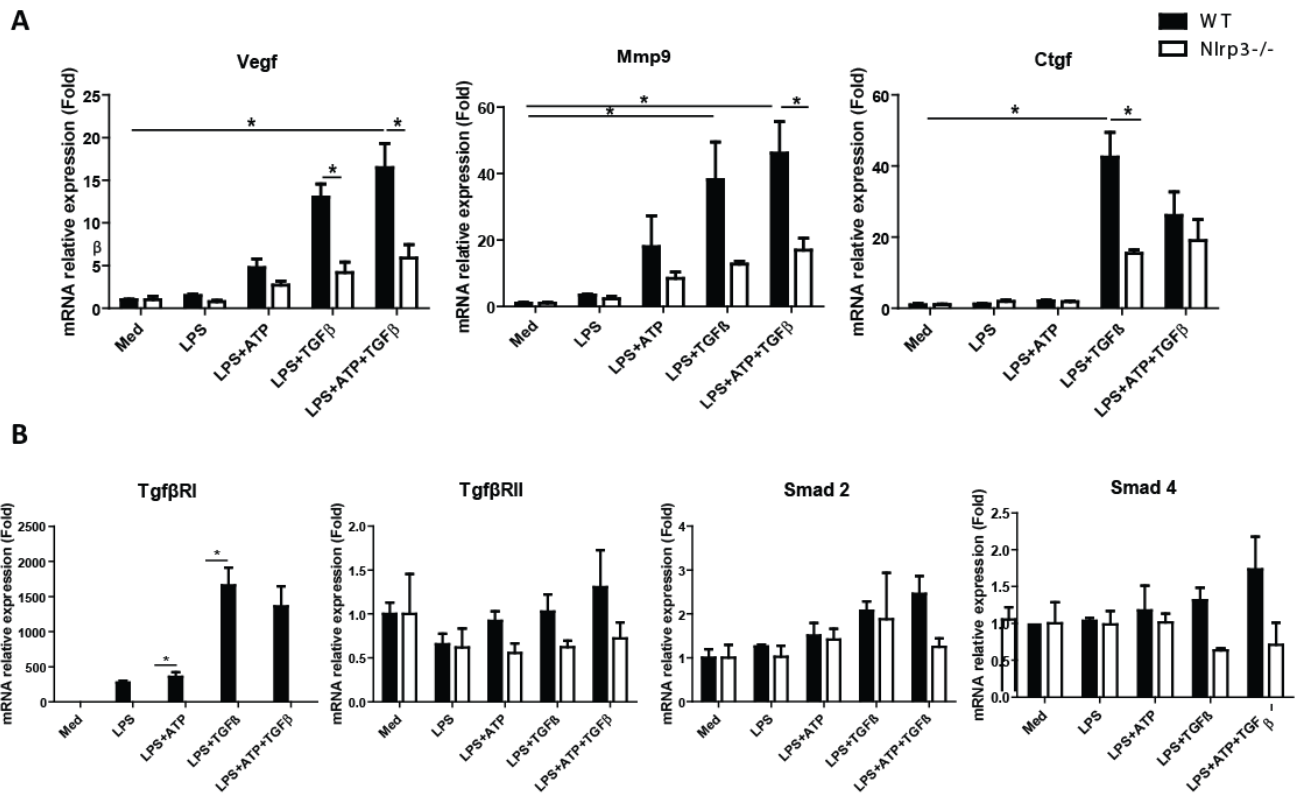


Figure 37: LPS and TGF-β1 stimulation increased TGF-β1-dependent gene expression in WT pMEFs and not in *Nlrp3*-deficient pMEFs. pMEFs from WT and *Nlrp3*^{-/-} mice were primed with LPS (100 ng/ml), ATP (5 mM) and mouse TGF-β1 (10 ng/ml) for 2, 5 and 18 hrs respectively. (A) Total mRNA expression was quantified with RT-PCR. TGF-β1 dependent genes such as *Vegf*, *Mmp-9*, *Ctgf*, and genes involved in TGF-β1 signaling, (B) *TGFβRI* and *TGFβRII*, *Smad2* and *Smad3* expression showed a marked increase in WT pMEFs compared to *Nlrp3*^{-/-} pMEFs. Data are expressed x-fold increase of the target gene over the 18s mRNA expression. These values represent one out of two independent experiments. Abb.: *Vegf*: vascular endothelial growth factor, *Mmp-9*: Matrix metalloproteinase 9, *Ctgf*: connective tissue growth factor, *TGFβRI*: TGF-β receptor 1, *TGFβRII*: TGF-β receptor 2. med: medium, LPS: lipopolysaccharide, ATP: adenosinetriphosphate, TGF-β1: transforming growth factor beta 1. *p<0.05, **p<0.01

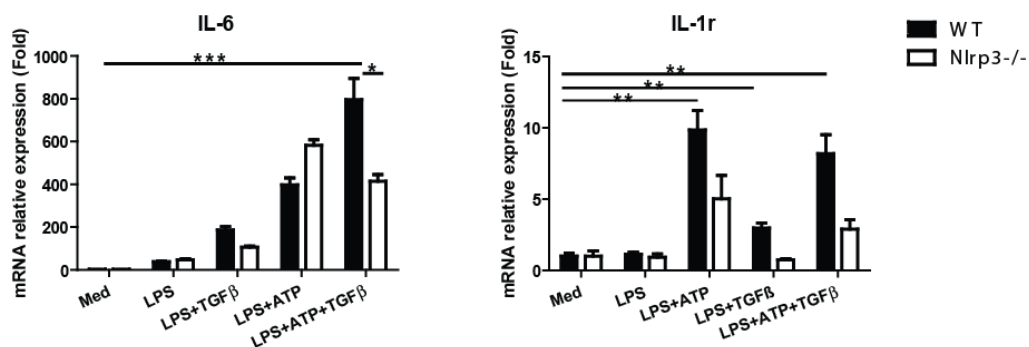


Figure 38: LPS and TGF-β1 stimulation increased proinflammatory gene expression in WT pMEFs and not in *Nlrp3*-deficient pMEFs. pMEFs from WT and *Nlrp3*^{-/-} mice were primed with LPS (100 ng/ml), ATP (5 mM) and mouse TGF-β1 (10 ng/ml) for 2, 5 and 8 hrs respectively. (A) Total mRNA expression was quantified with RT-PCR. Gene expression of proinflammatory cytokine *IL-6* and receptor *IL-1R* and were analyzed in both groups, showing a significant increase of these markers in WT pMEFs compared to the *Nlrp3*^{-/-} group. Data are expressed as x-fold increase of the target gene over the 18s mRNA expression. These values represent one out of two independent experiments. Abb.: IL-1r Interleukin-1 receptor, IL-6: interleukin 6. med: medium, LPS: lipopolysaccharide, ATP: adenosinetriphosphate, TGF-β1: transforming growth factor beta 1. *p<0.05, **p<0.01

Finally, immunofluorescence microscopy was used to determine the expression of α -SMA in WT and *Nlrp-3*-deficient pMEFs after stimulation with mouse TGF- β 1 (Figure 39 A). Although both groups showed increased expression and conformational changes upon TGF- β 1 stimulation, quantification analysis of α -SMA positivity revealed that WT pMEFs significantly increased the expression of α -SMA compared to *Nlrp-3*-deficient pMEFs (Figure 39 B).

Taken together, these results suggest that lack of *Nlrp-3* diminishes profibrotic and proinflammatory marker expression in pMEFs, thus regulating their activation and function as main ECM producers.

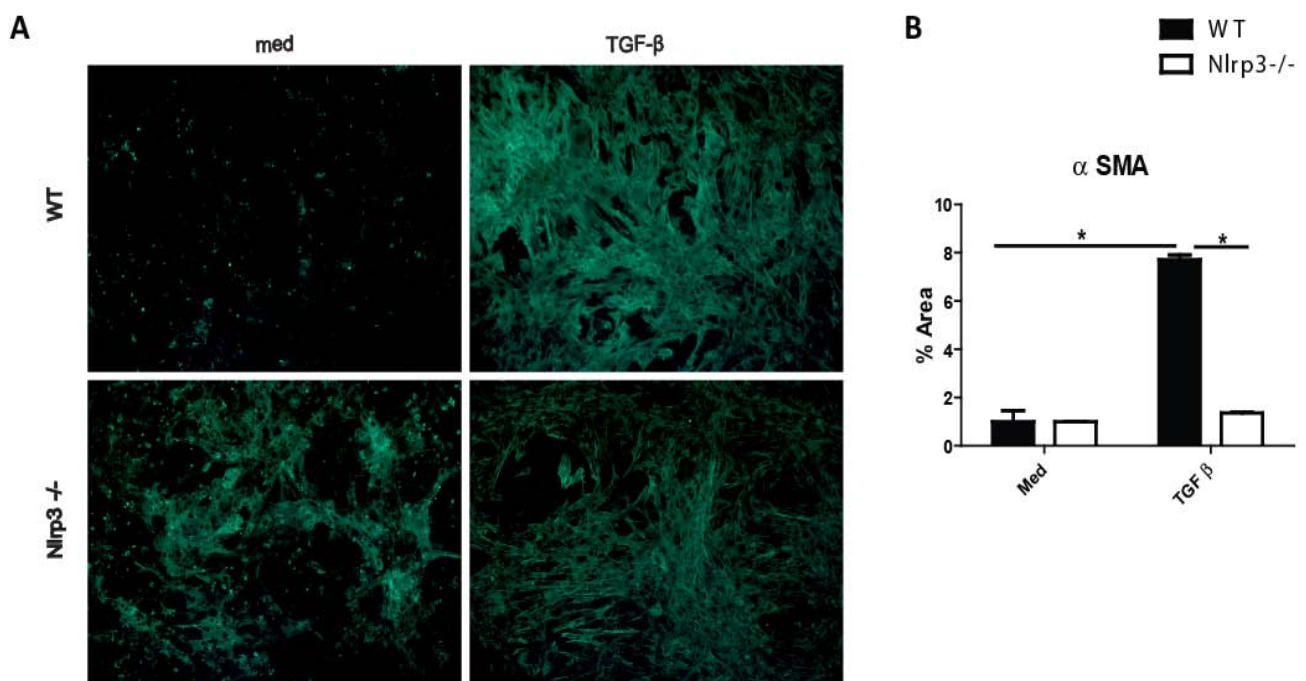


Figure 39: TGF- β 1 stimulation increased α -SMA expression in WT pMEFs and not in *Nlrp-3*-deficient pMEFs. PMEFs from WT and *Nlrp-3*^{-/-} mice were primed with mouse TGF- β 1 (10ng/ml) for 24 hrs (A) Immunofluorescence staining of α SMA in WT and *Nlrp-3*^{-/-} pMEFs after stimulation with mouse TGF- β 1. (B) Quantification of α -SMA positive areas in cells shows a significant increase in WT pMEFs and not in *Nlrp-3*^{-/-} pMEFs. Data are shown as mean % area in fold increase. These values represent one out of two independent experiments. *p<0.05 ,**p<0.01

3.2.6 TGF- β induced proliferation of pMEFs involves NLRP3 and ASC

Previous results imply that NLRP3 plays an important role in the expression of profibrotic genes in pMEFs. Fibrosis development involves not only the expression of ECM proteins but also the proliferation of fibroblasts.

We, therefore, analyzed whether the inflammasome components NLRP3 and ASC are involved in the proliferation of pMEFs. To address this, MTT proliferation assays were performed. WT and *Nlrp-3*-deficient pMEFs were stimulated with different doses of mouse TGF- β 1 for 48 hrs. Figure 40 A shows that both groups proliferated significantly upon TGF- β 1 stimulation; however *Nlrp-3*-deficient pMEFs were unable to achieve such a high proliferation rate as WT pMEFs. The significantly reduced proliferative ability in *Nlrp-3*-deficient pMEFs was observed in all groups, independent of the TGF- β 1 dose (Figure 40 A). Furthermore, a similar study including WT, *Nlrp-3*- and *Asc*-deficient pMEFs, revealed similar results showing a significantly higher proliferation rate in WT pMEFs compared to the *Nlrp-3* and *Asc*-deficient groups (Figure 40 B). Altogether, these results suggest that *Nlrp-3* or *Asc*-deficiency reduces fibroblast proliferation.

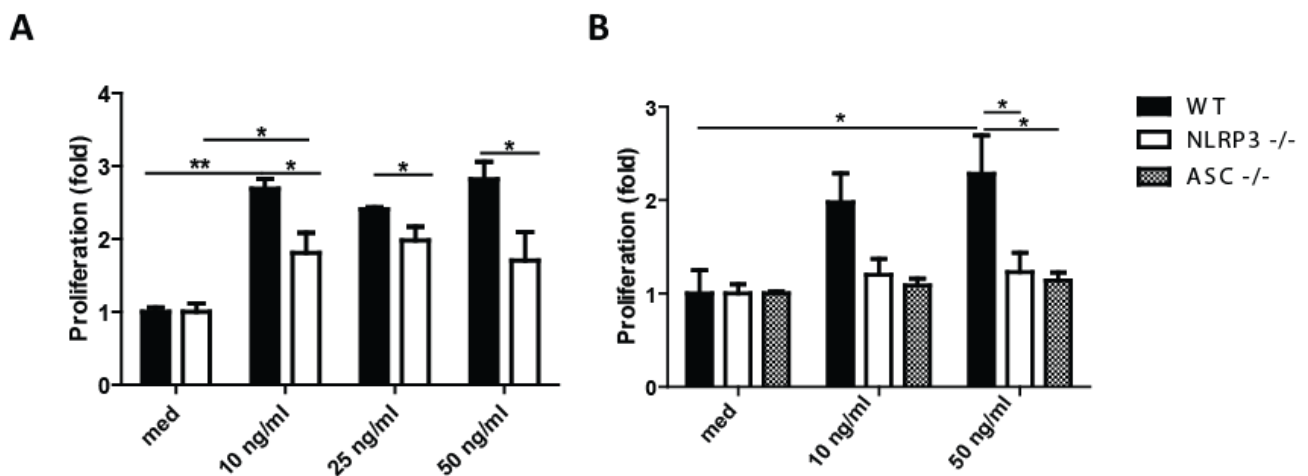


Figure 40: TGF- β 1-induced pMEF proliferation involves NLRP3 and ASC. (A) WT and *Nlrp-3*^{-/-} pMEFs were cultured and stimulated with TGF- β 1 in a dose dependent manner (10 ng/ml, 25 ng/ml, 50 ng/ml) respectively. After 48 hrs stimulation, MTT-proliferation assay was performed and absorbance was measured with ELISA reader at 490 nm. Significant increase in the proliferation rate is observed in stimulated WT and *Nlrp-3*^{-/-} pMEFs, although *Nlrp-3*^{-/-} pMEFs showed significantly less proliferation when compared to WT cells. (B) MTT-proliferation assay shows proliferation of WT, *Nlrp-3*^{-/-} and *Asc*^{-/-} pMEFs upon stimulation with mouse TGF- β 1 (10 ng/ml and 50ng/ml). Significant increase in proliferation is observed in the WT group compared to the *Nlrp-3*^{-/-} and *Asc*^{-/-} pMEFs. Data is shown in fold increase. These values represent one out of two independent experiments. Abb.: TGF- β 1: transforming growth factor β 1. * n <0.05 . ** n <0.01

3.2.7 NIH-3t3 fibroblasts and pMEFs do not release IL-1 β

All the previously described experiments indicated that the inflammasome components NLRP3 and ASC play an important role in the regulation of fibroblasts proliferation and ECM production. Nevertheless, an inflammasome activation and thus Casp-1-dependent IL-1 β cleavage cannot be excluded. The experiments in figure 20 suggested that NIH-3t3 fibroblasts proliferation did not depend on the Casp-1-mediated IL-1 β cleavage and thus excluding an inflammasome-dependent NLRP3 signaling for the proliferation of these fibroblasts. Moreover, the secretion of IL-1 β by fibroblasts has not yet been defined, as several opposing findings have been reported [178-180]. Therefore, we designed an experiment to detect IL-1 β secretion from NIH-3t3 cells, WT pMEFs and *Nlrp-3*-deficient pMEFs upon inflammasome stimulation. Bone marrow dendritic cells (BMDCs) were used as a control. Cells were primed with LPS (signal 1) and ATP (signal 2) for 24 hrs and supernatants analyzed for inflammasome-dependent IL-1 β release using ELISA detection kit. Results did not show any detectable production of IL-1 β in NIH-3t3, WT pMEFs or *Nlrp-3*-deficient pMEFs, compared to BMDCs, which produced large amounts of IL-1 β upon priming with LPS and ATP. This indicates that the lack of IL-1 β secretion in pMEFs is due to a Casp-1-independent role of NLRP3 in fibroblast proliferation, ECM production and thus in fibrogenesis.

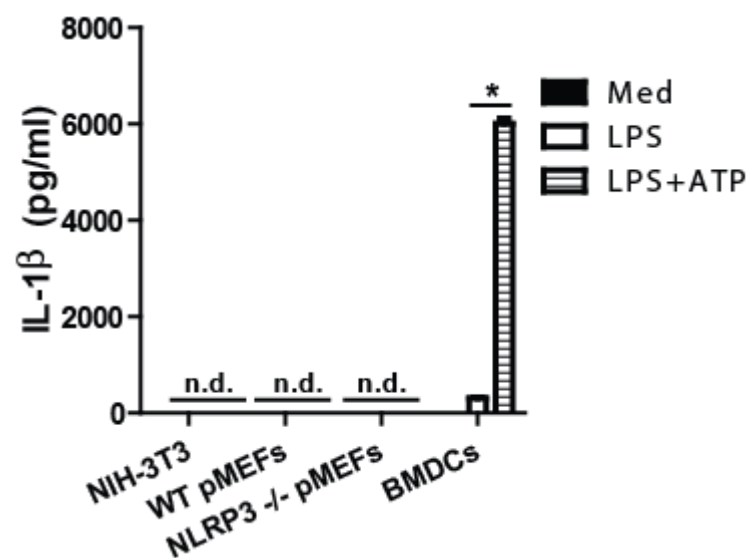


Figure 41: NIH-3t3 fibroblasts and pMEFs do not secrete IL-1 β . NIH-3t3 cells, WT pMEFs, *Nlrp-3*^{-/-} and BMDCs were primed with LPS (100ng/ml) and ATP (5mM) for 24 hrs. Supernatant was then analyzed with IL-1 β enzyme-linked immunosorbent assay (ELISA) and quantified using ELISA Reader with a 490nm absorbance filter. Cytokine production was not detectable in NIH-3t3, WT pMEFs or *Nlrp-3*^{-/-} pMEFs compared to primed BMDCs. Data is presented in pg/ml. These values represent one out of two independent experiments. Abb.: Med: medium, ATP: adenosinetriphosphate, LPS: lipopolysaccharide. BMDCs: Bone marrow dendritic cells **p*<0,05

4. Discussion

CKD is the result of progressive nephron loss aggravated by a prolonged inflammatory response, which in time enhances an exaggerated mesenchymal healing process, tissue remodeling and extensive scarring of the renal interstitium. This overshooting inflammatory response comprises the release of DAMPs, cytokines and chemokines that further promote a persistent damage of functional tubular epithelial cells, which consequently die. This epithelial leak undergoes a tissue-repair process, which predominantly involves the accumulation and proliferation of resident kidney fibroblast and the recruitment of bone-marrow fibroblasts or, to a lesser extent, a phenotype change of the tubular epithelial cells turning them into fibroblasts (a process called EMT) [181]. Finally, the exaggerated fibroblast accumulation and ECM deposition result in a significant renal interstitial fibrosis [181-183]. The exact molecular mechanisms and signaling pathways involved in this process, especially the role of the innate immunity and PRRs are of particular interest in the scientific community today [184, 185].

The cytosolic NLRP3 inflammasome is a PRR capable of recognizing a wide variety of ligands presented in form of PAMPs and DAMPs. This multiprotein complex acts as a platform for Casp-1 activation, leading to the proteolytic cleavage and activation of IL-1 β and IL-18 [56, 186, 187]. A variety of diseases have been associated with this complex including hereditary syndromes (CAPS) and other much more common acquired pathologies such as atherosclerosis and diabetes mellitus [56, 186, 187]. The kidney has not been an exception to this. Strong evidence advocates an important role of the NLRP3 inflammasome in kidney pathologies, including AKI [144, 147] and CKD [137, 152]. Its contribution to kidney disease has been mainly associated with the extensive activation of IL-1 β and IL-18, and thus exaggerated inflammatory response. However, recent data suggested a novel inflammasome-independent role of NLRP3, i.e. regardless of Casp-1-mediated IL-1 β and IL-18 release [138, 153, 188].

This study complements the recent findings regarding an inflammasome-independent role of NLRP3 in renal fibrogenesis by augmenting TGF- β receptor signaling independent of Casp-1-mediated IL-1 β release.

The main questions in this study were:

1. What role do NLRP3 and ASC play in renal interstitial fibrosis *in vivo*? Are these effects exclusively related to a reduced Casp-1-mediated IL-1 β release?

-
2. What is the role of NLRP3 or ASC in hyperoxaluria and nephrocalcinosis-induced CKD? Does their contribution to the pathogenesis of hyperoxaluria-induced CKD rely entirely on the IL-1-mediated IL-1 receptor activation?
 3. Do fibroblasts as main protagonists of fibrogenic processes express NLRP3? If yes, does that influence their function and proliferation in an inflammasome-dependent or independent manner?

4.1 NLRP3 and ASC in the UUO model

The results in this thesis revealed that mice lacking NLRP3 resulted in reduced renal injury, inflammation and interstitial fibrosis upon UUO, which was consistent with recently published data by Vilaysane et al. [152]. We reported less tubular injury and less infiltration of inflammatory cells (monocyte/macrophages), whereas the infiltration of T-lymphocytes was not significantly impaired in mice lacking NLRP3. Similar results have been observed by other groups showing that the number of CD3+ T-lymphocytes did not significantly change in a model of autoimmune encephalomyelitis in *Nlrp-3*-deficient mice [189]. NLRP3 is also essential for the development of interstitial fibrosis as evidenced by reduced collagen I and α -SMA deposition in mice lacking NLRP3.

The protective effects of NLRP3 deficiency observed in our experiments are consistent with a recently published paper by Guo H. et al. [190]. In this study, they demonstrated in a time-dependent manner that the expression of the NLRP3 inflammasome components and interleukin release increases in WT mice upon UUO, an effect, which was abolished in mice lacking NLRP3 [190]. Both Vilaysane et al. [152] and Guo H. et al. [190] proposed the reduced inflammasome-dependent cytokine maturation as the leading mechanism protecting *Nlrp-3*-deficient mice from renal injury, inflammation and fibrosis upon UUO. Additionally, NLRP3-mediated cytokine release was associated with mitochondrial dysfunction in mice upon UUO [190]. This theory was supported in other murine models of renal injury such as albumin-induced renal injury and 5/6 nephrectomy [191-193]. On the other hand, studies using an aldosterone-induced renal injury model indicated that mitochondrial dysfunction involves increased ROS production triggering the activation of the NLRP3 inflammasome, thus leading to tubular cell injury [194, 195].

But the fact that tubular epithelial cells do not secrete IL-1 β in spite of expressing the inflammasome components NLRP3, ASC and Casp-1 [138] suggests that other mechanisms, which do not involve a cytokine-mediated injury are involved in this process. This is also supported by studies which showed that the protective effects observed in *Nlrp-3*-deficient mice were not only due to less

infiltration of inflammatory cells but also due to reduced NLRP3 expression in renal parenchymal cells [152].

In this thesis, we propose a novel mechanism that involves an inflammasome-independent function of NLRP3 in the development of renal injury upon UUO. To prove this, mice were treated with the pan-caspase inhibitor zVAD, thus inhibiting the proteolytic activation of IL-1 β and IL-18. ZVAD-treated mice also showed significant protection compared to non-treated mice regarding tissue injury and interstitial inflammation. However, the protective effect in mice lacking NLRP3 went beyond the effects observed in zVAD-treated mice. Also, renal interstitial fibrosis was partially ameliorated in zVAD-treated mice, but collagen I deposition did not differ between the WT and zVAD-treated group. Our results highly suggest that further interleukin-independent mechanisms contribute to the development of CKD.

But the link between IL-1-independent NLRP3 signaling is still not well understood. Some studies regarding inflammasome-independent mechanisms have suggested that the NLRP3 regulates TGF- β receptor signaling [138, 153]. Consequently, we tested this hypothesis in mice upon UUO. Our data revealed that phosphorylation of the TGF receptor signaling components SMAD 2/3 was significantly reduced in *Nlrp-3*-deficient mice compared to zVAD-treated mice upon UUO, indicating that NLRP3 augments SMAD 2/3 phosphorylation, a mechanism that does not involve Casp-1-mediated IL-1 release.

It is worth mentioning that while our studies were ongoing another group proposed a mechanism involving both mitochondrial dysfunction and regulation of TGF- β signaling by the NLRP3 in an inflammasome-independent manner [180], whereby the inflammasome component NLRP3 (most likely through its NACHT domain) promoted R-SMAD signaling during fibroblast activation in cardiac fibroblasts. Interestingly, NLRP3 was found to be localized to the mitochondria without evidencing any translocation in the process of myofibroblast activation. Additionally, mitochondrial ROS production strongly correlated with NLRP3 expression. It is not clear whether ROS-mediated mitochondrial dysfunction is regulated by NLRP3 activation, or whether NLRP3-mediated mitochondrial ROS production regulates SMAD2 phosphorylation in TGF- β signaling.

Furthermore and contrary to our data, a recent *in vitro* study using HPTCs (human proximal tubular cells) showed that prolonged stimulation with TGF- β 1 resulted in an initial increase of NLRP3 expression on day 3 followed by a subsequent decrease 7 days after stimulation with TGF- β 1 [141]. The stimulation of HPTCs with TGF- β 1 also resulted in a phenotypical change associated with a loss

of the epithelial markers ZO-1 and E-cadherin as well as increased expression of the mesenchymal markers α -SMA and SMAD2/3 nuclear translocation. Kidney biopsies from patients with severe IgA-nephropathy revealed an increased expression of NLRP3 in the tubular epithelium compared to normal kidneys, whereby the α -SMA positive areas did not co-localize with NLRP3 in the renal interstitial area, thus rejecting the presence of NLRP3 in myofibroblasts [141]. Nevertheless, these findings might be related only to cells undergoing phenotypical changes such as fibroblasts that originated from TECs (accounting only for approximately 5% of the renal myofibroblasts that contribute to renal interstitial fibrosis) [181]. Furthermore, the role of the NLRP3 may vary according to the cell type as proven in studies involving NLRP3-mediated hepatocyte pyroptosis [196] and NLRP3-mediated fibroblast activation, as shown in this thesis. Contrary to many other findings an increased NLRP3 expression was associated with a better clinical outcome in patients with IgA nephropathy [141].

However, our hypothesis has been supported by several other studies. Our group found that *Nlrp3*- and *Asc*-deficient lupus mice had a marked lymphoproliferative syndrome and worsening of the clinical outcome as well as lupus nephritis, an effect that resulted from the regulation of TGF- β signaling by the inflammasome component NLRP-3, which was not mediated by interleukin release [153].

Interestingly, similar effects were also observed *Asc*-deficient mice, which also presented less tubular injury and interstitial fibrosis upon UUO despite the increase in F4/80+ macrophage numbers in *Asc*-deficient mouse kidneys. On the other hand, the precise role of ASC in regulating renal interstitial fibrosis remains unclear. Komanda T. et al. indicated a significant protection from renal injury, interstitial inflammation and fibrosis in *Asc*-deficient mice upon UUO [197]. Moreover, this group remarked the importance of ASC in renal collecting duct cells, as the expression of ASC was significantly up-regulated upon UUO [197]. The protective effects in *Asc*-deficient mice were most probably a result of IL-1 β releasing collecting duct cells, as shown in *in vitro* experiments, whereby LPS and ATP were used to prime and activate the inflammasome leading to IL-1 β secretion in collecting duct cells [197].

Together, we conclude that the inflammasome component NLRP3 modulates renal interstitial inflammation and fibrosis in obstructive nephropathy *via* regulation of TGF- β receptor signaling, an effect that goes beyond inflammasome activation by involving a novel inflammasome-independent NLRP3 signaling pathway.

4.2 The NLRP3 inflammasome and the Chronic Oxalate Model

As previously mentioned in the introduction, the UUO mouse model has several limitations in mimicking human CKD. Therefore, we used an alternative CKD mouse model: the chronic oxalate-induced CKD mouse model. This model has been established in our laboratory as described thoroughly in chapter 1.6 [163].

Previous studies from our laboratory described a role for the NLRP3 inflammasome in a model of acute calcium oxalate crystal-induced kidney injury [64], whereby calcium oxalate crystals trigger an inflammatory response associated with the activation of signaling pathways including the NLRP3 inflammasome. Additionally, these crystals induce tubular cell death leading to release of DAMPs, alarmins, proteases as well as other proinflammatory mediators, which are sensed by resident immune cells and parenchymal cells, augmenting the inflammatory response [198]. Mononuclear phagocytes and resident DCs can ingest calcium oxalate crystals that consequently lead to lysosomal leakage and activation of the NLRP3 inflammasome. Tubular epithelial cells on the other hand also express NLRP3 but are unable to produce IL-1 β [138, 188, 199]. In this regard, mice lacking *Nlrp-3*, *Asc*- or *Casp-1* were protected from calcium oxalate-induced AKI. This was also the case following IL-1 blockade with anakinra, which resulted in reduced renal damage upon injury, indicating that oxalate nephropathy-induced AKI mostly relies on the intrarenal inflammatory response from resident mononuclear cells and DCs [64].

In a model of chronic oxalate-induced nephropathy, Knauf F. et al. found that *Nlrp-3*-deficient mice were also protected as indicated by a normal renal pathology compared to WT mice [164]. This renal protective effect was due to the lack of intrarenal calcium oxalate crystal deposition in *Nlrp-3*-deficient mice. However, the role of ASC, Casp-1 and IL-1 β were not assessed in this study. Therefore, we performed experiments using *Asc*- as well as *Nlrp-3*-deficient mice in a murine model of hyperoxaluria-induced CKD. As predicted, *Nlrp-3*- and *Asc*-deficient mice did not show any differences in the renal functional parameters compared to the WT group due to the lack of intrarenal calcium oxalate crystal deposition, in spite of elevated plasma and urine oxalate levels. Contrary to the acute oxalate nephropathy model [64], mutant mouse strains were unable to develop nephrocalcinosis in a chronic oxalate model of CKD.

According to Knauf et al. the increased intrarenal crystal deposition observed in WT mice upon a high-soluble oxalate diet is a product of a vicious cycle between oxalate-induced systemic inflammation and progression of kidney disease. They argue that reduced GFR in WT mice (product of a systemic inflammation due to elevated plasma-oxalate levels) impedes oxalate excretion, thus

leading to accumulation of plasma-oxalate and further progression of CKD [164, 200]. Our findings showed no relevant differences in the plasma oxalate concentration between the groups, but did show differences in the urinary oxalate concentrations, which were higher in *Nlrp-3*- and *Asc*-deficient mice compared to the WT mice. More importantly, our findings show that *Nlrp-3*- and *Asc*-deficient mice did not develop nephrocalcinosis despite hyperoxaluria, and hence no nephrocalcinosis-induced renal inflammation, fibrosis and thus no CKD. The lack of intrarenal calcium deposition in *Nlrp-3*- and *Asc*-null mice precludes the assessment of the role of these proteins in hyperoxaluria and nephrocalcinosis-induced CKD.

One possible explanation for this phenomenon involves the presence of passenger mutations in genetically modified congenic mice, which confound the interpretation of experiments performed in these knockout mice [201]. Most genetically modified mouse strains are generated by germline transmission competent embryonic stem cells derived from the 129 mouse strain. In order to avoid passenger mutations flanking the gene, these mice are backcrossed to another particular mouse strain such as C57BL/6J, which reduces the probability of passenger mutations, although not excluding them completely [201]. A study performed by Kayagaki et al. demonstrated that the profound protection observed in *Casp-1*-deficient mice against lethal LPS challenge was due to an inactivating passenger mutation in the *Casp-11* gene [202]. Whether this is also the case for *Nlrp-3*- and *Asc*-deficient mice is not known. Certainly, both mutant mouse strains are not appropriate for the study of hyperoxaluria and nephrocalcinosis-induced CKD and thus an inflammasome-dependent or independent function of the NLRP3 cannot be assessed in this model.

In order to overcome this genetic issue, C57BL/6N mice with nephrocalcinosis were treated with the IL-1 receptor antagonist anakinra or a vehicle. Surprisingly, anakinra-treated mice with nephrocalcinosis showed a significant elevation of plasma BUN (similar to the vehicle-treated mice) but decreased plasma creatinine levels compared to the vehicle-treated mice, whereby intrarenal crystal deposition revealed no significant differences between both groups. It is important to note that the reduced urine oxalate concentrations observed in anakinra-treated mice correlated with increased accumulation of crystals in the renal parenchyma compared to vehicle-treated mice. No convincing explanation could be given to this finding. In contrast, mice deficient in IL-1 receptor were protected from acute calcium oxalate-induced kidney injury [64], indicating that the IL-1 receptor-mediated inflammatory response is crucial in AKI.

Furthermore, assessment of renal injury revealed no significant differences between anakinra- and vehicle-treated mice, whereas the inflammatory response associated with macrophage infiltration and

T_h -cell infiltration into the kidneys was significantly less in anakinra-treated mice implying a certain degree of protection. Surprisingly, anakinra treatment did not protect mice from renal interstitial fibrosis. Although histological analysis revealed a reduction in the intrarenal α -SMA expression in anakinra-treated mice compared to the vehicle group, collagen I deposition was significantly higher in the anakinra group compared to vehicle-treated mice. An explanation for this difference has not yet been found, as both parameters are known to positively correlate with the degree of renal interstitial fibrosis [203]. Consequently, assessment of the TGF- β receptor signaling pathway in hyperoxaluric mice upon anakinra treatment revealed no significant difference compared to the vehicle-treated mice, ruling out a link between the IL-1 receptor and the TGF- β receptor signaling pathway. Interestingly, the reduced inflammatory response observed upon anakinra treatment did not influence the profibrotic mechanisms induced by chronic hyperoxaluria. Taken together, these findings suggest that the NLRP3 inflammasome-IL-1-axis is not involved in hyperoxaluria and nephrocalcinosis-induced CKD. Unfortunately, differentiating whether these results are a product of an inflammasome-dependent or independent mechanism is currently impossible.

Recently, a novel NLRP3 inflammasome inhibitor called CP-456,773 was tested in crystal-induced CKD animal models [204]. Ludwig-Portugall et al. demonstrated that early application of CP-456,773 in mice upon adenine- or oxalate-induced nephropathy results in significant protection from renal interstitial fibrosis and progressive CKD. Unfortunately, the delayed application of the compound, which was associated with a significant reduction of IL-1 concentrations, could not resolve renal interstitial fibrosis [204]. The *in vivo* data indicated a novel approach in preventing crystal-induced nephropathy and its complications by using CP-456,773. Also, the results from this study suggest that NLRP3 and ASC can mediate crystal-induced chronic kidney injury and interstitial fibrosis through mechanisms, which do not imply inflammasome-dependent, i.e. Casp-1-mediated IL-1 β release and modulation of TGF- β downstream signaling.

4.3 Fibroblasts and the NLRP3 inflammasome

The presence of NLRP3 in non-immune cells has been extensively reported [140, 173 [138, 205], but its role in these cells is not completely understood as most of them do not secrete IL-1 β . Wang et al. reported that tubular epithelial cells from humans and mice express NLRP3 and that its expression was induced upon TGF- β 1 stimulation [138]. This was surprising as TGF- β is known for inducing epithelial cell apoptosis and exerting potent anti-inflammatory functions [131]. Interestingly, the

increased expression of NLRP3 correlated with the degree of phenotypical differentiation of TECs. Based on these findings, we investigated whether fibroblasts as main protagonists of fibrogenic processes needed the NLRP3 inflammasome for their function and proliferation. LPS-primed NIH-3t3 cells and pMEFs revealed that NLRP3 expression was inducible in fibroblasts and that this correlated with increased fibroblast activation and expression of profibrotic markers. Proliferation of pMEFs was dependent on NLRP3 and ASC. The degree of myofibroblast activation and expression of ECM components upon TGF- β 1 stimulation was decreased in cells lacking NLRP3, supporting previous studies performed in other fibroblasts including gingival and cardiac fibroblasts, where the latter also enhanced NLRP3 expression upon stimulation with TGF- β 1 [143, 180]. Stimulation of pMEFs with the inflammasome complex activator ATP did not influence the activation and function of fibroblasts. Consequently, caspase inhibition had no effect on the proliferative ability of NIH-3t3 cells, excluding an inflammasome-dependent effect on the proliferative ability of fibroblasts. This was further corroborated by the non-detectable production of IL-1 β in NIH-3t3 cells and pMEFs when compared to BMDCs. Other studies performed in cardiac fibroblasts claim that these cells can produce IL-1 β [206], although further studies on cardiac fibroblasts revealed that these cells produce negligible amounts of this cytokine compared to other inflammatory cells such as macrophages or DCs [180]. These results suggest that fibroblasts may produce small amounts of IL-1 β in a rather secondary manner. Several fibroblast subsets have been described previously where functional differences should not be ignored [103, 207] due to the tissue- and environment-specific activity of these cells. It is important to note that while our studies were ongoing, Bracey N. et al. published similar results in the heart [180]. They show in both *in vitro* and *in vivo* studies the involvement of the NLRP3 inflammasome in cardiac fibrosis and refer to the inflammasome-independent signaling pathway of NLRP3. Using cardiac fibroblasts, *in vitro* experiments demonstrate that NLRP3 regulates their differentiation into myofibroblasts in a Casp-1-independent manner [180].

In conclusion, we show that the inflammasome component NLRP3 is pivotal for fibroblast activation, function and proliferation, and that this effect relies mainly on the regulation of TGF- β 1 signaling and not on the caspase-1-mediated interleukin release.

Further research supported this theory and found an inflammasome-independent, non-canonical role for NLRP3. Recently, Wang H. et al. revealed that NLRP3 is required for EMT in colon cancer cells, a response that is independent of Casp-1-mediated IL-1 β secretion [208]. They also reported that this effect was dependent on the activation of NF- κ B signaling and regulated the expression of Snail [208]. Additionally, caspase-11 (equivalent in mice to caspase-4 and caspase-5 in humans) induces

NLRP3 inflammasome activation [186], whereby intracellular LPS binds to caspase-11 *via* Guanylate-binding proteins (GBPs) for the activation and cleavage of Gasdermine D, leading to pyroptotic cell death. Caspase-11-induced non-canonical NLRP3 activation has shown to be related to K⁺ efflux [202]. Furthermore, Chung H. et al. reported a novel non-canonical pathway for NLRP3 involving the regulation of a non-canonical platform for caspase-8 activation during epithelial cell apoptosis [209]. They propose that NLRP3 and ASC form a platform for activating caspase-8 mediated type II apoptosis in tubular epithelial cells. These effects vary from cell type to cell type and the localization of the NLRP3 in the cell might also be pivotal, e.g. NLRP3 localizes mostly to the cytosol in macrophages, but mainly to the mitochondria in TECs. Thus suggesting that NLRP3 acts in a cell-context-specific manner balancing between inflammation and cell death [209].

4.4 Study limitations

The limitations of the current thesis are among others that most of the *in vitro* studies were performed in pMEFs instead of using renal fibroblasts. Whether renal fibroblasts behave in a similar manner like pMEFs is not addressed in this thesis. Also, the possible effects of IL-18 could not be evaluated in these cells.

Furthermore, using zVAD for *in vivo* studies is rather unspecific for the inhibition of caspases, i.e. other caspase-specific functions such as regulation of apoptosis were probably also influenced in this study, but could not be directly assessed. Another limitation involving the use of anakinra as IL-1 receptor inhibitor was the limited quantification of the inhibitory effect on the IL-1 receptor, which could not be directly assessed in this thesis. The reduced inflammatory responses observed in the study already suggest an effect of anakinra, although a direct quantification was not possible. A study using a dose-dependent anakinra application *in vivo* could be supportive in this manner. Nevertheless, the assessment of this was beyond the aims of this study.

As described before the lack of intrarenal calcium oxalate crystal deposition in hyperoxaluric *Nlrp-3*- and *Asc*-deficient mice made it impossible to assess the role of these proteins in mice with nephrocalcinosis.

Finally, experiments performed in mice only reflect to a limited extent human disease, due to the genetic and pathophysiological differences between both species.

4.5 Conclusion and further perspectives

The results of this thesis identify NLRP3-TGF- β receptor signaling as a novel pathomechanism involved in renal fibrogenesis and CKD progression. From a therapeutic perspective, blocking NLRP3 is a potential target that can abrogate the inflammasome-dependent as well as -independent functions, and thus preventing the inflammatory and fibrotic response in CKD.

Figure 42 shows a schematic representation of the proposed mechanism involving the regulation of the TGF- β receptor signaling pathway by NLRP3. Hence, the novel NLRP3 inflammasome inhibitors viz. β -hydroxybutyrate [210], glyburide[211], parthenolide, Bay11_7082 [212] and MCC950 (or CP-456773) [213] could be used as potential therapeutic approaches for CKD.

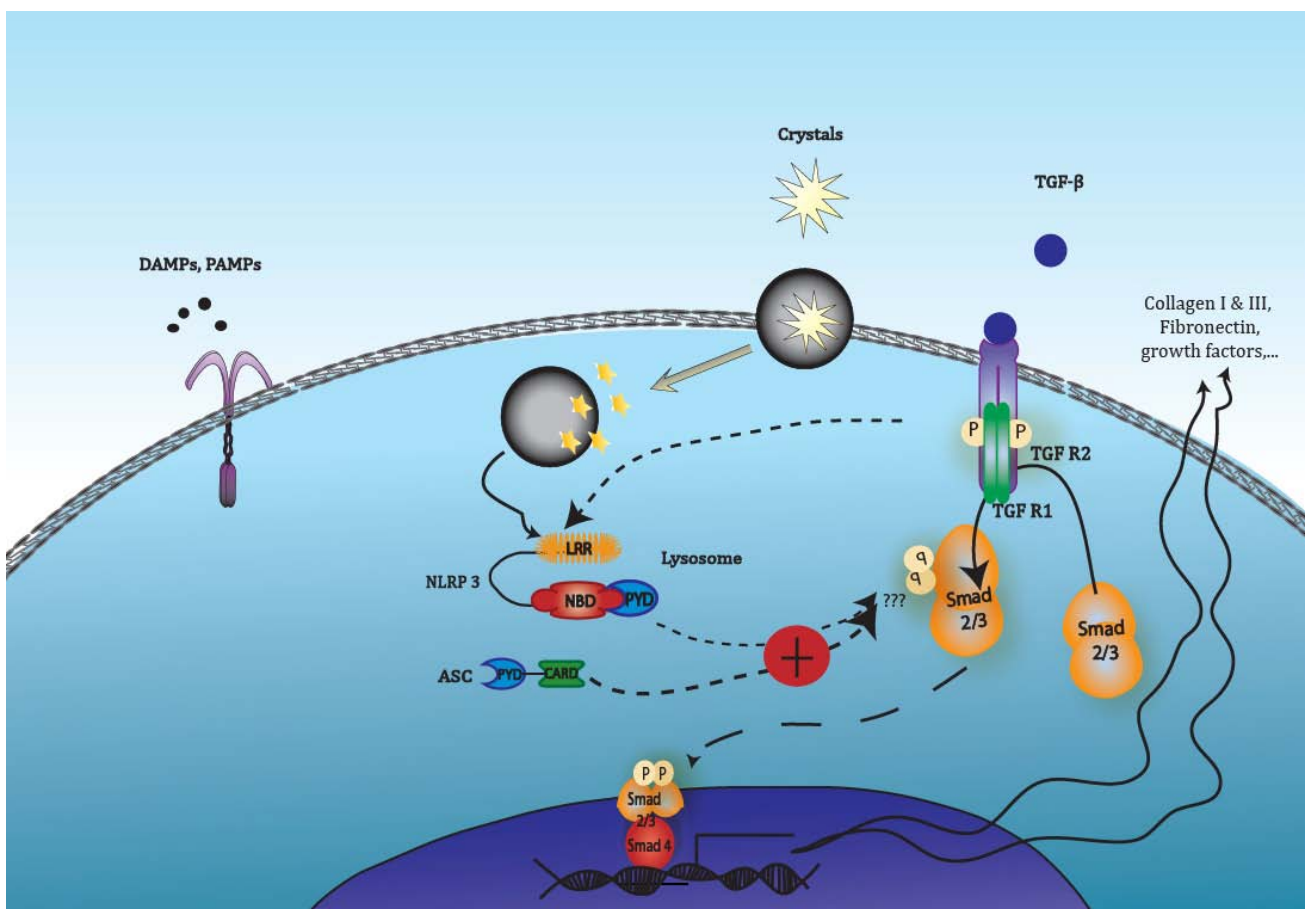


Figure 42: Schematic representation of the modulation of NLRP3-mediated TGF- β receptor signaling. Stimulation with PAMPs, DAMPs and TGF- β induces NLRP3 activation. Increased expression of NLRP3 enhances Smad2/3 phosphorylation augmenting TGF- β signaling and thus the production of profibrotic proteins (Collagen I, -III, Fibronectin) and other profibrotic growth factors.

Abb.: ASC: Apoptosis-associated speck-like protein containing a CARD NLRP3: Nod-like receptor protein 3, TGF- β : transforming growth factor beta 1, PAMP: pathogen-associated molecular patterns, DAMP: damage-associated molecular patterns, Smad 2/3/4: Mothers Against Decapentaplegic Homolog 2,3 and 4, P: phosphor group, TGF R 1/2: transforming growth factor beta receptor 1 and 2.

5. Abbreviations

| | |
|-------------------------------|---|
| AKI | Acute kidney injury |
| AP | Alkali phosphatase |
| APC | Antigen presenting cell |
| ASC | Apoptosis-associated speck-like protein containing a CARD |
| ATP | Adenosine triphosphate |
| BMP | Bone morphogenic protein |
| BUN | Blood urea nitrogen |
| C57Bl6 | C57 black 6 |
| CAPS | Cryopyrin associated periodic syndromes |
| Casp-1 | Caspase 1 |
| CCL2 | chemokine (C-C motif) ligand 2 |
| CD3 | Cluster of differentiation 3 |
| CKD | Chronic kidney disease |
| CTGF | Connecting tissue growth factor |
| CXCL2 | Chemokine (C-X-C motif) ligand 2 |
| DAMPs | Danger associated molecular patterns |
| DCs | Dendritic cells |
| ECM | Extracellular matrix |
| ECS | Extracellular space |
| ED-A FN | ED-A Fibronectin |
| EMT | Epithelial to mesenchymal transition |
| EndMT | Endothelial to mesenchymal transition |
| EPO | Erythropoietin |
| ERK | Extra-cellular signal regulated kinases |
| ESRD | End stage renal disease |
| GFR | Glomerular filtration rate |
| H ₂ O ₂ | Hydrogen peroxide |
| IL-(1, 6, 8,18) | Interleukin (1, 6, 8, 18) |
| INF | Interferon |
| IRI | Ischemia reperfusion injury |
| KDIGO | Kidney Disease: Improving Global Outcomes (KDIGO) |
| KDOQI | Kidney Disease Outcomes Quality Initiative |
| KIM 1 | Kidney injury molecule 1 |
| LPS | Lipopolysaccharide |
| LTA | Lipoteichoic acid |
| LTBP | Latent TGF- β Binding Protein |
| MCP-1 | Monocyte chemotactic protein 1 |
| mRNA | Messenger Ribonucleic acid |
| NLR | NOD like receptor |
| NLRP3 | NOD like receptor binding PYD 3 |

| | |
|------------------|--|
| NOD | nucleotide-binding oligomerization domain |
| P2X ₇ | P2X Purigenic receptor 7 |
| PAMPs | Pattern associated molecular patterns |
| PAS | Periodic acid shiff |
| PDGF | Platelet derived growth factor |
| pMEFs | Primary Mouse embryonic fibroblasts |
| PRRs | Pattern recognition receptors |
| PTH | Parathormon |
| RAAS | Rennin-Angiotensine-aldosteron-system |
| SMAD | Mothers Against Decapentaplegic Homolog |
| STZ | Streptozotocin |
| TECs | Tubular epithelial cells |
| TGF- β | Transforming growth factor β |
| TIMPs | Tissue inhibitor metalloproteinases |
| TNF- α | Tumor necrosis factor α |
| UTI | Urinary tract infection |
| UTO | Urinary tract obstruction |
| UTP | Uridine triphosphate |
| UUO | Unilateral ureteral model |
| VEGF | Vascular endothelial growth factor |
| zVAD | Pan caspase inhibitor: carbobenzoxy-valyl-alanyl-aspartyl-[O- |
| α /II-GST | methyl]- fluoromethylketone α/π – Gluthation-S-transferase |

6. References

1. Janeway Jr, C.A. and R. Medzhitov, *Innate immune recognition*. Annual review of immunology, 2002. **20**(1): p. 197-216.
2. Medzhitov, R., *Toll-like receptors and innate immunity*. Nature Reviews Immunology, 2001. **1**(2): p. 135-145.
3. Longo, D.L. and T.R. Harrison, *Harrison's principles of internal medicine. Vol. 2 Vol. 2*. 2012, New York: McGraw-Hill, Medical.
4. Kidney Disease: Improving Global, O., *KDIGO clinical practice guideline for the diagnosis, evaluation, prevention, and treatment of chronic kidney disease-mineral and bone disorder (CKD-MBD)*. 2009, New York: Nature Pub. Group.
5. Data, U.U.S.r., *CKD in the United States*. USRD Annual data Report, 2015. **1**.
6. DGFN. *Daten und Fakten zur Nephrologie 2014*; Available from: <http://www.dgfn.eu/presse/downloadbereich/daten-und-fakten-zur-nephrologie.html>.
7. Krankheitskostenrechnung, S.B., Zweigstelle Bonn. *Krankheitskosten in Mio. € durch Niereninsuffizienz (ICD10: N17-N19) nach Alter (2002-2008)*. 2010; Available from: http://www.gbe-bund.de/oowa921-install/servlet/oowa/aw92/dboowasys921.xwdevkit/xwd_init?gbe.isgbetol/xs_start_neu/&p_a_id=i&p_aid=9179515&nummer=553&p_sprache=D&p_indsp=50545&p_aid=57565345.
8. William G Couser¹, G.R., Shanthi Mendis³ and Marcello Tonelli² *The Contribution of Chronic Kidney Disease to the Global Burden of Major Noncommunicable Diseases*. Kidney International, 2011.
9. Sharma, S.K., et al., *Burden of CKD, proteinuria, and cardiovascular risk among Chinese, Mongolian, and Nepalese participants in the International Society of Nephrology screening programs*. Am J Kidney Dis, 2010. **56**(5): p. 915-27.
10. Ritz, E., et al., *Prenatal programming-effects on blood pressure and renal function*. Nat Rev Nephrol, 2011. **7**(3): p. 137-44.
11. Levey, A.S., et al., *Chronic kidney disease as a global public health problem: approaches and initiatives - a position statement from Kidney Disease Improving Global Outcomes*. Kidney Int, 2007. **72**(3): p. 247-59.
12. Parsa , A., et al., *APOL1 Risk Variants, Race, and Progression of Chronic Kidney Disease*. New England Journal of Medicine, 2013. **369**(23): p. 2183-2196.
13. Herold, G., *Innere Medizin 2013 eine vorlesungsorientierte Darstellung ; unter Berücksichtigung des Gegenstandskataloges für die Ärztliche Prüfung ; mit ICD 10-Schlüssel im Text und Stichwortverzeichnis*. 2013, Köln: Selbstverl.
14. Collins, A.J., et al., *The state of chronic kidney disease, ESRD, and morbidity and mortality in the first year of dialysis*. Clinical Journal of the American Society of Nephrology, 2009. **4**(Supplement 1): p. S5-S11.
15. Bricker, N.S., *On the meaning of the intact nephron hypothesis*. The American Journal of Medicine. **46**(1): p. 1-11.
16. Hagemann, J., et al., *Danger Control Programs Cause Tissue Injury and Remodeling*. International Journal of Molecular Sciences, 2013. **14**(6): p. 11319.
17. Anders, H.J., *Four danger response programs determine glomerular and tubulointerstitial kidney pathology: clotting, inflammation, epithelial and mesenchymal healing*. Organogenesis, 2012. **8**(2): p. 29-40.
18. Zhai, X.Y., et al., *Cubilin- and megalin-mediated uptake of albumin in cultured proximal tubule cells of opossum kidney*. Kidney International. **58**(4): p. 1523-1533.

-
19. Boswell, R.N., et al., *Interleukin 6 production by human proximal tubular epithelial cells in vitro: analysis of the effects of interleukin-1 α (IL-1 α) and other cytokines*. Nephrology Dialysis Transplantation, 1994. **9**(6): p. 599-606.
 20. Imig, J.D. and M.J. Ryan, *Immune and Inflammatory Role in Renal Disease*. Comprehensive Physiology, 2013. **3**(2): p. 957-976.
 21. Silverstein, D.M., *Inflammation in chronic kidney disease: role in the progression of renal and cardiovascular disease*. Pediatr Nephrol, 2009. **24**(8): p. 1445-52.
 22. Kuncio, G.S., E.G. Neilson, and T. Haverty, *Mechanisms of tubulointerstitial fibrosis*. Kidney international, 1991. **39**(3): p. 550-556.
 23. Du Pasquier, L., *The immune system of invertebrates and vertebrates*. Comparative Biochemistry and Physiology Part B: Biochemistry and Molecular Biology, 2001. **129**(1): p. 1-15.
 24. Janeway, C. and K.P. Murphy, *Janeway Immunologie*. 2009, Heidelberg: Spektrum, Akad. Verl.
 25. Janeway, C.A., Jr. and R. Medzhitov, *Innate immune recognition*. Annu Rev Immunol, 2002. **20**: p. 197-216.
 26. Medzhitov, R. and C. Janeway, Jr., *Innate immune recognition: mechanisms and pathways*. Immunol Rev, 2000. **173**: p. 89-97.
 27. Medzhitov, R. and C.A. Janeway, Jr., *Innate immunity: impact on the adaptive immune response*. Curr Opin Immunol, 1997. **9**(1): p. 4-9.
 28. Cruse, J.M. and R.E. Lewis, *Illustrated dictionary of immunology*. 2003, Boca Raton: CRC Press.
 29. Medzhitov, R. and C. Janeway, Jr., *Innate immunity*. N Engl J Med, 2000. **343**(5): p. 338-44.
 30. Aderem, A., *Phagocytosis and the inflammatory response*. J Infect Dis, 2003. **187** Suppl 2: p. S340-5.
 31. Kaissling, B. and M. Le Hir, *Characterization and distribution of interstitial cell types in the renal cortex of rats*. Kidney international, 1994. **45**(3): p. 709-720.
 32. Kruger, T., et al., *Identification and functional characterization of dendritic cells in the healthy murine kidney and in experimental glomerulonephritis*. J Am Soc Nephrol, 2004. **15**(3): p. 613-21.
 33. Woltman, A., et al., *Quantification of dendritic cell subsets in human renal tissue under normal and pathological conditions*. Kidney international, 2007. **71**(10): p. 1001-1008.
 34. Anders, H.J., *Innate versus adaptive immunity in kidney immunopathology*. BMC Nephrol, 2013. **14**: p. 138.
 35. Turvey, S.E. and D.H. Broide, *Innate immunity*. Journal of Allergy and Clinical Immunology, 2010. **125**(2): p. S24-S32.
 36. Janeway, C.A. *Approaching the asymptote? Evolution and revolution in immunology*. in *Cold Spring Harbor symposia on quantitative biology*. 1989. Cold Spring Harbor Laboratory Press.
 37. Sauvage, E., et al., *The penicillin-binding proteins: structure and role in peptidoglycan biosynthesis*. FEMS microbiology reviews, 2008. **32**(2): p. 234-258.
 38. Matzinger, P., *Tolerance, danger, and the extended family*. Annual review of immunology, 1994. **12**(1): p. 991-1045.
 39. Matzinger, P., *The danger model: a renewed sense of self*. Science, 2002. **296**(5566): p. 301-305.
 40. Matzinger, P., *Friendly and dangerous signals: is the tissue in control?* Nature immunology, 2007. **8**(1): p. 11-13.

-
41. Seong, S.-Y. and P. Matzinger, *Hydrophobicity: an ancient damage-associated molecular pattern that initiates innate immune responses*. *Nature Reviews Immunology*, 2004. **4**(6): p. 469-478.
 42. Kaczmarek, A., P. Vandenabeele, and D.V. Krysko, *Necroptosis: the release of damage-associated molecular patterns and its physiological relevance*. *Immunity*, 2013. **38**(2): p. 209-223.
 43. Lotze, M.T. and K.J. Tracey, *High-mobility group box 1 protein (HMGB1): nuclear weapon in the immune arsenal*. *Nature Reviews Immunology*, 2005. **5**(4): p. 331-342.
 44. Krysko, D.V., et al., *Emerging role of damage-associated molecular patterns derived from mitochondria in inflammation*. *Trends in Immunology*, 2011. **32**(4): p. 157-164.
 45. Kawai, T. and S. Akira, *The role of pattern-recognition receptors in innate immunity: update on Toll-like receptors*. *Nat Immunol*, 2010. **11**(5): p. 373-384.
 46. Gordon, S., *Pattern recognition receptors: doubling up for the innate immune response*. *Cell*, 2002. **111**(7): p. 927-930.
 47. Loop, T. and H. Pahl, *Activators and Target Genes of Rel/NF- κ B Transcription Factors*, in *Nuclear Factor κ B*. 2003, Springer. p. 1-48.
 48. Mantovani, A., et al., *Pentraxins in innate immunity: from C-reactive protein to the long pentraxin PTX3*. *Journal of clinical immunology*, 2008. **28**(1): p. 1-13.
 49. Areschoug, T. and S. Gordon, *Pattern recognition receptors and their role in innate immunity: focus on microbial protein ligands*, in *Trends in Innate Immunity*. 2008, Karger Publishers. p. 45-60.
 50. Loo, Y.M. and M. Gale, *Immune signaling by RIG-I-like receptors*. *Immunity*, 2011. **34**(5): p. 680-92.
 51. Laing, K.J., et al., *A genomic view of the NOD-like receptor family in teleost fish: identification of a novel NLR subfamily in zebrafish*. *BMC Evolutionary Biology*, 2008. **8**(1): p. 42.
 52. Tattoli, I., et al., *NLRX1 is a mitochondrial NOD-like receptor that amplifies NF- κ B and JNK pathways by inducing reactive oxygen species production*. *EMBO reports*, 2008. **9**(3): p. 293-300.
 53. Chen, G., et al., *NOD-like receptors: role in innate immunity and inflammatory disease*. *Annual Review of Pathological Mechanical Disease*, 2009. **4**: p. 365-398.
 54. Kanneganti, T.-D., M. Lamkanfi, and G. Núñez, *Intracellular NOD-like Receptors in Host Defense and Disease*. *Immunity*, 2007. **27**(4): p. 549-559.
 55. Ting, J.P.-Y., et al., *The NLR gene family: an official nomenclature*. *Immunity*, 2008. **28**(3): p. 285.
 56. Schroder, K. and J. Tschopp, *The inflammasomes*. *Cell*, 2010. **140**(6): p. 821-832.
 57. Martinon, F., K. Burns, and J. Tschopp, *The inflammasome: a molecular platform triggering activation of inflammatory caspases and processing of proIL- β* . *Molecular cell*, 2002. **10**(2): p. 417-426.
 58. Dinarello, C.A., *Interleukin-1 β , Interleukin-18, and the Interleukin-1 β Converting Enzyme*. *Annals of the New York Academy of Sciences*, 1998. **856**(1): p. 1-11.
 59. Kummer, J.A., et al., *Inflammasome components NALP 1 and 3 show distinct but separate expression profiles in human tissues suggesting a site-specific role in the inflammatory response*. *Journal of Histochemistry & Cytochemistry*, 2007. **55**(5): p. 443-452.
 60. Guarda, G., et al., *Differential expression of NLRP3 among hematopoietic cells*. *The Journal of Immunology*, 2011. **186**(4): p. 2529-2534.
 61. Netea, M.G., et al., *Differential requirement for the activation of the inflammasome for processing and release of IL-1 β in monocytes and macrophages*. *Blood*, 2009. **113**(10): p. 2324-2335.

-
62. Pétrilli, V., et al., *The inflammasome: a danger sensing complex triggering innate immunity*. Current opinion in immunology, 2007. **19**(6): p. 615-622.
 63. Bortoluci, K.R. and R. Medzhitov, *Control of infection by pyroptosis and autophagy: role of TLR and NLR*. Cellular and Molecular Life Sciences, 2010. **67**(10): p. 1643-1651.
 64. Mulay, S.R., et al., *Calcium oxalate crystals induce renal inflammation by NLRP3-mediated IL-1beta secretion*. J Clin Invest, 2013. **123**(1): p. 236-46.
 65. Martinon, F., et al., *Gout-associated uric acid crystals activate the NALP3 inflammasome*. Nature, 2006. **440**(7081): p. 237-241.
 66. Darisipudi, M.N., et al., *Uromodulin triggers IL-1beta-dependent innate immunity via the NLRP3 inflammasome*. J Am Soc Nephrol, 2012. **23**(11): p. 1783-9.
 67. Mariathasan, S., et al., *Cryopyrin activates the inflammasome in response to toxins and ATP*. Nature, 2006. **440**(7081): p. 228-232.
 68. Cruz, C.M., et al., *ATP activates a reactive oxygen species-dependent oxidative stress response and secretion of proinflammatory cytokines in macrophages*. Journal of Biological Chemistry, 2007. **282**(5): p. 2871-2879.
 69. Franchi, L., R. Muñoz-Planillo, and G. Núñez, *Sensing and reacting to microbes through the inflammasomes*. Nature immunology, 2012. **13**(4): p. 325-332.
 70. Walle, L.V., et al., *Negative regulation of the NLRP3 inflammasome by A20 protects against arthritis*. Nature, 2014. **512**(7512): p. 69-73.
 71. Martinon, F., et al., *Identification of bacterial muramyl dipeptide as activator of the NALP3/cryopyrin inflammasome*. Curr Biol, 2004. **14**(21): p. 1929-34.
 72. Kanneganti, T.-D., et al., *Bacterial RNA and small antiviral compounds activate caspase-1 through cryopyrin/Nalp3*. Nature, 2006. **440**(7081): p. 233-236.
 73. Kim, S., et al., *Listeria monocytogenes is sensed by the NLRP3 and AIM2 inflammasome*. European journal of immunology, 2010. **40**(6): p. 1545-1551.
 74. Craven, R.R., et al., *Staphylococcus aureus alpha-hemolysin activates the NLRP3-inflammasome in human and mouse monocytic cells*. PloS one, 2009. **4**(10): p. e7446.
 75. Allen, I.C., et al., *The NLRP3 inflammasome mediates in vivo innate immunity to influenza A virus through recognition of viral RNA*. Immunity, 2009. **30**(4): p. 556-565.
 76. Dostert, C., et al., *Malarial hemozoin is a Nalp3 inflammasome activating danger signal*. PLoS One, 2009. **4**(8): p. e6510.
 77. Ea, H.K., et al., *Basic calcium phosphate crystals induce NLRP3 inflammasome activation: the in vitro and in vivo face to face*. Proc Natl Acad Sci U S A, 2011. **108**(50): p. E1361; author reply E1362.
 78. Martinon, F., et al., *Gout-associated uric acid crystals activate the NALP3 inflammasome*. Nature, 2006. **440**(7081): p. 237-41.
 79. Duewell, P., et al., *NLRP3 inflammasomes are required for atherogenesis and activated by cholesterol crystals*. Nature, 2010. **464**(7293): p. 1357-61.
 80. Prencipe, G., et al., *Inflammasome activation by cystine crystals: implications for the pathogenesis of cystinosis*. J Am Soc Nephrol, 2014. **25**(6): p. 1163-9.
 81. Demento, S.L., et al., *Inflammasome-activating nanoparticles as modular systems for optimizing vaccine efficacy*. Vaccine, 2009. **27**(23): p. 3013-21.
 82. Dostert, C., et al., *Innate immune activation through Nalp3 inflammasome sensing of asbestos and silica*. Science, 2008. **320**(5876): p. 674-7.
 83. Nakagawa, K., et al., *Somatic NLRP3 mosaicism in Muckle-Wells syndrome. A genetic mechanism shared by different phenotypes of cryopyrin-associated periodic syndromes*. Annals of the rheumatic diseases, 2015. **74**(3): p. 603-610.
 84. Kümmerle-Deschner, J.B., et al., *Risk factors for severe Muckle-Wells syndrome*. Arthritis & Rheumatism, 2010. **62**(12): p. 3783-3791.

-
85. Ichinohe, T., I.K. Pang, and A. Iwasaki, *Influenza virus activates inflammasomes via its intracellular M2 ion channel*. Nature immunology, 2010. **11**(5): p. 404-410.
 86. Broz, P., et al., *Redundant roles for inflammasome receptors NLRP3 and NLRC4 in host defense against Salmonella*. The Journal of experimental medicine, 2010. **207**(8): p. 1745-1755.
 87. Chow, M.T., et al., *NLRP3 promotes inflammation-induced skin cancer but is dispensable for asbestos-induced mesothelioma*. Immunology and cell biology, 2012. **90**(10): p. 983-986.
 88. Dostert, C., et al., *Innate immune activation through Nalp3 inflammasome sensing of asbestos and silica*. Science, 2008. **320**(5876): p. 674-677.
 89. He, J., Y. Yang, and D.-Q. Peng, *Monosodium urate (MSU) crystals increase gout associated coronary heart disease (CHD) risk through the activation of NLRP3 inflammasome*. International journal of cardiology, 2012. **160**(1): p. 72-73.
 90. Kingsbury, S.R., P.G. Conaghan, and M.F. McDermott, *The role of the NLRP3 inflammasome in gout*. J Inflamm Res, 2011. **4**: p. 39-49.
 91. Singh, D. and K.K. Huston, *IL-1 inhibition with anakinra in a patient with refractory gout*. JCR: Journal of Clinical Rheumatology, 2009. **15**(7): p. 366.
 92. Pope, R.M. and J. Tschopp, *The role of interleukin-1 and the inflammasome in gout: implications for therapy*. Arthritis & Rheumatism, 2007. **56**(10): p. 3183-3188.
 93. Esser, N., et al., *Inflammation as a link between obesity, metabolic syndrome and type 2 diabetes*. Diabetes research and clinical practice, 2014. **105**(2): p. 141-150.
 94. Stienstra, R., et al., *The inflammasome-mediated caspase-1 activation controls adipocyte differentiation and insulin sensitivity*. Cell Metab, 2010. **12**(6): p. 593-605.
 95. Yan, Y., et al., *Omega-3 fatty acids prevent inflammation and metabolic disorder through inhibition of NLRP3 inflammasome activation*. Immunity, 2013. **38**(6): p. 1154-1163.
 96. Lee, H.-M., et al., *Upregulated NLRP3 inflammasome activation in patients with type 2 diabetes*. Diabetes, 2013. **62**(1): p. 194-204.
 97. Mandrup-Poulsen, T., L. Pickersgill, and M.Y. Donath, *Blockade of interleukin 1 in type 1 diabetes mellitus*. Nature Reviews Endocrinology, 2010. **6**(3): p. 158-166.
 98. Duewell, P., et al., *NLRP3 inflammasomes are required for atherogenesis and activated by cholesterol crystals*. Nature, 2010. **464**(7293): p. 1357-1361.
 99. Badylak, S.F., *The extracellular matrix as a biologic scaffold material*. Biomaterials, 2007. **28**(25): p. 3587-3593.
 100. Frantz, C., K.M. Stewart, and V.M. Weaver, *The extracellular matrix at a glance*. J Cell Sci, 2010. **123**(24): p. 4195-4200.
 101. Daley, W.P. and K.M. Yamada, *ECM-modulated cellular dynamics as a driving force for tissue morphogenesis*. Current Opinion in Genetics & Development, 2013. **23**(4): p. 408-414.
 102. Virchow, R., *Die Cellularpathologie in ihrer Begründung auf physiologische und pathologische Gewebelehre: 20 Vorlesungen, gehalten während d. Monate Febr., März u. April 1858 im Patholog. Inst. zu Berlin*. 1858: Hirschwald.
 103. Maxwell, P.H., et al., *Identification of the renal erythropoietin-producing cells using transgenic mice*. Kidney international, 1993. **44**(5): p. 1149-1162.
 104. Paliege, A., et al., *Hypoxia-inducible factor-2 α -expressing interstitial fibroblasts are the only renal cells that express erythropoietin under hypoxia-inducible factor stabilization*. Kidney international, 2010. **77**(4): p. 312-318.
 105. Paszek, M.J. and V.M. Weaver, *The tension mounts: mechanics meets morphogenesis and malignancy*. Journal of mammary gland biology and neoplasia, 2004. **9**(4): p. 325-342.
 106. Migita, K., et al., *Serum amyloid A protein induces production of matrix metalloproteinases by human synovial fibroblasts*. Laboratory investigation; a journal of technical methods and pathology, 1998. **78**(5): p. 535-539.

-
107. Mott, J.D. and Z. Werb, *Regulation of matrix biology by matrix metalloproteinases*. Current Opinion in Cell Biology, 2004. **16**(5): p. 558-564.
 108. Wang, L., J. Luo, and S. He, *Induction of MMP-9 release from human dermal fibroblasts by thrombin: involvement of JAK/STAT3 signaling pathway in MMP-9 release*. BMC Cell Biol, 2007. **8**: p. 14.
 109. Boor, P. and J. Floege, *The renal (myo-) fibroblast: a heterogeneous group of cells*. Nephrology Dialysis Transplantation, 2012. **27**(8): p. 3027-3036.
 110. Xu, J., S. Lamouille, and R. Derynck, *TGF- β -induced epithelial to mesenchymal transition*. Cell research, 2009. **19**(2): p. 156-172.
 111. Zeisberg, M., et al., *Fibroblasts derive from hepatocytes in liver fibrosis via epithelial to mesenchymal transition*. Journal of Biological Chemistry, 2007. **282**(32): p. 23337-23347.
 112. Lovisa, S., et al., *Epithelial-to-mesenchymal transition induces cell cycle arrest and parenchymal damage in renal fibrosis*. Nature medicine, 2015.
 113. Feghali, C.A. and T.M. Wright, *Cytokines in acute and chronic inflammation*. Front Biosci, 1997. **2**(1): p. d12-d26.
 114. Scotton, C.J. and R.C. Chambers, *Molecular targets in pulmonary fibrosis: the myofibroblast in focus*. CHEST Journal, 2007. **132**(4): p. 1311-1321.
 115. Gordon, M. and R. Hahn, *Collagens Cell Tissue Res. 2010, 339, 247–257*. DOI.
 116. Farris, A.B. and R.B. Colvin, *Renal Interstitial fibrosis: mechanisms and evaluation in: current opinion in nephrology and hypertension*. Current opinion in nephrology and hypertension, 2012. **21**(3): p. 289.
 117. Darby, I.A., et al., *Fibroblasts and myofibroblasts in wound healing*. Clin Cosmet Investig Dermatol, 2014. **7**: p. 301-11.
 118. Schainuck, L.I., et al., *Structural-functional correlations in renal disease: Part II: the correlations*. Human pathology, 1970. **1**(4): p. 631-641.
 119. Bohle, A., et al., *The role of the interstitium of the renal cortex in renal disease*, in *Interstitial Nephropathies*. 1979, Karger Publishers. p. 109-114.
 120. Zeisberg, M. and E.G. Neilson, *Mechanisms of tubulointerstitial fibrosis*. Journal of the American Society of Nephrology, 2010. **21**(11): p. 1819-1834.
 121. Lee, T.Y., et al., *Expression of transforming growth factor beta 1, 2, and 3 proteins in keloids*. Annals of plastic surgery, 1999. **43**(2): p. 179&hyphen.
 122. Wang, R., et al., *Hypertrophic scar tissues and fibroblasts produce more transforming growth factor- β 1 mRNA and protein than normal skin and cells*. Wound Repair and Regeneration, 2000. **8**(2): p. 128-137.
 123. Chou, D., W. Lee, and C. McCulloch, *TNF-alpha inactivation of collagen receptors: implications for fibroblast function and fibrosis*. The Journal of Immunology, 1996. **156**(11): p. 4354-4362.
 124. Baroni, G.S., et al., *Interferon gamma decreases hepatic stellate cell activation and extracellular matrix deposition in rat liver fibrosis*. Hepatology, 1996. **23**(5): p. 1189-1199.
 125. Sporn, M.B., et al., *Transforming growth factor-beta: biological function and chemical structure*. Science, 1986. **233**(4763): p. 532-534.
 126. Crowe, M.J., T. Doetschman, and D.G. Greenhalgh, *Delayed wound healing in immunodeficient TGF- β 1 knockout mice*. Journal of Investigative Dermatology, 2000. **115**(1): p. 3-11.
 127. Saharinen, J., et al., *Latent transforming growth factor- β binding proteins (LTBPs)—structural extracellular matrix proteins for targeting TGF- β action*. Cytokine & growth factor reviews, 1999. **10**(2): p. 99-117.

-
128. Yu, Q. and I. Stamenkovic, *Cell surface-localized matrix metalloproteinase-9 proteolytically activates TGF- β and promotes tumor invasion and angiogenesis*. Genes & development, 2000. **14**(2): p. 163-176.
 129. Schultz-Cherry, S. and J.E. Murphy-Ullrich, *Thrombospondin causes activation of latent transforming growth factor-beta secreted by endothelial cells by a novel mechanism*. The Journal of cell biology, 1993. **122**(4): p. 923-932.
 130. Roberts, A.B., *TGF- β signaling from receptors to the nucleus*. Microbes and Infection, 1999. **1**(15): p. 1265-1273.
 131. Attisano, L. and J.L. Wrana, *Signal transduction by the TGF- β superfamily*. Science, 2002. **296**(5573): p. 1646-1647.
 132. Verrecchia, F. and A. Mauviel, *Transforming Growth Factor- β ; Signaling Through the Smad Pathway: Role in Extracellular Matrix Gene Expression and Regulation*. Journal of Investigative Dermatology, 2002. **118**(2): p. 211-215.
 133. Savage, C., et al., *Caenorhabditis elegans genes sma-2, sma-3, and sma-4 define a conserved family of transforming growth factor beta pathway components*. Proceedings of the National Academy of Sciences, 1996. **93**(2): p. 790-794.
 134. Heldin, C.-H., K. Miyazono, and P. Ten Dijke, *TGF- β signalling from cell membrane to nucleus through SMAD proteins*. Nature, 1997. **390**(6659): p. 465-471.
 135. Kretzschmar, M., et al., *A mechanism of repression of TGF β /Smad signaling by oncogenic Ras*. Genes & development, 1999. **13**(7): p. 804-816.
 136. Kopp, J.B., *TGF- β signaling and the renal tubular epithelial cell: too much, too little, and just right*. Journal of the American Society of Nephrology, 2010. **21**(8): p. 1241-1243.
 137. Anders, H.J. and D.A. Muruve, *The inflammasomes in kidney disease*. J Am Soc Nephrol, 2011. **22**(6): p. 1007-18.
 138. Wang, W., et al., *Inflammasome-independent NLRP3 augments TGF- β signaling in kidney epithelium*. The Journal of Immunology, 2013. **190**(3): p. 1239-1249.
 139. Abais, J.M., et al., *Nod-like receptor protein 3 (NLRP3) inflammasome activation and podocyte injury via thioredoxin-interacting protein (TXNIP) during hyperhomocysteinemia*. Journal of Biological Chemistry, 2014. **289**(39): p. 27159-27168.
 140. Xia, M., et al., *Inhibition of hyperhomocysteinemia-induced inflammasome activation and glomerular sclerosis by NLRP3 gene deletion*. Cellular Physiology and Biochemistry, 2014. **34**(3): p. 829-841.
 141. Chun, J., et al., *NLRP3 Localizes to the Tubular Epithelium in Human Kidney and Correlates With Outcome in IgA Nephropathy*. Sci Rep, 2016. **6**.
 142. Sandanger, Ø., et al., *The NLRP3 inflammasome is up-regulated in cardiac fibroblasts and mediates myocardial ischaemia-reperfusion injury*. Cardiovascular research, 2013. **99**(1): p. 164-174.
 143. Belibasakis, G.N., B. Guggenheim, and N. Bostanci, *Down-regulation of NLRP3 inflammasome in gingival fibroblasts by subgingival biofilms: involvement of Porphyromonas gingivalis*. Innate immunity, 2013. **19**(1): p. 3-9.
 144. Furuichi, K., et al., *Interleukin-1-dependent sequential chemokine expression and inflammatory cell infiltration in ischemia-reperfusion injury*. Critical care medicine, 2006. **34**(9): p. 2447-2455.
 145. Iyer, S.S., et al., *Necrotic cells trigger a sterile inflammatory response through the Nlrp3 inflammasome*. Proceedings of the National Academy of Sciences, 2009. **106**(48): p. 20388-20393.
 146. Lee, D.W., S. Faubel, and C.L. Edelstein, *A pan caspase inhibitor decreases caspase-1, IL-1 α and IL-1 β , and protects against necrosis of cisplatin-treated freshly isolated proximal tubules*. Renal failure, 2015. **37**(1): p. 144-150.

-
147. Faubel, S., et al., *Caspase-1-deficient mice are protected against cisplatin-induced apoptosis and acute tubular necrosis*. *Kidney international*, 2004. **66**(6): p. 2202-2213.
 148. Parikh, C.R., et al., *Urine IL-18 is an early diagnostic marker for acute kidney injury and predicts mortality in the intensive care unit*. *Journal of the American Society of Nephrology*, 2005. **16**(10): p. 3046-3052.
 149. Isaka, Y., et al., *Hyperuricemia-induced inflammasome and kidney diseases*. *Nephrology Dialysis Transplantation*, 2015: p. gfv024.
 150. Kim, S.-M., et al., *Hyperuricemia-induced NLRP3 activation of macrophages contributes to the progression of diabetic nephropathy*. *American Journal of Physiology-Renal Physiology*, 2015. **308**(9): p. F993-F1003.
 151. Shahzad, K., et al., *Nlrp3-inflammasome activation in non-myeloid-derived cells aggravates diabetic nephropathy*. *Kidney international*, 2015. **87**(1): p. 74-84.
 152. Vilaysane, A., et al., *The NLRP3 inflammasome promotes renal inflammation and contributes to CKD*. *Journal of the American Society of Nephrology*, 2010. **21**(10): p. 1732-1744.
 153. Lech, M., et al., *NLRP3 and ASC suppress lupus-like autoimmunity by driving the immunosuppressive effects of TGF-beta receptor signalling*. *Ann Rheum Dis*, 2015. **74**(12): p. 2224-35.
 154. Yang, H.C., Y. Zuo, and A.B. Fogo, *Models of chronic kidney disease*. *Drug Discov Today Dis Models*, 2010. **7**(1-2): p. 13-9.
 155. Johnston, D.L., et al., *Contemporary Management of Vesicoureteral Reflux*. *Curr Treat Options Pediatr*, 2016. **2**(2): p. 82-93.
 156. Chevalier, R.L., *Obstructive nephropathy: towards biomarker discovery and gene therapy*. *Nat Clin Pract Nephrol*, 2006. **2**(3): p. 157-68.
 157. Chevalier, R.L., M.S. Forbes, and B.A. Thornhill, *Ureteral obstruction as a model of renal interstitial fibrosis and obstructive nephropathy*. *Kidney Int*, 2009. **75**(11): p. 1145-52.
 158. Curhan, G.C. and E.N. Taylor, *24-h uric acid excretion and the risk of kidney stones*. *Kidney Int*, 2008. **73**(4): p. 489-96.
 159. Nazzari, L., S. Puri, and D.S. Goldfarb, *Enteric hyperoxaluria: an important cause of end-stage kidney disease*. *Nephrology Dialysis Transplantation*, 2015.
 160. McMartin, K., *Are calcium oxalate crystals involved in the mechanism of acute renal failure in ethylene glycol poisoning?* *Clin Toxicol (Phila)*, 2009. **47**(9): p. 859-69.
 161. Mulay, S.R., A. Evan, and H.-J. Anders, *Molecular mechanisms of crystal-related kidney inflammation and injury. Implications for cholesterol embolism, crystalline nephropathies and kidney stone disease*. *Nephrology Dialysis Transplantation*, 2014. **29**(3): p. 507-514.
 162. Khan, S.R., *Crystal-induced inflammation of the kidneys: results from human studies, animal models, and tissue-culture studies*. *Clin Exp Nephrol*, 2004. **8**(2): p. 75-88.
 163. Mulay, S.R., et al., *Oxalate-induced chronic kidney disease with its uremic and cardiovascular complications in C57BL/6 mice*. 2016: p. ajprenal.00488.2015.
 164. Knauf, F., et al., *NALP3-mediated inflammation is a principal cause of progressive renal failure in oxalate nephropathy*. *Kidney Int*, 2013. **84**(5): p. 895-901.
 165. Principle of MTT Assay. Available from: https://www.researchgate.net/figure/279778205_fig2_Figure-2-Principle-of-MTT-assay.
 166. scientific, T. 260/280 and 260/230 Ratios. T009-TECHNICAL BULLETIN NanoDrop 1000 & 8000; Available from: <http://www.nanodrop.com/Library/T009-NanoDrop%201000-&-NanoDrop%208000-Nucleic-Acid-Purity-Ratios.pdf>.
 167. Biosystems, A. *Real-Time PCR Vs. Traditional PCR*. Support-Tutorials; Available from: http://www6.appliedbiosystems.com/support/tutorials/pdf/rtpcr_vs_tradpcr.pdf.
 168. Gateway, H.M. *Real-Time PCR Quantification Analysis*. Available from: <http://www.highveld.com/pcr/real-time-pcr-quantification-analysis.html>.

-
169. abcam. *Immunocytochemistry and immunofluorescence protocol*. IHC protocols; Available from: <http://www.abcam.com/protocols/immunocytochemistry-immunofluorescence-protocol>.
 170. OptEIA, B. *Mouse IL-1beta ELISA Set*. Technical data sheet; Cat. No. 559603]. Available from: <http://www.bdbiosciences.com/ds/pm/tds/559603.pdf4>.
 171. BIO-RAD. *Quick Start Bradford Protein Assay - Instruction Manual*. Available from: <http://www.nature.com/protocolexchange/protocols/2925#/procedure>.
 172. LI-COR. *Western Blot protocol - Troubleshooting*. Available from: Mahmood T, Yang PC. Western blot: Technique, theory, and trouble shooting. *North Am J Med Sci* 2012;4:429-34.
 173. Mulay, S.R., *Role of murine double minute (MDM)-2 in kidney injury and repair*. 2013, lmu.
 174. SCIENCES, E.M. *Pizzolato method for Calcium Oxalate*. EMS Catalog #26212]. Available from: <https://www.emsdiasum.com/microscopy/technical/datasheet/26212.aspx>.
 175. abcam. *Product datasheet: Anti-alpha smooth muscle Actin antibody [1A4] ab7817*. Available from: <http://www.abcam.com/alpha-smooth-muscle-actin-antibody-1a4-ab7817.html>.
 176. Garber, S.L., et al., *Relaxin decreases renal interstitial fibrosis and slows progression of renal disease I*. *Kidney international*, 2001. **59**(3): p. 876-882.
 177. Knauf, F., et al., *NALP3-mediated inflammation is a principal cause of progressive renal failure in oxalate nephropathy*. *Kidney international*, 2013. **84**(5): p. 895-901.
 178. Lonnemann, G., et al., *Cytokines in human renal interstitial fibrosis. II. Intrinsic interleukin (IL)-1 synthesis and IL-1-dependent production of IL-6 and IL-8 by cultured kidney fibroblasts*. *Kidney international*, 1995. **47**(3): p. 845-854.
 179. Baum, J. and H.S. Duffy, *Fibroblasts and Myofibroblasts: What are we talking about?* *J Cardiovasc Pharmacol*, 2011. **57**(4): p. 376-9.
 180. Bracey, N.A., et al., *Mitochondrial NLRP3 protein induces reactive oxygen species to promote Smad protein signaling and fibrosis independent from the inflammasome*. *Journal of Biological Chemistry*, 2014. **289**(28): p. 19571-19584.
 181. LeBleu, V.S., et al., *Origin and Function of Myofibroblasts in Kidney Fibrosis*. *Nature medicine*, 2013. **19**(8): p. 1047-1053.
 182. Meng, X.-M., D.J. Nikolic-Paterson, and H.Y. Lan, *Inflammatory processes in renal fibrosis*. *Nature Reviews Nephrology*, 2014. **10**(9): p. 493-503.
 183. Eddy, A.A., *Molecular basis of renal fibrosis*. *Pediatric nephrology*, 2000. **15**(3-4): p. 290-301.
 184. Kurts, C., et al., *The immune system and kidney disease: basic concepts and clinical implications*. *Nat Rev Immunol*, 2013. **13**(10): p. 738-753.
 185. Anders, H.-J., *Innate versus adaptive immunity in kidney immunopathology*. *BMC nephrology*, 2013. **14**(1): p. 138.
 186. Broz, P. and V.M. Dixit, *Inflammasomes: mechanism of assembly, regulation and signalling*. *Nat Rev Immunol*, 2016. **16**(7): p. 407-420.
 187. Guo, H., J.B. Callaway, and J.P. Ting, *Inflammasomes: mechanism of action, role in disease, and therapeutics*. *Nature medicine*, 2015. **21**(7): p. 677-687.
 188. Lorenz, G., M.N. Darisipudi, and H.J. Anders, *Canonical and non-canonical effects of the NLRP3 inflammasome in kidney inflammation and fibrosis*. *Nephrol Dial Transplant*, 2014. **29**(1): p. 41-8.
 189. Dumas, A., et al., *The inflammasome pyrin contributes to pertussis toxin-induced IL-1beta synthesis, neutrophil intravascular crawling and autoimmune encephalomyelitis*. *PLoS Pathog*, 2014. **10**(5): p. e1004150.

-
190. Guo, H., et al., *NLRP3 Deficiency Attenuates Renal Fibrosis and Ameliorates Mitochondrial Dysfunction in a Mouse Unilateral Ureteral Obstruction Model of Chronic Kidney Disease*. 2017. **2017**: p. 8316560.
 191. Gong, W., et al., *NLRP3 deletion protects against renal fibrosis and attenuates mitochondrial abnormality in mouse with 5/6 nephrectomy*. *Am J Physiol Renal Physiol*, 2016. **310**(10): p. F1081-8.
 192. Zhuang, Y., et al., *NLRP3 inflammasome mediates albumin-induced renal tubular injury through impaired mitochondrial function*. *J Biol Chem*, 2014. **289**(36): p. 25101-11.
 193. Zhuang, Y., et al., *Mitochondrial dysfunction confers albumin-induced NLRP3 inflammasome activation and renal tubular injury*. *Am J Physiol Renal Physiol*, 2015. **308**(8): p. F857-66.
 194. Ding, W., et al., *Rotenone Attenuates Renal Injury in Aldosterone-Infused Rats by Inhibiting Oxidative Stress, Mitochondrial Dysfunction, and Inflammasome Activation*. *Med Sci Monit*, 2015. **21**: p. 3136-43.
 195. Ding, W., et al., *Mitochondrial reactive oxygen species-mediated NLRP3 inflammasome activation contributes to aldosterone-induced renal tubular cells injury*. *Oncotarget*, 2016. **7**(14): p. 17479-91.
 196. Wree, A., et al., *NLRP3 inflammasome activation results in hepatocyte pyroptosis, liver inflammation and fibrosis*. *Hepatology (Baltimore, Md.)*, 2014. **59**(3): p. 898-910.
 197. Komada, T., et al., *ASC in renal collecting duct epithelial cells contributes to inflammation and injury after unilateral ureteral obstruction*. *Am J Pathol*, 2014. **184**(5): p. 1287-98.
 198. Mulay, S.R. and H.J. Anders, *Crystallopathies*. *N Engl J Med*, 2016. **374**(25): p. 2465-76.
 199. Anders, H.J., *Of Inflammasomes and Alarmins: IL-1beta and IL-1alpha in Kidney Disease*. *Mediators Inflamm*, 2016. **27**(9): p. 2564-75.
 200. Ermer, T., et al., *Oxalate, inflammasome, and progression of kidney disease*. *Current opinion in nephrology and hypertension*, 2016. **25**(4): p. 363-371.
 201. Vanden Berghe, T., et al., *Passenger Mutations Confound Interpretation of All Genetically Modified Congenic Mice*. *Immunity*, 2015. **43**(1): p. 200-9.
 202. Kayagaki, N., et al., *Non-canonical inflammasome activation targets caspase-11*. *Nature*, 2011. **479**(7371): p. 117-121.
 203. Boukhalfa, G., et al., *Relationship between alpha-smooth muscle actin expression and fibrotic changes in human kidney*. *Exp Nephrol*, 1996. **4**(4): p. 241-7.
 204. Ludwig-Portugall, I., et al., *An NLRP3-specific inflammasome inhibitor attenuates crystal-induced kidney fibrosis in mice*. *Kidney Int*, 2016. **90**(3): p. 525-39.
 205. Shahzad, K., et al., *Nlrp3-inflammasome activation in non-myeloid-derived cells aggravates diabetic nephropathy*. *Kidney International*. **87**(1): p. 74-84.
 206. Kawaguchi, M., et al., *Inflammasome activation of cardiac fibroblasts is essential for myocardial ischemia/reperfusion injury*. *Circulation*, 2011. **123**(6): p. 594-604.
 207. Kostadinova-Kunovska, S., et al., *Morphology of renal interstitial fibroblasts*. *Prilozi*, 2012. **33**(1): p. 15-25.
 208. Wang, H., et al., *Inflammasome-independent NLRP3 is required for epithelial-mesenchymal transition in colon cancer cells*. *Exp Cell Res*, 2016. **342**(2): p. 184-92.
 209. Chung, H., et al., *NLRP3 regulates a non-canonical platform for caspase-8 activation during epithelial cell apoptosis*. *Cell Death Differ*, 2016. **23**(8): p. 1331-46.
 210. Youm, Y.H., et al., *The ketone metabolite beta-hydroxybutyrate blocks NLRP3 inflammasome-mediated inflammatory disease*. *Nat Med*, 2015. **21**(3): p. 263-9.
 211. Lamkanfi, M., et al., *Glyburide inhibits the Cryopyrin/Nalp3 inflammasome*. *J Cell Biol*, 2009. **187**(1): p. 61-70.
 212. Juliana, C., et al., *Anti-inflammatory compounds parthenolide and Bay 11-7082 are direct inhibitors of the inflammasome*. *J Biol Chem*, 2010. **285**(13): p. 9792-802.

-
213. Coll, R.C., et al., *A small-molecule inhibitor of the NLRP3 inflammasome for the treatment of inflammatory diseases*. 2015. **21**(3): p. 248-55.

7. Eidesstattliche Versicherung

Ich erkläre hiermit an Eides statt,

dass ich die vorliegende Dissertation mit dem Thema **Inflammasome-Independent NLRP3 Signaling in Chronic Kidney Disease** selbständig verfasst, mich außer der angegebenen keiner weiteren Hilfsmittel bedient und alle Erkenntnisse, die aus dem Schrifttum ganz oder annähernd übernommen sind, als solche kenntlich gemacht und nach ihrer Herkunft unter Bezeichnung der Fundstelle einzeln nachgewiesen habe.

Ich erkläre des Weiteren, dass die hier vorgelegte Dissertation nicht in gleicher oder in ähnlicher Form bei einer anderen Stelle zur Erlangung eines akademischen Grades eingereicht wurde. Der Hauptteil meiner Dissertation wurde im September 2017 in der Fachzeitschrift *Kidney International* mit dem Titel „*The inflammasome component NLRP3 contributes to nephrocalcinosis-related chronic kidney disease independent from IL-1-mediated tissue injury. Role of macrophage phenotypes and NLRP3-mediated fibrogenesis*“ zur Veröffentlichung zugelassen. Als einer von drei geteilten Erstautoren wurde ein Teil der Arbeit mit Hilfe von Beatriz Suarez Alvarez und Orestes Foresto-Neto durchgeführt, welche mit mir die *in vivo* Experimente mit dem NLRP3 Inflammasom Inhibitor 1,3-Butandiol durchgeführt haben.

München, den 28. August 2018

Melissa Sofia Grigorescu Vlass

8. Acknowledgments

First and foremost I would like to thank Prof. Hans-Joachim Anders and my supervisor PD. Dr. hum. biol. Shrikant R. Mulay, who gave me the opportunity to participate in this project and thought me from a very close perspective what science really is, thus allowing me to know the incredibly interesting but also frustrating sides of it, waking a deep sense of passion for science and especially nephrology in me. Without their guidance, intellectual talent, encouragement and professional expertise, none of this would have been possible. Thank you for the support, for instilling confidence in me and encouraging the physician-scientist in me.

I would also like to thank my co-workers Beatriz Suarez Alvarez and Orestes Foresto-Neto, who kindly provided their talent to support this project by helping me with experiments that nicely complemented this thesis and lead to the publication of our paper. In this regard I would also like to thank Stefanie Steiger, who with her technical expertise, knowledge and natural love for science provided us with interesting ideas that gave that special touch to our paper. Also, many thanks to external contributors Jutta Jordan and Tobias Bäuerle who performed MRI Images, Lisa Müller and Nicolai Burzlaff who kindly agreed to support this project. Many special thanks to Jyaysi, Julian, Mohsen and Chongxu, who also put some of their precious time for supporting this project. To Dan Draganovici and Janina Mandelbaum also many thanks for the preparation of histological sections. Especially I would like to thank all my lab colleges, Alex, John, Heni, Jyaysi, Santhosh, Simo, Shrikant, Julian, Anja and Steffi for the amazing moments shared, for all the fun, the friendship, the international dinners, and unconditional support. I will never forget you!

And last but not least, I would like to thank my parents Sanda and Tiberiu, my sister Andrea and Daniel, who gave me their unconditional support and patience, encouraging me even in the toughest times. Thank you for being such an inspiration to me and for your unconditional love.

